UNIVERSITY OF OKLAHOMA

GRADUATE COLLEGE

METABOLOMIC ANALYSIS OF LIVE SINGLE CELLS AND SPHEROID SECRETIONS USING MASS SPECTROMETRY: TOWARDS UNDERSTANDING OF CELLULAR METABOLISM

A DISSERTATION

SUBMITTED TO THE GRADUATE FACULTY

in partial fulfillment of the requirements for the

Degree of

Doctor of Philosophy

By

Mei Sun

Norman, Oklahoma

2019

METABOLOMIC ANALYSIS OF LIVE SINGLE CELLS AND SPHEROID SECRETIONS USING MASS SPECTROMETRY: TOWARDS UNDERSTANDING OF CELLULAR METABOLISM

A DISSERTATION APPROVED FOR THE DEPARTMENT OF CHEMISTRY AND BIOCHEMISTRY

BY

Dr. Zhibo Yang, Chair

Dr. Bin Wang

Dr. Chuanbin Mao

Dr. Si Wu

Dr. Yihan Shao

Acknowledgment

I am extremely grateful for the mentorship provided by my advisor Dr. Zhibo Yang. Without the support and guidance from him, a doctoral thesis would not have been possible. I would like to sincerely acknowledge Dr. Yang for his unconditional support, encouragement and patient in the past five years. Dr. Yang's supervision made my research work more efficient and productive.

I would like to thank all my committee members, Dr. Si Wu, Dr. Yihan Shao, Dr. Bin Wang, Dr. Chuanbin Mao, Dr. Ann West and Dr. Boris Wawrik. Their kind guidance and suggestions throughout my graduate research are very much appreciated.

I also would like to give special thanks to both past and present members in Dr. Yang's group. They are Ning Pan, Wei Rao, Xiang Tian, Renmeng Liu, Shawna Standke, Yanlin Zhu, Xingxiu Chen, Zhu Zou, Jon Pope, Zongkai Peng, Tra Nguyen and Yunpeng Lan. Their suggestions and help contribute to the completion of my thesis.

Finally, I would like to express my very profound gratitude to my parents for providing me with continuous encouragement and support throughout my Ph.D. study. This accomplishment would not have been possible without them.

Table of Contents

List of Tables

List of Figures

Abstract

This dissertation describes the single cell metabolomics analysis and microscale extracellular metabolites analysis using the Single-probe mass spectrometry (MS) techniques.

Chapter one summarizes the current technique for single cell analysis, including the exploration of single cell genome, transtriptome, proteome, and metabolome. Techniques used for extracellular metabolites analysis were also briefly described.

Chapter two introduces the metabolomic analysis of single cancer stem cells (CSCs) using the Single-probe MS technique. CSCs are rare types of cells responsible for tumor development, relapse, and metastasis. However, current research in CSC biology is largely limited by the difficulty of obtaining sufficient CSCs. Single-cell analysis techniques are promising tools for CSC-related studies. The Single-probe MS technique was used to investigate the metabolic features of live colorectal CSCs at the single-cell level. Experimental data were analyzed using statistical analysis methods, including the t-test and partial least squares discriminant analysis. The overall metabolic profiles of CSCs are distinct from non-stem cancer cells (NSCCs). Specifically, tricarboxylic acid (TCA) cycle metabolites are more abundant in CSCs compared to NSCCs, indicating their major energy production pathways are different. Moreover, CSCs have relatively higher levels of unsaturated lipids. Inhibiting the activities of stearoyl-CoA desaturase-1 (SCD1), nuclear factor κB (NF-κB), and aldehyde dehydrogenases (ALDH1A1) in CSCs significantly reduced the abundances of unsaturated lipids and hindered the formation of spheroids, resulting in reduced stemness of CSCs. Our techniques and experimental protocols can be potentially used for metabolomic studies of other CSCs and rare types of

cells and provide a new approach to discovering functional biomarkers as therapeutic targets.

Chapter three demonstrates the investigation of metabolic features of single algae cells under different environment stress. Traditional approaches for the assessment of physiological responses of microbes in the environment rely on bulk filtration techniques that obscure differences among populations as well as among individual cells. The Single-probe MS technique was used to directly extract metabolites from living, individual phytoplankton cells for analysis. Marine dinoflagellate Scrippsiella trochoidea cells were grown under different illumination levels and under nitrogen (N) limiting conditions. In both experiments, significant differences in the cellular metabolome of individual cells could readily be identified, though the vast majority of detected metabolites could not be assigned to KEGG pathways. Using the same approach, significant changes in cellular lipid complements were observed, with individual lipids being both up- and down-regulated under light vs. dark conditions. Conversely, lipid content increased across the board under N limitation, consistent with an adjustment of Redfield stoichiometry to reflect higher C:N and C:P ratios. Overall, these data suggest that the Single-probe MS technique has the potential to allow for near in situ metabolomic analysis of individual phytoplankton cells, opening the door to targeted analyses that minimize cell manipulation and sampling artifacts, while preserving metabolic variability at the cellular level.

Chapter four describes comprehensive studies of early-stage drug resistance cells using single cell MS metabolomics combined with other techniques. Efficacy of chemotherapy is often limited by *de novo* or acquired drug resistance in clinic treatment. Studying the

underlying mechanisms of drug resistance is necessary for better development of novel therapeutic strategies. Studies in this field are generally conducted through bulk analysis of samples obtained from long-term chemotherapy. Investigating the metabolic changes occurred in the early-stage of drug resistance at the single-cell level provides insights into drug resistant mechanisms, and the developed techniques can be potentially used for early monitoring of drug resistance in clinic. Comprehensive studies were carried out using multiple techniques, including single cell MS metabolomics, western blotting, flow cytometry, and reverse transcription polymerase chain reaction (RT-PCR), to explore mechanisms of irinotecan resistance at the initial stage at the single cell level. Results illustrate that SCD1 is upregulated in the irinotecan-resistant cells, which show increased levels of stemness and decreased degrees of ROS.

Chapter 5 demonstrates the critical roles of extracellular compounds in intercellular communication, tumor proliferation, and cancer cell metastasis. However, the lack of appropriate techniques leads to limited studies of extracellular metabolite. Here, we introduced a microscale collection device, the Micro-funnel, fabricated from biocompatible fused silica capillary. With a small probe size (~25 μm), the Micro-funnel can be implanted into live multicellular tumor spheroids to accumulate the extracellular metabolites produced by cancer cells. Metabolites collected in the Micro-funnel device were thenextracted by a microscale sampling and ionization device, the Single-probe, for real-time mass spectrometry (MS) analysis. We successfully detected the abundance change of anticancer drug irinotecan and its metabolites inside spheroids treated under a series of conditions. Moreover, we found that irinotecan treatment dramatically altered the composition of extracellular compounds. Specifically, we observed the increased

abundances of a large number of lipids, which are potentially related to the drug resistance of cancer cells. This study provides a novel way to detect the extracellular compounds inside live spheroids, and the successful development of our technique can benefit the research in multiple areas, including the microenvironment inside live tissues, cell−cell communication, biomarker discovery, and drug development.

Chapter 1. Introduction

1.1 Background

A single cell is the basic functional biological unit, and cellular status and molecular compositions can vary based on different external influence and internal process. To study cellular functional and structural roles in bioanalytical system, many traditional bioanalytical methods rely on a bulk analysis, providing the averaged results from the analyzed specimen. In many cases it is suitable to conduct the traditional bulk analysis for samples with adequate amounts. However, there is an increasing need to study extremely limited amounts of samples requiring measurements to be performed at the single-cell or even subcellular level.[1-3] For example, the rare cells such as circulating tumor cells (CTC) have limited populations, and one of the biggest challenges in CTCs' studies is to obtain sufficient cells.[4, 5] Therefore, techniques performing meaningful biological research from individual cells would provide a great advantage for the study of CTCs.[6, 7] Single-cell analysis allows us to study the individual cells with limited population, and investigate the heterogeneity of similar cells, which further promote the development of the understanding of cellular physiological phenomena and fundamental biology. In addition, single cell analysis is an important step to facilitate the investigation of cellular and subcellular genomics, transcriptomics, proteomics, and metabolomics.[2]

1.2 Techniques for single cell intracellular analysis

The advancement in bioanalytical techniques provide the opportunity to investigate complex biological systems from individual cells. Analysis of genome, transcriptome, proteome, and metabolome at the single-cell level promotes system biological study of gene-expression dynamics, cell heterogeneity and disease pathogenesis.[2, 8] Moreover, advanced single cell analysis techniques provide novel and significant insight into studies of biology, medicine, toxicology, and clinical pathology.

1.2.1 Challenges in single cell studies

Despite the significant advance, single cell analysis has been considered as a challenge task. The major challenge for single cell analysis is the extremely limited amount of cellular contents with very complex compositions available from a single cell. In addition, intracellular molecules present as wide ranges of concentrations.[9, 10] Thus, it is obligatory that techniques for single cell analysis need to have high spatial resolution, detection sensitivity, molecular selectivity, and reliability.[11]

1.2.2 Single cell genomics and transcriptomics analysis

Recent advancement of sequencing technique allows us to detect genome, transcriptome, and epigenome at the single-cell level to investigate the cell heterogeneity and status. Figure1.1 presents the development of single cell sequencing.[2] The PCR method permits the analysis of DNA in single cell, and developments of whole genome amplification (WGA)[12, 13] and whole transcriptome amplification (WTA)[14] promote the quantitative analysis of DNA and RNA in individual cells. Later, the genome-wide analysis of DNA and RNA has been realized by the invention of next generation sequencing, and several methods have been further applied to study the single cell DNA methylation and proteome analysis.[15] With the ability to detect both genome

and transcriptome from the same single cell, multi-omics profile for the same cell could be performed.[16] The integrated analysis of the genome and transcriptome promotes the study of regulatory variation[17], DNA structural alteration[18], and RNA editing[19]. In order to perform the integrated analysis at the single cell level, several methods have been applied to separate RNA from genomic DNAs.[8, 20-23]

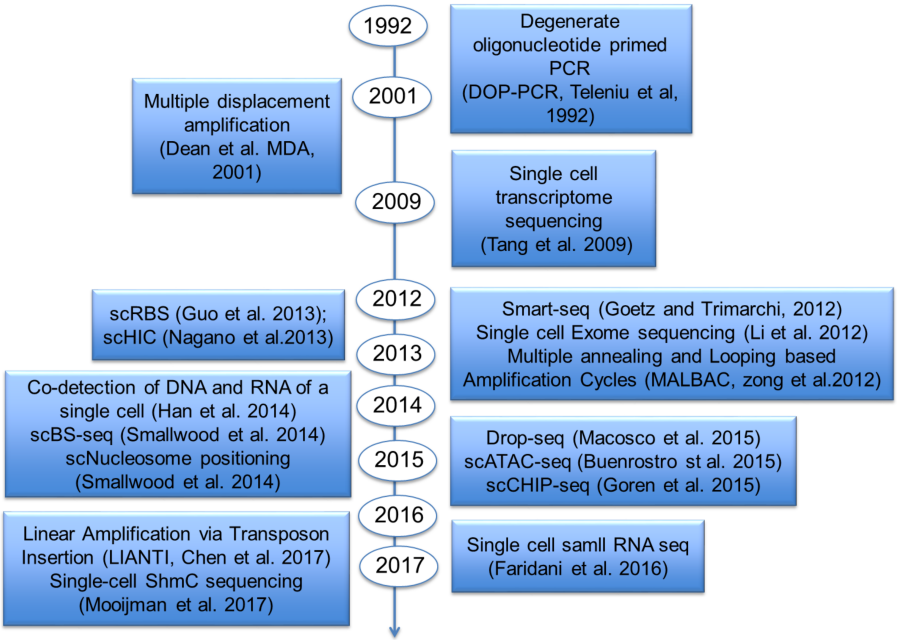

Figure 1.1 Development timeline of single cell sequencing methods.

Han *et al.* developed the microfluidic platform to achieve cell lysate, separation, and amplification of gDNA and cytoplasmic mRNA on a chip. DNA and RNA will be further detected using on-chip PCR, gel electrophoresis, and Sanger sequencing.[21] This is the first measurement of genome and transcripts from single cells. Microfluidic device designed for single cell analysis based on separate extraction process, while later several techniques have been developed to extract genome and transcript in parallel.[22-25] Parallel extraction minimizes sample preparation steps to reduce the sample loss and

contamination compared to separate extraction. GDNA-mRNA sequencing (DR-seq)[23] and genome and transcriptome sequencing (G&T-seq)[26] are developed to perform simultaneously analysis DNA and cytoplasmic RNA without separating nucleus and cytoplasm. Based on the technique of G&T-seq, single-cell methylation and transcriptome sequencing (scM&T-seq) methods were developed to detect the methylation and transcriptome expression level.[27] In addition, more techniques have been reported to study single cell epigenomics such as transposase-accessible chromatin sequencing (ATAC-seq)[28] and single-cell DNase sequencing (scDNase-seq).[29] These techniques allow new co-measurement of single cell epigenomics and transcriptomics in the future.

1.2.3 Single cell protein analysis

Techniques for single cell DNA and RNA analysis provide the information on the gene-products level, but they are incapable to study the expression, post-translational modification, and interactions of proteins in single cells. Recent advancements in microscopy, flow cytometry, microfluidics, and mass spectrometry allow the detection of proteins at the single-cell level.[30, 31] Fluorescent flow cytometry is a well-established technique for single-cell surface protein analysis. This technique utilizes single cells, which are stained with up to 10-15 specific fluorescent-labeled antibodies, and flows them through a capillary tube to be detected by photomultiplier tubes[32, 33]. Fluorescent flow cytometry is able to semi-quantify multiple proteins in single cells related to a variety of disease.[34] However, traditional flow cytometry normally requires a large of amount of cells to be processed, and therefore, it is not suitable for the analysis of cells with limited numbers such as CTCs. In order to overcome the limitation, microfluidic

flow cytometry has been developed to study the cells with limited numbers (10-100).[35] Moreover, the microfluidic flow cytometry also make it possible to study protein in a single cell with two orthogonal methods: imaging and cytometry.[1, 36-38] As show in Figure 1.2, a parallel microfluidic flow cytometry has been developed to perform cell culture and cell preparation combined with fluorescence microscope and microfluidic flow cytometer to investigate the immune response.[39]

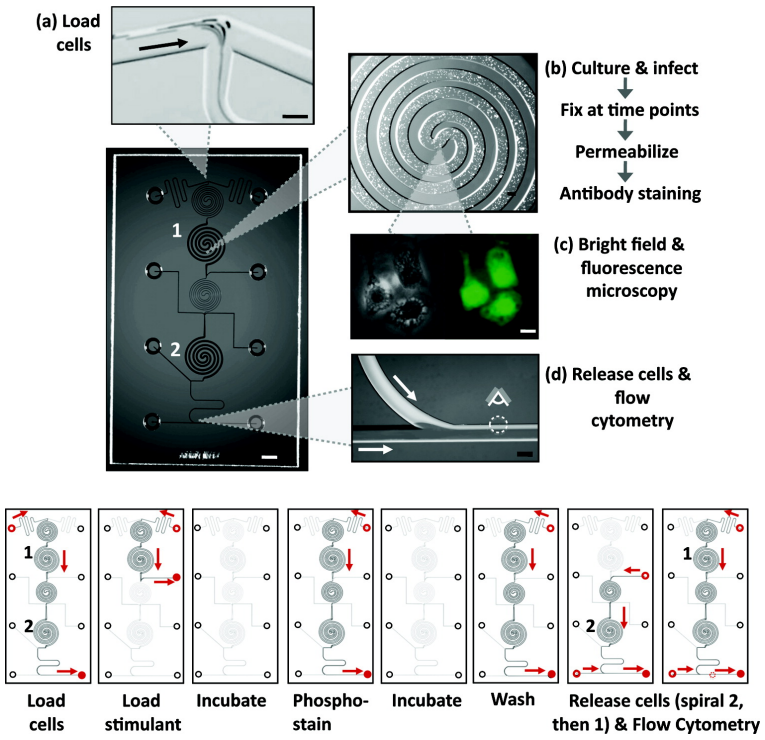

Figure 1.2. A parallel microfluidic flow cytometer for single cell protein screening. (a) Cells are loaded into the phosphoflow chip (pFC) by pressure-driven flow. (b) pFC phosphorylation assay in incubation chambers proceeds as (1) cell culture and infection, (2) phospho-profiling, (c) imaging, and (d) flow cytometry.

[Reprinted with the permission from Srivastava, Nimisha, et al., Analytical Chemistry 81.9 (2009): 3261-3269. Copyright © 2009, American Chemical Society]

Besides flow cytometry, single cell western blot has been developed to study single cell proteins.[40] Single cell western blot targets specific proteins by coupling antibody based detection and sodium dodecyl sulfate–polyacrylamide gel electrophoresis (SDS-PAGE) separation as shown in Figure 1.3. [41] Antibody based methods provide the golden standard method in protein analysis at single cell level. However, these technique cannot simultaneously analyze more than 20 proteins, limiting the study of system-level biological pathways that requires multiple correlation measurements.[30]

Single cell mass spectrometry allows the detection of whole proteome simultaneously at single cell level. [42] With the advantage of label-free and high sensitivity, mass spectrometry technique has the potential to quantify entire proteome in a single cell. [30]

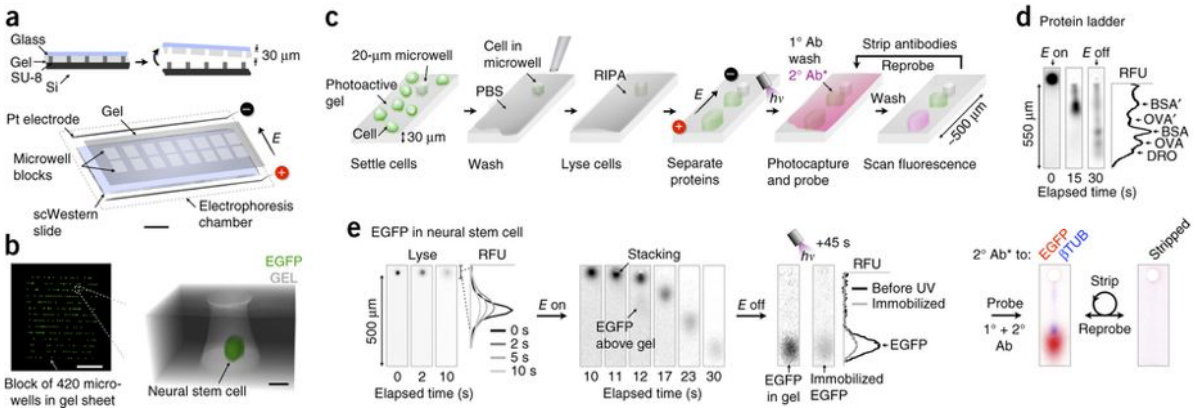

Figure 1.3. Single cell western blotting workflow. (a) Thousands of microwells patterned in a photoactive polyacrylamide gel seated on a glass slide. (b) Fluorescent microspheres are blocked in a microwell. (c) Open-gel single cell western analysis including cell setting and cell lysis. (d) PAGE separates five fluorescently labeled proteins. (e) Single cell western detects proteins from a single cell.

[Reprinted with the permission from Hughes, Alex J., et al., Nature Methods 11.7 (2014): 749. Copyright © 2014, Springer Nature]

1.2.3 Single cell metabolomics analysis

Compared to results obtained from single cell analysis of genomics, transcriptomics, and proteomics, single cell metabolomics presents more immediate and dynamic status of a single cells. Metabolites are directly related to a variety of biological mechanisms, and they are regarded as indicators of phenotypic heterogeneity.[43] Analysis of metabolites in individual cells is challenging, because metabolites changed rapidly and the cellular contents are very complex. Therefore, high selectivity and sensitivity are needed for analytical techniques to perform single cell metabolomics analysis. Currently, many analytical techniques, including capillary electrophoresis, Raman spectroscopy, microfluidics, and mass spectrometry (MS), have been applied to study the metabolites at single cell level.[44-49] Among them, MS is becoming a powerful method and playing an important role in single cell analysis due to its outstanding properties of high sensitivity, high resolution, and label-free detection.[49]

According to the sample ionization environment, there are two major groups of MS based techniques for single cell metabolomics analysis: vacuum-based and ambient-based MS techniques.[50, 51] Secondary ion mass spectrometry (SIMS) [52] and matrix-assisted laser desorption ionization (MALDI)[53, 54] are dominant vacuum-based MS techniques, and they provide important advancements in bioanalytical method development. For example, MALDI desorbs and ionizes the metabolites by incorporating the metabolites into a suitable matrix. With an excellent spatial resolution (~5 μm),

MALDI is becoming the dominant approaches for single cell analysis (Figure 1.4).[53] However, vacuum-based MS techniques still have their drawbacks, such as obligatory sample preparation and high vacuum conditions, limiting the studies of live cells.

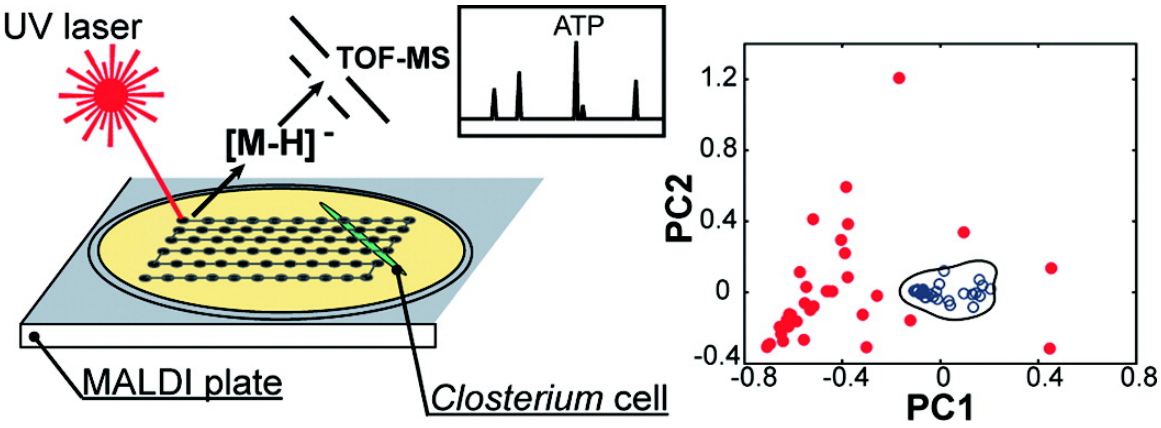

Figure 1.4. Single cell MALDI-MS analysis. Single cells are mixed with matrix and subjected to MALDI-MS measurement of metabolites.

[Reprinted with the permission from Amantonico, Andrea, et al., Analytical Chemistry 82.17 (2010): 7394-7400. Copyright © 2010, American Chemical Society]

With the development of ambient sampling and ionization techniques, ambient-based MS has been used to perform live single cell analysis with minimal preparation, which offers direct, rapid, *in vivo* investigation of the heterogeneity of individual cells.[50] Live single-cell video-mass spectrometry utilizes the gold-coated nanospray tip to insert into a single cell under a video microscope, and the cellular metabolites are sucked into the tip acting as a micropipette. Then the nanospray tip is directly coupled with MS for the detection of the cellular metabolites (Figure 1.5). Hundreds of small molecules can be detected by the live single-cell video-mass spectrometry.[55] Microprobe single-cell capillary electrophoresis electrospray ionization mass

spectrometry (CE-ESI-MS) technique integrates micro sampling, microscale extraction, and CE-MS to investigate the metabolic feature of single embryonic cells (Figure 1.6).[56, 57] Particularly, with the exquisite separation efficiency, microprobe single-cell CE-ESI MS could address the complex metabolome to offer complementary advantages for single-cell studies.[56]

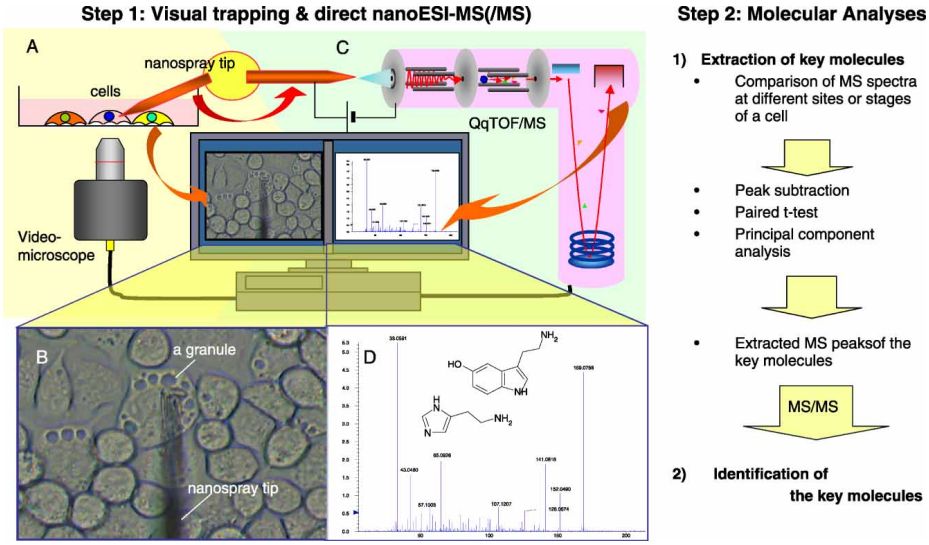

Figure 1.5. Live single-cell video mass spectrometry. The analysis process has two steps. In the first step, video microscope is used to monitor single cells, and cellular contents are directly sucked into a nanospray ionization tip, which is transferred to a mass spectrometer. A voltage is then applied to start the nanospray. In the second step, MS spectra are exported and data analysis is performed to extract key metabolites. Some targeted MS peaks were subjected to MS/MS analysis for identification.
[Reprinted with the permission from Mizuno, Hajime, et al., Journal of Mass Spectrometry 43.12 (2008): 1692-1700. © John Wiley & Sons Ltd]

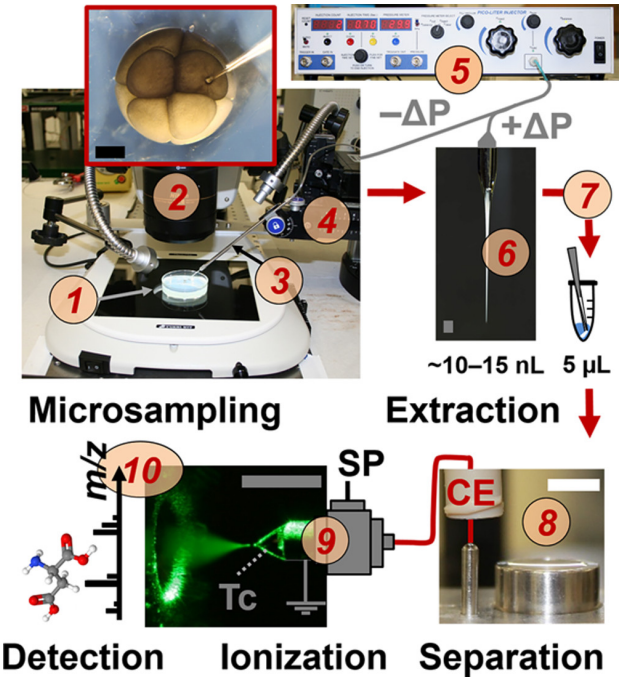

Figure 1.6. Microprobe single-cell CE-ESI-MS for metabolomic analysis of singe live embryos. (1) The status of single cells is monitored using a stereomicroscope. (2) Cellular content are sucked into a pulled capillary. (3) A multiaxis translation stage coupled with (4) a microinjector and (5) a delivering vacuum. (6) The enriched cell contents are injected into a tube for extraction. (7) The extracted metabolites are measured by a microloading CE platform. (8) CE platform is connected to an ESI source. (9) Metabolites are ionized for detection using a high-resolution tandem mass spectrometer. (10) Metabolites peaks detected by MS.

[Reprinted with the permission Onjiko, Rosemary M., et al., Analytical Chemistry 89.13 (2017): 7069-7076. Copyright © 2017, American Chemical Society]

The Single-probe MS is another single-cell ambient MS method. The Single-probe is a miniaturized multifunctional sampling and ionization device that can be coupled with MS for the real-time single cell analysis.[48, 58, 59] This device is

composed of dual-bore quartz tubing pulled by a laser pipette puller, a fused silica capillary, and a nano-ESI emitter. With an extremely small sampling probe size (<10 μm), the Single-probe cab be inserted into single cells to efficiently extract cellular contents for ionization and MS analysis (Figure 1.7).[48]

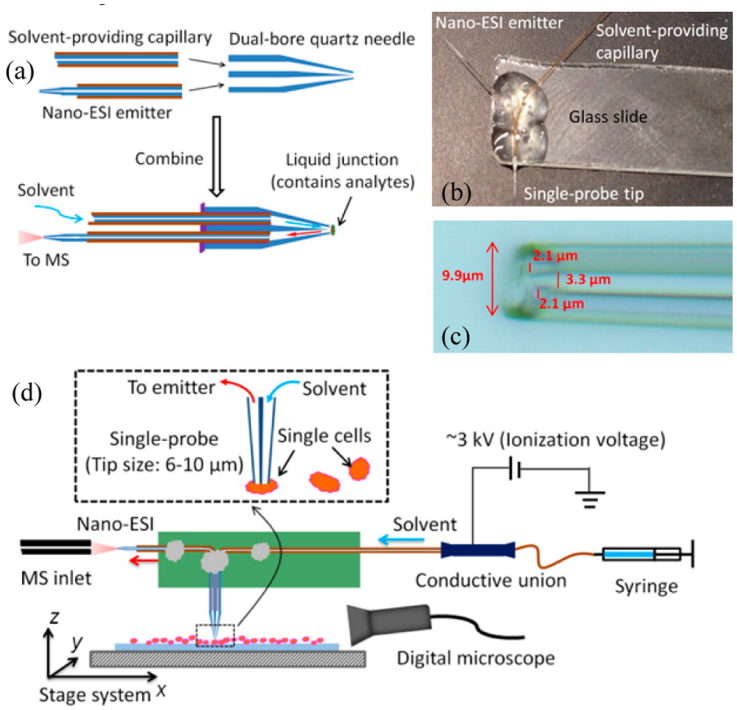

Figure 1.7. The Single-probe MS system. (a) Fabrication of Single-probe. (b) Photograph of a Single-probe. (C) Calibrated microscopic photo of a Single-probe tip. (D) Single cell MS analysis setup.

[Reprinted with the permission Pan, Ning, et al., Analytical Chemistry 86.19 (2014): 9376-9380. Copyright © 2014, American Chemical Society]

In general, single cell analysis promotes the understanding of cell function and heterogeneity based on genome, transcriptome, proteome and metabolome study abstained at single cell level. Single cell multi-omics analysis will allow us to explore the

correlation and mechanism of cell genetic variation and expression dynamics of proteins and metabolites, enabling more detailed investigation of cellular status in multiple diseases.[22, 60]

1.3. Microscale analysis of extracellular metabolites

In addition to intracellular analysis, previous studies indicate that microenvironment is essential for biological function of tumors, including cell−cell communication and cancer cell migration and metastasis.[61] Investigation of extracellular compounds produced by tumor cells enable us to potentially discover specific cancer biomarkers, and provide guidelines for the amelioration of current cancer therapies. However, studies of extracellular metabolites have not been widely performed due to the lack of appropriate analytical techniques.[62, 63] In a long time, the detection of extracellular biomolecules is limited by their low concentrations and loss through diffusion into cell culture medium. Microdialysis technique utilizes microdialysis probes that contain semipermeable membranes to enrich extracellular molecules. However, the general sizes of microdialysis probe range between 200 and 500 μm, resulting in limited spatial resolution and studies of small tumors.[64-66] Micro-funnel device with small tip size (~25 μm) has been developed to study extracellular molecules in multicellular spheroids. Micro-funnel can be implanted into a live spheroid for direct collection of extracellular compounds without being diluted and selected. Micro-funnel can be coupled with the Single-probe MS to monitor extracellular drug and metabolites inside live spheroids for real-time analysis (Figure 1.8).[59] In general, the development of extracellular components detection technique can benefit the research in multiple areas, including the microenvironment inside live tissues, cell−cell communication, biomarker discovery, and drug development.

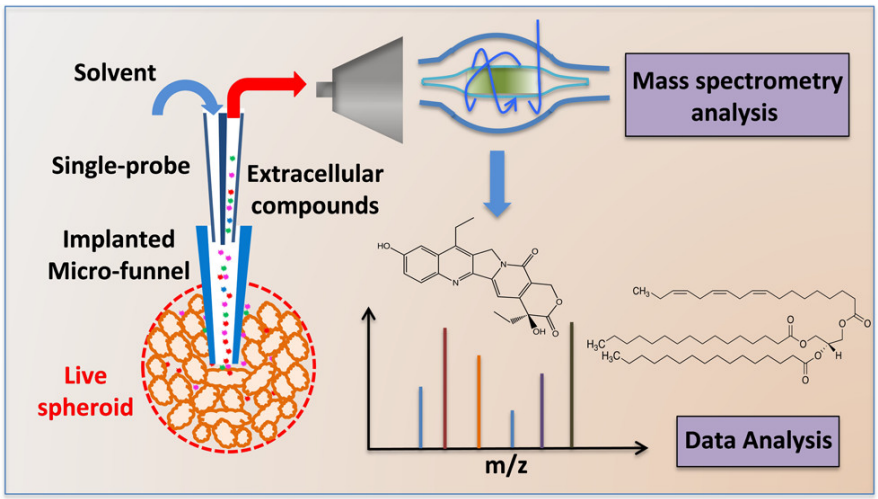

Figure 1.8 The Micro-funnel coupled with the Single-probe MS analysis for extracellular compounds detection in live spheroids.

[Reprinted with the permission Sun, Mei, et al., Analytical Chemistry 89.17 (2017): 9069-9076. Copyright © 2017, American Chemical Society]

1.4 Reference

[1] S. Lindström, H. Andersson-Svahn, Overview of single-cell analyses: microdevices and applications, Lab Chip, 10 (2010) 3363-3372.

[2] Y. Hu, Q. An, K. Sheu, B. Trejo, S. Fan, Y. Guo, Single cell multi-omics technology: methodology and application, Front Cell Dev Biol., 6 (2018).

[3] E. Levy, N. Slavov, Single cell protein analysis for systems biology, Essays Biochem., 62 (2018) 595-605.

[4] D. Heymann, M. Téllez-Gabriel, Circulating tumor cells: the importance of single cell analysis, Single Cell Biomedicine, Springer2018, pp. 45-58.

[5] A.A. Powell, A.H. Talasaz, H. Zhang, M.A. Coram, A. Reddy, G. Deng, M.L. Telli, R.H. Advani, R.W. Carlson, J.A. Mollick, Single cell profiling of circulating tumor cells: transcriptional heterogeneity and diversity from breast cancer cell lines, PloS one, 7 (2012) e33788.

[6] C.L. Chen, D. Mahalingam, P. Osmulski, R.R. Jadhav, C.M. Wang, R.J. Leach, T.C. Chang, S.D. Weitman, A.P. Kumar, L. Sun, Single‐cell analysis of circulating tumor cells identifies cumulative expression patterns of EMT‐related genes in metastatic prostate cancer, The Prostate, 73 (2013) 813-826.

[7] D.T. Ting, B.S. Wittner, M. Ligorio, N.V. Jordan, A.M. Shah, D.T. Miyamoto, N. Aceto, F. Bersani, B.W. Brannigan, K. Xega, Single-cell RNA sequencing identifies extracellular matrix gene expression by pancreatic circulating tumor cells, Cell reports, 8 (2014) 1905-1918.

[8] Y. Song, X. Xu, W. Wang, T. Tian, Z. Zhu, C. Yang, Single cell transcriptomics: moving towards multi-omics, Analyst, (2019).

[9] G.-C. Yuan, L. Cai, M. Elowitz, T. Enver, G. Fan, G. Guo, R. Irizarry, P. Kharchenko, J. Kim, S. Orkin, Challenges and emerging directions in single-cell analysis, Genome Biol., 18 (2017) 84.

[10] P. Angerer, L. Simon, S. Tritschler, F.A. Wolf, D. Fischer, F.J. Theis, Single cells make big data: New challenges and opportunities in transcriptomics, Curr Opin Syst Biol., 4 (2017) 85-91.

[11] A.L. Roy, R. Conroy, J. Smith, Y. Yao, A.C. Beckel-Mitchener, J.M. Anderson, E.L. Wilder, Accelerating a paradigm shift: The Common Fund Single Cell Analysis Program, Sci Adv., 4 (2018) eaat8573.

[12] M. Hosokawa, Y. Nishikawa, M. Kogawa, H. Takeyama, Massively parallel whole genome amplification for single-cell sequencing using droplet microfluidics, Sci. Rep., 7 (2017) 5199.

[13] D. Wells, J.K. Sherlock, J.D. Delhanty, A.H. Handyside, Detailed chromosomal and molecular genetic analysis of single cells by whole genome amplification and comparative genomic hybridisation, Nucleic Acids Res, 27 (1999) 1214-1218.

[14] S.A. Tomlins, R. Mehra, D.R. Rhodes, R.B. Shah, M.A. Rubin, E. Bruening, V. Makarov, A.M. Chinnaiyan, Whole transcriptome amplification for gene expression profiling and development of molecular archives, Neoplasia, 8 (2006) 153-162.

[15] I.D. Karemaker, M. Vermeulen, Single-cell DNA methylation profiling: technologies and biological applications, Trends Biotechnol, (2018).

[16] I.C. Macaulay, C.P. Ponting, T. Voet, Single-cell multiomics: multiple measurements from single cells, Trends Genet., 33 (2017) 155-168.

[17] F. Grubert, J.B. Zaugg, M. Kasowski, O. Ursu, D.V. Spacek, A.R. Martin, P. Greenside, R. Srivas, D.H. Phanstiel, A. Pekowska, Genetic control of chromatin states in humans involves local and distal chromosomal interactions, Cell, 162 (2015) 1051-1065.

[18] X. Wang, H. Chen, N.R. Zhang, DNA copy number profiling using single-cell sequencing, Brief. Bioinform, 19 (2017) 731-736.

[19] J.B. Li, E.Y. Levanon, J.-K. Yoon, J. Aach, B. Xie, E. LeProust, K. Zhang, Y. Gao, G.M. Church, Genome-wide identification of human RNA editing sites by parallel DNA capturing and sequencing, Science, 324 (2009) 1210-1213.

[20] H. Guo, P. Zhu, X. Wu, X. Li, L. Wen, F. Tang, Single-cell methylome landscapes of mouse embryonic stem cells and early embryos analyzed using reduced representation bisulfite sequencing, Genome Res., 23 (2013) 2126-2135.

[21] L. Han, X. Zi, L.X. Garmire, Y. Wu, S.M. Weissman, X. Pan, R. Fan, Co-detection and sequencing of genes and transcripts from the same single cells facilitated by a microfluidics platform, Sci. Rep., 4 (2014) 6485.

[22] Y. Hou, H. Guo, C. Cao, X. Li, B. Hu, P. Zhu, X. Wu, L. Wen, F. Tang, Y. Huang, Single-cell triple omics sequencing reveals genetic, epigenetic, and transcriptomic heterogeneity in hepatocellular carcinomas, Cell Res., 26 (2016) 304.

[23] S.S. Dey, L. Kester, B. Spanjaard, M. Bienko, A. Van Oudenaarden, Integrated genome and transcriptome sequencing of the same cell, Nat. Biotechnol., 33 (2015) 285.

[24] I.C. Macaulay, M.J. Teng, W. Haerty, P. Kumar, C.P. Ponting, T. Voet, Separation and parallel sequencing of the genomes and transcriptomes of single cells using G&T-seq, Nat. Protoc., 11 (2016) 2081.

[25] S. Picelli, Å.K. Björklund, O.R. Faridani, S. Sagasser, G. Winberg, R. Sandberg, Smart-seq2 for sensitive full-length transcriptome profiling in single cells, Nat. Methods, 10 (2013) 1096.

[26] I.C. Macaulay, W. Haerty, P. Kumar, Y.I. Li, T.X. Hu, M.J. Teng, M. Goolam, N. Saurat, P. Coupland, L.M. Shirley, G&T-seq: parallel sequencing of single-cell genomes and transcriptomes, Nat. Methods, 12 (2015) 519.

[27] C. Angermueller, S.J. Clark, H.J. Lee, I.C. Macaulay, M.J. Teng, T.X. Hu, F. Krueger, S.A. Smallwood, C.P. Ponting, T. Voet, Parallel single-cell sequencing links transcriptional and epigenetic heterogeneity, Nat. Methods, 13 (2016) 229.

[28] J.D. Buenrostro, B. Wu, H.Y. Chang, W.J. Greenleaf, ATAC‐seq: a method for assaying chromatin accessibility genome‐wide, Curr Protoc Mol Biol, 109 (2015) 21.29. 21-21.29. 29.

[29] H.H. He, C.A. Meyer, M.-W. Chen, C. Zang, Y. Liu, P.K. Rao, T. Fei, H. Xu, H. Long, X.S. Liu, Refined DNase-seq protocol and data analysis reveals intrinsic bias in transcription factor footprint identification, Nat. Methods, 11 (2014) 73.

[30] M. Wu, A.K. Singh, Single-cell protein analysis, Curr Opin Biotechnol 23 (2012) 83-88.

[31] B. Fan, J. Wang, Y. Xu, J. Chen, Single-Cell Protein Assays: A Review, in: T. Huang (Ed.) Computational Systems Biology: Methods and Protocols, Springer New York, New York, NY, 2018, pp. 293-309.

[32] S.C. De Rosa, L.A. Herzenberg, L.A. Herzenberg, M. Roederer, 11-color, 13-parameter flow cytometry: identification of human naive T cells by phenotype, function, and T-cell receptor diversity, Nat. Med., 7 (2001) 245.

[33] S.P. Perfetto, P.K. Chattopadhyay, M. Roederer, Seventeen-colour flow cytometry: unravelling the immune system, Nat. Rev. Immunol., 4 (2004) 648.

[34] K. Sachs, O. Perez, D. Pe'er, D.A. Lauffenburger, G.P. Nolan, Causal protein-signaling networks derived from multiparameter single-cell data, Science, 308 (2005) 523-529.

[35] A.B. Shrirao, Z. Fritz, E.M. Novik, G.M. Yarmush, R.S. Schloss, J.D. Zahn, M.L. Yarmush, Microfluidic flow cytometry: The role of microfabrication methodologies, performance and functional specification, Technology, 6 (2018) 1-23.

[36] V.V. Lychagov, A.A. Shemetov, R. Jimenez, V.V. Verkhusha, Microfluidic System for In-Flow Reversible Photoswitching of Near-Infrared Fluorescent Proteins, Anal. Chem., 88 (2016) 11821-11829.

[37] B.K. McKenna, J.G. Evans, M.C. Cheung, D.J. Ehrlich, A parallel microfluidic flow cytometer for high-content screening, Nat. Methods, 8 (2011) 401.

[38] X. Li, B. Fan, S. Cao, D. Chen, X. Zhao, D. Men, W. Yue, J. Wang, J. Chen, A microfluidic flow cytometer enabling absolute quantification of single-cell intracellular proteins, Lab Chip, 17 (2017) 3129-3137.

[39] N. Srivastava, J.S. Brennan, R.F. Renzi, M. Wu, S.S. Branda, A.K. Singh, A.E. Herr, Fully integrated microfluidic platform enabling automated phosphoprofiling of macrophage response, Anal. Chem., 81 (2009) 3261-3269.

[40] A.J. Hughes, D.P. Spelke, Z. Xu, C.-C. Kang, D.V. Schaffer, A.E. Herr, Single-cell western blotting, Nat. Methods, 11 (2014) 749.

[41] C.-C. Kang, J.-M.G. Lin, Z. Xu, S. Kumar, A.E. Herr, Single-cell western blotting after whole-cell imaging to assess cancer chemotherapeutic response, Anal. Chem., 86 (2014) 10429-10436.

[42] B. Budnik, E. Levy, G. Harmange, N. Slavov, SCoPE-MS: mass spectrometry of single mammalian cells quantifies proteome heterogeneity during cell differentiation, Genome Biol., 19 (2018) 161.

[43] R. Zenobi, Single-cell metabolomics: analytical and biological perspectives, Science, 342 (2013) 1243259.

[44] X. Zhang, M.B. Roeffaers, S. Basu, J.R. Daniele, D. Fu, C.W. Freudiger, G.R. Holtom, X.S. Xie, Label‐free live‐cell imaging of nucleic acids using stimulated Raman scattering microscopy, ChemPhysChem, 13 (2012) 1054-1059.

[45] D. Di Carlo, L.Y. Wu, L.P. Lee, Dynamic single cell culture array, Lab Chip, 6 (2006) 1445-1449.

[46] W.-H. Tan, S. Takeuchi, A trap-and-release integrated microfluidic system for dynamic microarray applications, Proc. Natl. Acad. Sci. , 104 (2007) 1146-1151.

[47] P. Nemes, A.M. Knolhoff, S.S. Rubakhin, J.V. Sweedler, Metabolic differentiation of neuronal phenotypes by single-cell capillary electrophoresis–electrospray ionization-mass spectrometry, Anal. Chem., 83 (2011) 6810-6817.

[48] N. Pan, W. Rao, N.R. Kothapalli, R. Liu, A.W. Burgett, Z. Yang, The single-probe: a miniaturized multifunctional device for single cell mass spectrometry analysis, Anal. Chem., 86 (2014) 9376-9380.

[49] K.D. Duncan, J. Fyrestam, I. Lanekoff, Advances in mass spectrometry based single-cell metabolomics, Analyst, 144 (2019) 782-793.

[50] J.T. Shelley, S.P. Badal, C. Engelhard, H. Hayen, Ambient desorption/ionization mass spectrometry: evolution from rapid qualitative screening to accurate quantification tool, Anal. Bioanal. Chem, 410 (2018) 4061-4076.

[51] L. Zhang, A. Vertes, Single‐Cell Mass Spectrometry Approaches to Explore Cellular Heterogeneity, Angew Chem. Int. Ed., 57 (2018) 4466-4477.

[52] S. Chandra, Quantitative imaging of chemical composition in single cells by secondary ion mass spectrometry: cisplatin affects calcium stores in renal epithelial cells, Mass spectrometry imaging, Springer2010, pp. 113-130.

[53] A. Amantonico, P.L. Urban, S.R. Fagerer, R.M. Balabin, R. Zenobi, Single-cell MALDI-MS as an analytical tool for studying intrapopulation metabolic heterogeneity of unicellular organisms, Anal. Chem., 82 (2010) 7394-7400.

[54] L. Li, R.W. Garden, J.V. Sweedler, Single-cell MALDI: a new tool for direct peptide profiling, Trends Biotechnol, 18 (2000) 151-160.

[55] H. Mizuno, N. Tsuyama, T. Harada, T. Masujima, Live single‐cell video‐mass spectrometry for cellular and subcellular molecular detection and cell classification, J. Mass Spectrom., 43 (2008) 1692-1700.

[56] R.M. Onjiko, E.P. Portero, S.A. Moody, P. Nemes, In situ microprobe single-cell capillary electrophoresis mass spectrometry: metabolic reorganization in single differentiating cells in the live vertebrate (Xenopus laevis) embryo, Anal. Chem., 89 (2017) 7069-7076.

[57] R.M. Onjiko, E.P. Portero, S.A. Moody, P. Nemes, Microprobe Capillary Electrophoresis Mass Spectrometry for Single-cell Metabolomics in Live Frog (Xenopus laevis) Embryos, J. Vis. Exp., (2017).

[58] N. Pan, W. Rao, S.J. Standke, Z. Yang, Using Dicationic Ion-Pairing Compounds To Enhance the Single Cell Mass Spectrometry Analysis Using the Single-Probe: A Microscale Sampling and Ionization Device, Anal. Chem., 88 (2016) 6812.

[59] M. Sun, X. Tian, Z. Yang, Microscale Mass Spectrometry Analysis of Extracellular Metabolites in Live Multicellular Tumor Spheroids, Anal. Chem., (2017).

[60] Y. Hou, H. Guo, C. Cao, X. Li, B. Hu, P. Zhu, X. Wu, L. Wen, F. Tang, Y. Huang, Single-cell triple omics sequencing reveals genetic, epigenetic, and transcriptomic heterogeneity in hepatocellular carcinomas, Cell research, 26 (2016) 304.

[61] T. Nederman, B. Norling, B. Glimelius, J. Carlsson, U. Brunk, Demonstration of an extracellular matrix in multicellular tumor spheroids, Cancer Res., 44 (1984) 3090-3097.

[62] M. Sun, X. Tian, Z. Yang, Microscale Mass Spectrometry Analysis of Extracellular Metabolites in Live Multicellular Tumor Spheroids, Analytical Chemistry, (2017).

[63] R. Harisi, A. Jeney, Extracellular matrix as target for antitumor therapy, Onco Targets Ther., 8 (2015) 1387.

[64] N. Plock, C. Kloft, Microdialysis—theoretical background and recent implementation in applied life-sciences, Eur. J. Pharm. Sci., 25 (2005) 1-24.

[65] C. Liu, Q. Wu, A.C. Harms, R.D. Smith, On-line microdialysis sample cleanup for electrospray ionization mass spectrometry of nucleic acid samples, Anal. Chem., 68 (1996) 3295-3299.

[66] T.S. Shippenberg, A.C. Thompson, Overview of microdialysis, Curr Protoc Neurosci. , (1997) 7.1. 1-7.1. 22.

Chapter 2. Metabolomic Studies of Live Single Cancer Stem Cells Using Mass Spectrometry

2.1 Introduction

Cancer is one of the most common causes of death, and it threats the health of millions of people.[1] Cancer therapy is suffered from drug resistance, which leads to tumor recurrence and metastasis.[2] Cancer stem cells (CSCs) are a rare subset of cancer cells possessing the ability to self-renew and initiate tumors.[3] Recent studies indicate that CSCs are the main source of therapy resistance, and they are responsible for tumor recurrence and metastasis.[4] In particular, the heterogeneity of CSCs forcefully impedes anti-cancer therapies.[5] Unfortunately, the current understanding of the characters of CSCs and their roles in drug resistance is largely lacked, hindering the development of novel tumor diagnostic and therapeutic strategies.

One of the biggest challenges in CSC studies is to obtain sufficient cells, especially from patients, for analysis.[6] However, traditional approaches to studying cell metabolomics, such as HPLC/MS, typically require a large number of cells for sample preparation.[7] Therefore, techniques performing meaningful biological research from individual cells would provide a great advantage for the study of CSCs.[8] A number of single-cell analysis techniques, such as single-cell sorting and single-cell sequencing, have been developed to effectively utilize the limited resources of CSCs.[9, 10] As the final downstream products, metabolites reflect gene regulation, pathway interactions, and environmental perturbations, and they directly indicate cell status. Therefore, the single cell metabolomics study, particularly based on live single cells, can truly provide

chemical information of individual cells to effectively investigate their biological phenotypes.[11, 12] Due to its high detection sensitivity and broad range of molecular analysis, mass spectrometry (MS) has become a predominant technique for metabolomics research. However, the single cell MS (SCMS) analysis of single CSCs has been rarely performed. To the best of our knowledge, only one MS-based metabolomics study of single CSCs has been reported[13], in which the time-of-flight secondary ion mass spectrometry (TOF-SIMS) has been utilized. Due to complex background at low mass range and high degree of ion fragmentation, only a few molecules were identified. In addition, because cell metabolites can rapidly change upon the alteration of cell living environment[14, 15], any method requiring a vacuum environment (e.g., for sampling and ionization) and nontrivial sample preparation, such as SIMS and MALDI (Matrix Assisted Laser Desorption/Ionization), precludes the capability of obtaining molecular information from live cells. Thus, metabolomics of live single CSCs is largely unexplored.[16] Current methods used to detect the CSCs are mainly based on a number of common cell surface biomarkers, such as CD133, CD24, CD44, and the activity of aldehyde dehydrogenase (ALDH1).[17] Because CSCs are highly heterogeneous, using novel techniques to discover new candidates for CSC markers will provide additional approaches to identify target CSCs.[18] Moreover, many CSCs markers are selected without knowing their functional roles, leading to limited reliability as biomarkers.[19] Therefore, characteristic molecules identified using SCMS techniques can be potentially used as novel function-based biomarkers of CSCs.

Colorectal cancer (CRC) is the fourth leading cause of cancer-related death, and CSCs play a critical role in tumor relapse and metastasis[20]; however, the metabolomic

characteristics of colon CSCs in their living status are largely unknown. In this study, we used live CSCs derived from the HCT-116 (colorectal cancer) cells as the model system, and conducted metabolomic analysis at single cell level. In the comparison study, we utilized the regular HCT-116 as the model of non-stem cancer cells (NSCCs) to illustrate the metabolic differences between CSCs and NSCCs. All SCMS experiments were conducted using the Single-probe MS techniques (Figures 2.1A and 2.1B), which have been previously applied in live single cell analysis[21-24], mass spectrometry imaging of tissues[25], and metabolomic analysis of extracellular molecules in live multicellular spheroids.[26]

2.2 Experimental Section

2.2.1 Cell lines and cell culture

Enriched human colon cancer HCT-116 CSCs were purchased from ProMab Biotechnology (Richmond, CA), and HCT-116 cancer cells (NSCCs) were originally obtained from American Type Culture Collection (ATCC) (Rockville, MD, USA). The HCT-116 CSCs were cultured in Cancer Stem Premium™ medium (Probmab Biotechnology) to maintain their stemness (Figure 2.1C)[27], and the passage number of cells was limited within three to maintain the population of CSCs during cell culture. The HCT-116 NSCCs were cultured in McCoy's 5A cell culture medium containing 10% FBS (fetal bovine serum) and 1% Pen Strep (Life Technologies, Grand Island, NY, USA). All cells were cultured at 37°C in an incubator with 5% CO_2 supply (HeraCell, Heraeus, Germany).

2.2.2 Reagents for the treatment of CSCs

CAY10566 (SCD1 inhibitor, ≥98%), dimethylaminoparthenolide DMAPT (NF-κB inhibitor, ≥99%), CM037 (ALD1H1 inhibitor, ≥98%), and retinoic acid (≥98%) were purchased from Cayman Chemical Company (Ann Arbor, MI, USA). The stock solution of these compounds were prepared in dimethyl sulfoxide (DMSO, Sigma-Aldrich, St. Louis, MO, USA), and further diluted into McCoy's 5A cell culture medium to prepare inhibitor solutions. Based on previous studies, CSCs were treated by CAY10566 (1 μM), DMAPT (5 μM), CM037 (4.6 μM), or retinoic acid (1 μM) for 7 days prior to SCMS measurement.[28, 29]

2.2.3 CSC sorting

To purify CSCs for our SCMS experiments, we utilized florescence-activated cell sorting (FACS) (BD FACS Jazz flow cytometer, BD Biosciences, San Jose, CA, USA) under sterile conditions for cell isolation. Briefly, CSC spheroids formed during culture were dissociated using TrypLE reagents (Life Technologies, Grand Island, NY, USA), and then resuspended in the solution containing 0.5% bovine serum albumin BSA (Sigma-Aldrich, St. Louis, USA) and antibodies on ice. According to previous studies[18], $CD133^+/CD24^+$ population is recognized as CSCs, whereas $CD133^-/CD24^-$ cells (HCT-116 cells) are regarded as NSCCs. In our experiments, antibodies of CD133 conjugated with phycoerythrin (PE) and CD24 conjugated with allophycocyanin (APC) (Biolegend, San Diego, CA, USA) were added into cell suspension. CD133 and CD24 double-positive cells ($CD133^+/CD24^+$) were gated using control cells that are incubated with IgG_1 isotype controls (APC- and PE-conjugated antibodies, Biolegend, San Diego, CA, USA).

2.2.4 Fabrication of the Single-probe

The fabrication details of the Single-probe have been described in previous studies.[21] Briefly, there are three components in a Single-probe (Figure 2.1A): a needle pulled from dual-bore quartz tubing (outer diameter (OD): 500 μm; inner diameter (ID): 127 μm, Friedrich & Dimmock, Inc., Millville, NJ, USA) using a laser pipet puller (P-2000 micropipette puller, Sutter Instrument, Novato, CA, USA), a fused silica capillary (OD: 105 μm; ID: 40 μm, Polymicro Technologies, Phoenix, AZ, USA), and a nano-ESI emitter produced using the same type of fused silica capillary. A Single-probe is fabricated by embedding a laser-pulled dual-bore quartz needle with a fused silica capillary and a nano-ESI emitter.

2.2.5 The Single-probe SCMS Set-up

CSCs and NSCCs were attached onto the laminin-coated glass slides through over-night culture (Figure 2.1C), and the slides were placed on a motorized XYZ−translation stage system (Figure 2.1D), which was controlled by a LabView software package.[30] A syringe (250 μl; Hamilton Co., Reno, NV, USA) was used to continuously provide the sampling solvent (acetonitrile; Sigma-Aldrich St. Louis, MO, USA), and a stable liquid junction was formed at the Single-probe tip to extract cellular contents during the experiment. Using a microscope as a guide, a cell of interest was selected by controlling the stage system, and the selected cell was penetrated by lifting the Z-stage (Figure 2.1B). Cellular components were extracted by sampling solvent at the Single-probe tip, withdrawn towards the nano-ESI emitter through a self-aspiration process, and ionized for analysis using a Thermo LTQ Orbitrap XL mass spectrometer (Thermo Scientific, Waltham, MA, USA) (Figure 2.1D). MS scans were acquired for individual cells, whereas MS^2 experiments were conducted for ions of interest. MS analysis parameters

are listed as follows: mass resolution 60,000, ionization voltage +4.5 kV (positive ion mode) or -4 kV (negative ion mode), 1 microscan, 100 ms max injection time, and AGC (automatic gain control) on.

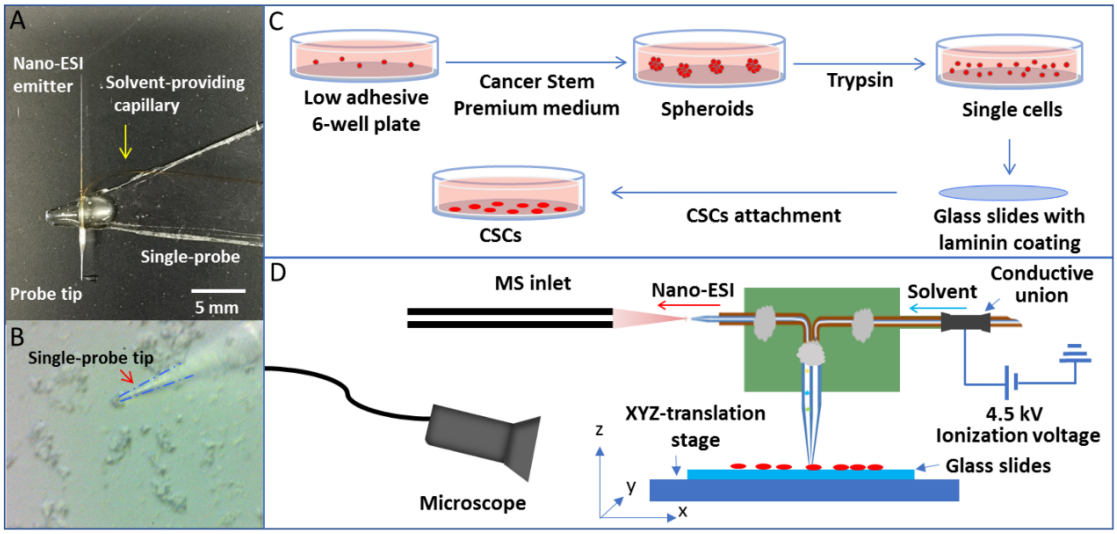

Figure 2.1 The Single-probe SCMS experimental set-up for the analysis of individual CSCs and NSCCs. (A) Photograph of a Single-probe device; (B) Zoomed-in photograph of the Single-probe tip probing a single cancer cell; (C) Workflow of CSC sample preparation; (D) The schematic diagram of the Single-probe SCMS set-up for the analysis of live single cells.

2.2.6 Data analysis

We performed the pretreatment of SCMS data prior to statistical analysis. We exported MS data (m/z values with their relative intensities) as tab-delimited data files using Thermo Xcalibur Qual Browser (Thermo Scientific, Waltham, MA, USA). Only relatively abundant peaks (intensity > 10^3) were exported, whereas background signals, such as peaks from solvent and cell culture medium, were subtracted from MS data.[31]

To minimize the influence induced by fluctuations of ion signals during experiments, we normalized ion intensities to the total ion current (TIC). We used Geena 2 online software tool (http://bioinformatics.hsanmartino.it/geena2/) to preform peak alignment. The pretreated data were subjected to Levene's test to assess the equality of variance of data, and Student's *t*-test (for data with equal variance) or Welch's *t*-test (for data with unequal variance) was then applied to obtain ions with significantly different abundance between two groups ($p < 0.05$). Metaboanalyst 4.0 (http://www.metaboanalyst.ca/) was used to conduct Partial Least Squares Discriminant Analysis (PLS-DA) to illustrate the overall differences of metabolomics profiles between CSCs and NSCCs. Finally we use online database METLIN (https://metlin.scripps.edu/metabo_batch.php) and human metabolome database (HMDB; http://www.hmdb.ca) to tentatively label all ions based on their accurate m/z values, whereas more confident identification of ions of interest was proposed based on tandem MS measurements. It is worth noting that, due to the lack of separation of cellular contents in the real-time SCMS measurement, we cannot completely exclude the coexistence of isomers producing common fragment ions in tandem MS.

2.3 Results and Discussion

2.3.1 Metabolic profiles of CSCs and NSCCs are significantly different

We used florescence-activated cell sorting (FACS) to isolate $CD133^+/CD24^+$ population from HCT-116 CSCs [18] prior to SCMS experiments, and utilized the regular HCT-116 cells as NSCCs for comparison studies. For SCMS experiments, CSCs and NSCCs were attached onto the laminin-coated glass sides through over-night culture

(Figure 2.1C), and the slides were placed on a motorized XYZ−translation stage system (Figure 2.1D). Using a microscope as a guide, a cell of interest was selected by controlling the stage system. The selected cell was penetrated by the Single-probe (tip size < 10 μm) for sampling of cellular contents followed by real-time MS analysis (Figures 2.1A and 2.1B). To obtain a broader coverage of cellular metabolites, we measured 60 and 40 cells from each group in the positive and negative ion modes, respectively. Our experimental results indicate that the positive ion mode is suitable for MS detection of the majority of cellular metabolites (e.g., lipids), whereas the negative ion mode is desired for certain organic acids (e.g., TCA cycle metabolites and fatty acids). Mass spectrum patterns obtained from CSCs and NSCCs are distinct, and PLS-DA results confirmed that their overall metabolomic features are significantly different as shown in Figure 2.2 ($p = 0.0015$ from the permutation test).

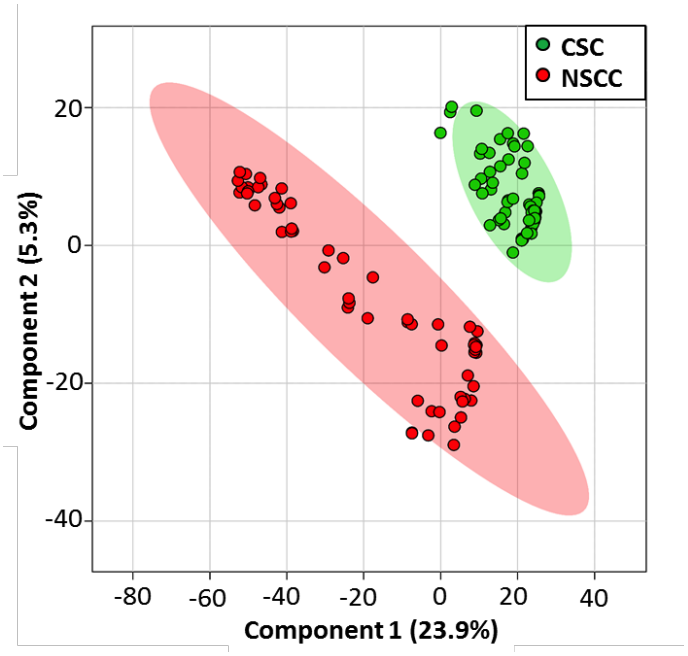

Figure 2.2 Results from Partial Least Squares Discriminant Analysis (PLS-DA) of SCMS data illustrate the overall difference of metabolites between CSCs and NSCC.

2.3.2 CSCs have higher abundances of metabolites of TCA cycle than NSCCs

We further investigated the specific metabolites that are different between CSCs and NSCCs. TCA cycle, a step in the aerobic oxidative respiration, plays a critical role in the energetic metabolism in normal mammalian cells (Figure 2.3A). We found that multiple metabolites of the TCA cycle, including malic acid, citric acid, succinic acid, and pyruvate, have significantly higher abundances in CSCs than NSCCs (Figures 2.3B). However, other relevant metabolites, including fumaric acid, α-ketoglutarate, and oxoglutaric acid, are present with comparable abundances (Figure 2.3B). All these metabolites of the TCA cycle were identified by MS^2 experiments at the single cell level.

Our results demonstrate that the activities of TCA cycle are different between colonic CSCs and NSCCs at the single cell level. According to previous studies, cancer cells have a distinct energy metabolism pathway compared to normal cells.[32] Aerobic glycolysis is the major energetic source for most of cancer cells even under sufficient oxygen environment (known as "the Warburg effect"), while normal cells rely on the mitochondrial oxidative phosphorylation (OXPHOS) to provide most energy.[33] The TCA cycle, a cellular process supplying the material to OXPHOS,[34] is downregulated in cancer cells. Studies based on bulk analysis (LC-MS) found that intermediates of the TCA cycle are decreased in human ovarian cancer and cervical cancer cells[35], whereas ovarian and cervical squamous CSCs obtain energy through OXPHOS by activating the TCA cycle.[36] In fact, CSCs can utilize different energy metabolism pathways based on their phenotypes,[36, 37] and they maintain the homeostasis by switching their energy metabolism pathways between OXPHOS and glycolysis.[38] In the present study, we identified multiple intermediates of the TCA cycle (including pyruvate, citric acid, malic

acid, and succinic acid), and demonstrated they are significantly upregulated in CSCs than NSCCs. Our results may suggest that the dominant energy metabolism pathways are different for HCT-116 CSCs and NSCCs under our experimental conditions (Figures 2.3A and 3B).

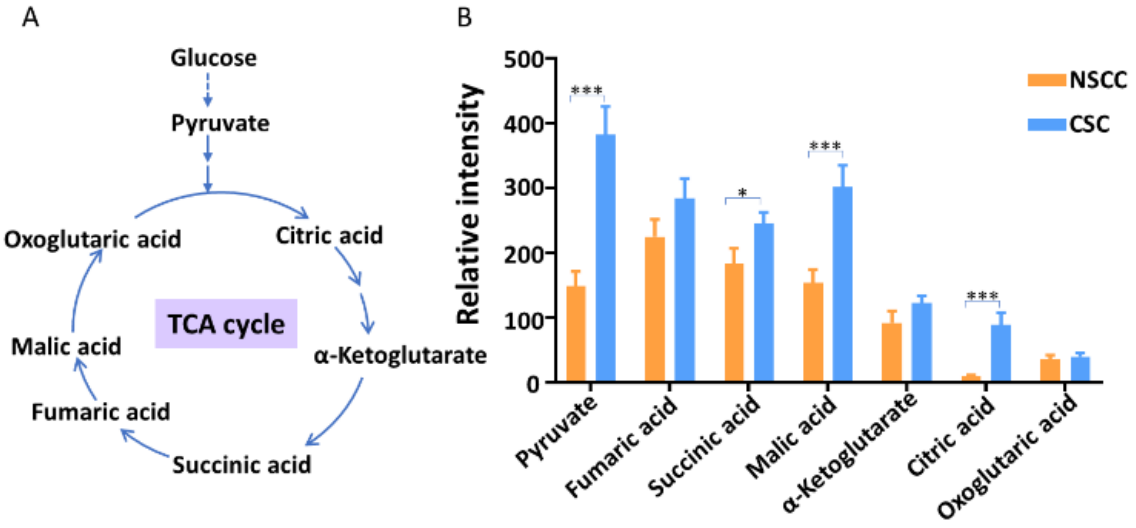

Figure 2.3 Comparison of abundances of metabolites in TCA cycle between CSCs and NSCCs (negative ion mode, n = 40 in each group). (A) TCA cycle pathway and the associated key metabolites. (B) Metabolites present at significantly higher levels in CSCs than in NSCCs are labeled. All metabolites were identified from MS^2 and MS^2 experiments at single cell level. (From *t*-test: *p < 0.05; **p < 0.001)

2.3.3 CSCs have higher levels of unsaturated lipids than NSCCs

In addition to the detection of small metabolites such as species involved in the TCA cycle, we observed a large number of lipids in both CSCs and NSCCs. Our experimental results indicate the levels of 13 unsaturated lipids are significantly higher in CSCs compared to NSCCs (in positive ion mode, Figure 2.4A). All of these lipids were

confirmed through MS^2 analysis from single cells. As the building blocks of lipids, fatty acids were also detected in both CSCs and NSCCs in the negative ion mode. The ratios of monounsaturated fatty acids (MUFAs) to saturated fatty acids (SFAs), e.g., palmitic acid/palmitoleic acid (C16:0/C16:1) and stearic acid/oleic acid (C18:0/C18:1), are significantly higher in CSCs compared to NSCCs (Figures 2.4B and 2.4C).

We observed drastically different levels of unsaturated lipids and fatty acids between CSCs and NSCCs through SCMS analysis (Figures 2.4A and 2.4B). Relatively higher abundances of unsaturated lipids in CSCs are likely related to the formation of lipid droplets.[39] Previous studies found that in CSCs *de novo* fatty acid synthesis pathway is upregulated, and lipids storage compartment, lipid droplets (LDs), are accumulated.[40] Increasing amount of evidence indicates that lipid molecules and lipid droplets are essential for the stemness and tumorigenicity of CSCs.[40] For example, a recent study reported a higher degree of LDs accumulation in different patient-derived colon CSCs than normal cancer cells using hyperspectral-stimulated Raman spectroscopy and LC/MS, and relatively more abundant LDs are positively correlated with the tumorigenic potential of CSCs.[41]

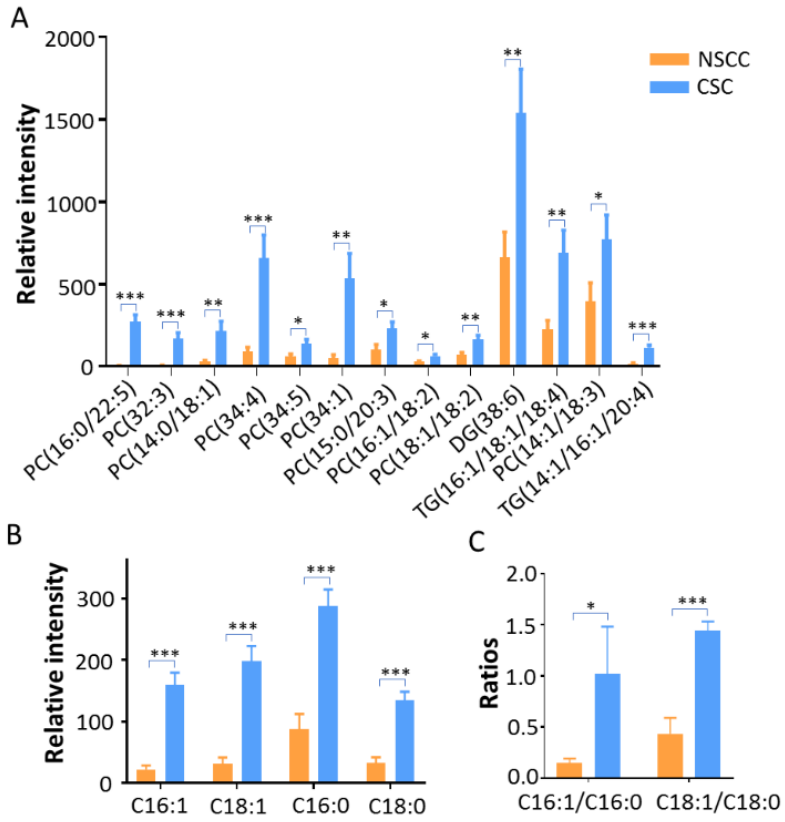

Figure 2.4 Saturation levels of lipids and fatty acids in CSCs and NSCCs. All species were identified from MS^2 experiments at single cell level. (A) CSCs contain relatively higher abundances of unsaturated lipids compared to NSCCs (positive ion mode, n = 60 in each group). (B) Relative abundances of fatty acids (C16:0, C16:1, C18:0, and C18:1) detected in CSCs and NSCCs (negative ion mode, n = 40 in each group). (C) Ratios of unsaturated fatty acid (UFA) to saturated fatty acid (SFA) in CSCs and NSCCs. (From *t*-test: *$p < 0.05$; **$p < 0.01$; ***$p < 0.001$).

Interestingly, correlations between metabolites of TCA cycle and unsaturated lipids were also discovered in CSCs. We conducted correlation analysis of species measured from same cells, and found positive correlations (correlation coefficinet > 0.6, $p < 0.01$) between pyruvate and each of these fatty acids: C16:0, C16:1, C18:0, and C18:1.

Because pyruvate can be converted into acetyl-CoA, which is directly involved in the sythesis of fatty acids, by pyruvate dehydrogenase,[42] higher levels of pyruvate likely lead to more production of fatty acids, including unsaturated fatty acids.

In addition to those species reported in previous LC-MS studies (i.e., palmitic (C16:0), palmitoleic (C16:1), stearic (C18:0), oleic (C18:1), linoleic (C18:2), arachidonic (C20:4), and docosahexaenoic acid (C22:6)), we discovered additional unsaturated lipids with drastically different abundances between CSCs and NSCCs. For example, phosphatidylcholines (PC(16:0/22:5), PC(32:3), PC(14:0/18:1), PC(34:4), PC(34:5), PC(34:1), PC(15:0/20:3), PC(16:1/18:2), PC(18:1/18:2), PC(14:1/18:3)), diglyceride (DG(38:6)), and triglycerides (TG(16:1/18:1/18:4), TG(14:1/16:1/20:4)) are present at significantly higher abundances in CSCs than NSCCs (Figures 2.4A and 2.4B). Higher levels of unsaturated lipids and fatty acids are mainly produced by stearoyl-CoA desaturase-1 (SCD1) enzyme, and they are directly associated with the stemness of CSCs.[28]

2.3.4 Inhibition of SCD1, NF-κB, and ALDH1A1 reduces the stemness of CSCs

Previous studies indicate that SCD1, nuclear factor κB (NF-κB), and aldehyde dehydrogenases (ALDH1A1) play critical roles in maintaining the abundances of unsaturated lipids in CSCs.[28] We conducted SCMS experiments to investigate their functions regulating the saturation level of lipids and fatty acids, and the consequential influence on the stemness of CSCs. Overall, PLS-DA indicates that metabolomic profiles of CSCs were significantly altered ($p < 0.05$ from permutatoin test) by these inhibitors. Because inhibitors used in our experiments can induce cell apoptosis[43-45], it is unclear

if changes of cell metabolites are related to cell apoptosis, although cells are still alive prior to the SCMS measurements.

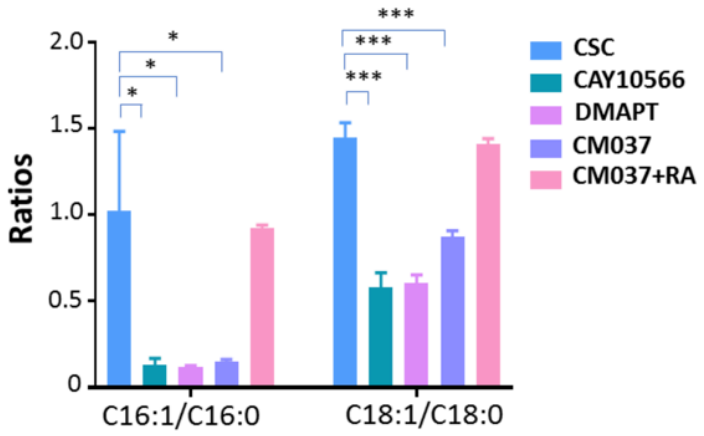

Figure 2.5 Ratios of monounsaturated fatty acid (MUFA) to its saturated fatty acid (SFA) in CSCs under different treatment conditions (negative ion mode, n = 40 in each group). (From *t*-test: *p < 0.05; ***p < 0.001).

Stearoyl-CoA desaturase-1 (SCD1) is one of the major lipid desaturases catalyzing the conversion of SFAs to MUFAs in mammalian cells, and the major products of SCD1 are palmitoleic (C16:1) and oleic acid (C18:1).[46] A recent study shows that SCD1 is a key factor mediating the expression of desaturated lipids and fatty acids in ovarian cancer cells.[28] To determine whether SCD1 plays a role in regulating the expression of unsaturation lipids and fatty acids in colorectal CSCs, we treated CSCs with CAY10566, a small molecule inhibitor of SCD1, to suppress the activity of SCD1.[47] As shown in Figures 2.5 and 2.6A, the ratios of MUFAs to SFAs (C16:1/C16:0 and C18:1/C18:0) and the abundances of numerous unsaturated lipids are drastically decreased in CSCs treated with CAY10566, indicating the expression of unsaturated lipids and fatty acids can be regulated by SCD1. Interestingly, PC(16:0/22:5) exhibits an opposite trend: its abundance

is increased after CAY10566 treatment. A reasonable explanation follows: inhibiting SCD1 can reduce the synthesis of C16:1 from C16:0, result in the accumulation of C16:0, and further increase the synthesis of lipids using C16:0, such as PC(16:0/22:5), through competative pathways. Moreover, we found that CSCs treated with CAY10566 possess significantly lower tendencies to form spheroids during cell culture. Because forming spheroids in serum-free medium is an important feature of CSCs[48], our results suggest CAY10566 impacts the formation of speroids and reduces the stemness of CSCs.[28] We conclude that levels of unsaturated lipids and fatty acids can be regulated by SCD1, and their abundances are important for the maintenance of the stemness of CSCs, which is consistent with the previous studies.[28]

In addition to directly suppressing the activity of SCD-1, we investigated the influence of nuclear factor κB (NF-κB) and aldehyde dehydrogenases (ALDH1A1), which are crucial for regulating SCD1 activities and maintaining the stemness of ovarian CSCs[28], on metabolites of CSCs. NF-κB is a protein complex that is essential for DNA transcription, cytokine production, and cell survival.[49, 50] NF-kB is extensively tied to cancer biology, and tightly related to cancer stem cell.[51, 52] Particularly, NF-κB signaling is highly sensitive to the inhibition of desaturase, which is related to the stemness of CSCs.[28] ALDH1A1 is one of the major enzymes producing retinoic acid (RA), which is also a well-known biomarker of colon CSCs.[53] To investigate whether NF-κB and ALDH1A1 are associated with lipid saturation and the stemness of CSCs, we treated CSCs with inhibitors of NF-κB and

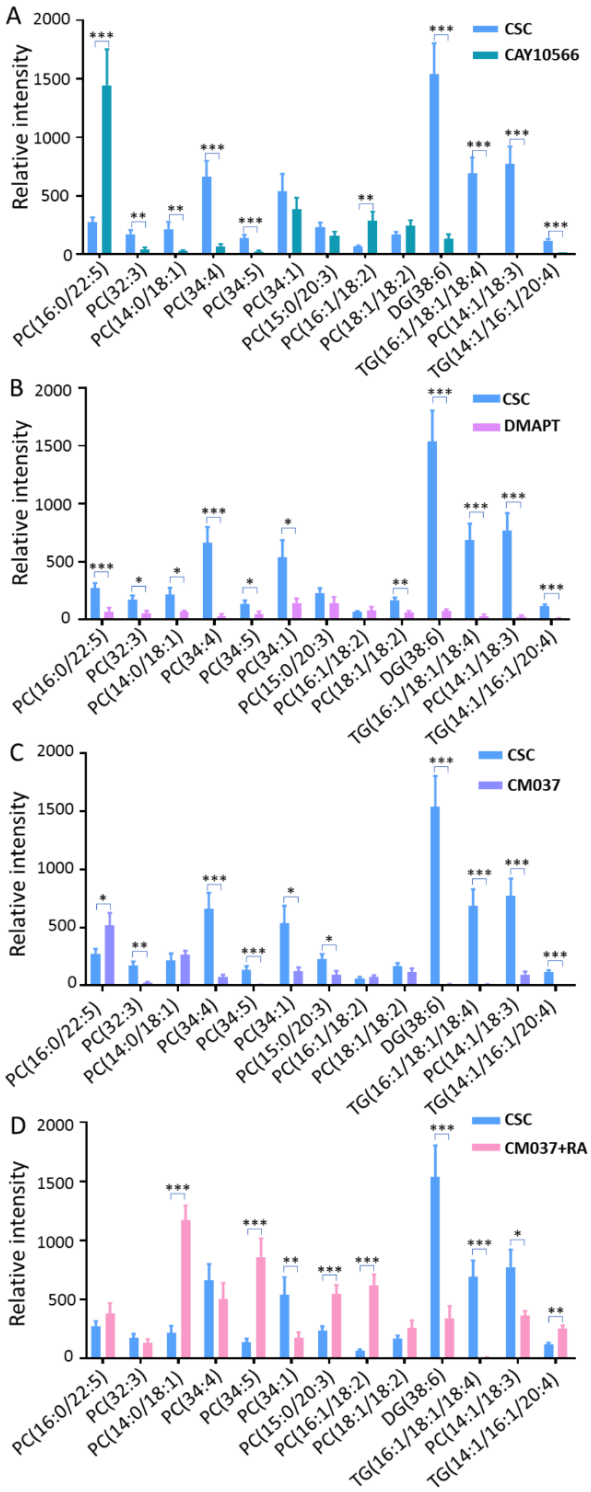

Figure 2.6 The investigation of roles of SCD1, NF-κB, and ALDH1A1 in regulating the saturation levels of lipids and fatty acids in CSCs (positive ion mode, n = 60 in each group). Expression of unsaturated lipids is decreased by inhibitors of (A) SCD1

(CAY10566), (B) NF-κB (DMART), and (C) ALDH1A1 (CM037). (D) Retinoic acid (RA) rescues the inhibition by CM037 and results in increased levels of unsaturated lipids. (From *t*-test: *p < 0.05; **p < 0.01; ***p < 0.001).

ALDH1A1 (i.e., dimethylaminoparthenolide (DMAPT) and CM037[29, 54], respectively). Experimental results show that these two inhibitors significantly suppressed the expression of unsaturated lipids and fatty acids (Figures 2.5, 2.6B, and 2.6C), and drastically hindered the formation of CSC spheroids, i.e., reduced stemness of CSCs. We conclude that the NF-κB and ALDH1A1 affect the growth of CSCs.

Because RA is an important product of ALDH1A1[55], inhibiting the activity of ALDH1A1 will apparently lead to a reduced production of RA. This consequence is likely related to the altered properties of CSCs such as the reduced stemness. It is reasonable to hypothesize that increasing RA supply during the cell culture will likely alleviate the inhibition by CM037. We then treated CM037-inhibited cells with RA, and observed that the levels of unsaturated fatty acids and lipids were significantly restored in CM037-inhibited CSCs (Figures 2.5 and 2.6D). Taken together, we demonstrate SCD1, NF-κB, and ALDH1A1 are important regulating factors in CSCs, and they are responsible for the expression of higher levels of unsaturated lipids and fatty acids to maintain the stemness of CSCs.

2.2.5 Activities of SCD1, NF-κB, and ALDH1A1 regulate the stemness of CSCs.

As summarized in Figure 2.7, we demonstrate that SCD1, NF-κB, and ALDH1A1 participate in the regulation of the saturation levels of lipids and fatty acids, and further affect the stemness of CSCs. First, we found SCD1 inhibitor (CAY10566) can reduce the

levels of unsaturated lipids in CSCs and inhibit the formation of CSC spheroids (Figures 2.6A), indicating that SCD1 activity is important for the stemness and tumorigenicity of CSCs. Second, we investigated the influence of inhibiting ALDH1A1, which is a known biomarker of CSCs.[56] ALDH1A1 converts retinaldehyde to RA, which functions as a ligand of transcription factor, i.e., retinoic acid receptor (RAR). RA regulates the activation of numerous nuclear transcription factors, and plays a central role in regulating lipid metabolism.[57] Treatment using ALDH1A1 inhibitor (CM037) significantly decreased levels of unsaturated lipids and suppressed spheroid forming of CSCs (Figures 2.6C). Our results indicate that ALDH1A1 is a mediating factor of the stemness and tumorigenicity of CSCs, which is consistent with a previous study of ovarian CSCs.[28] Last, we proved that the function of NF-κB is cruicial for the maintenance of the stemness of CSCs. NF-κB signaling pathway is responsible for maintaining the stemness of CSCs[58], and it is a crucial regulator of inflammation and immune responses as well as multiple cancer-associated processes such as proliferation, apoptosis, angiogenesis, and metastasis.[59] The hyper activation of NF-κB signaling in CSCs provides a proper niche for the survival and expansion of CSCs, and contribute to their capabilities of invasion, metastatic, and self-renewal.[58, 60, 61] In this study, we found that, similar to the treatment effects of using inhibitors of SCD1 and ALD1H1, inhibiting the activity of NF-κB using DMAPT changed the metabolomic profiles, as well as decreased the level of unsaturated lipid and the spheroid formation of colon CSCs (Figures 2.6B), indicating this transcription factor may important for maintaining stemness of CSCs.

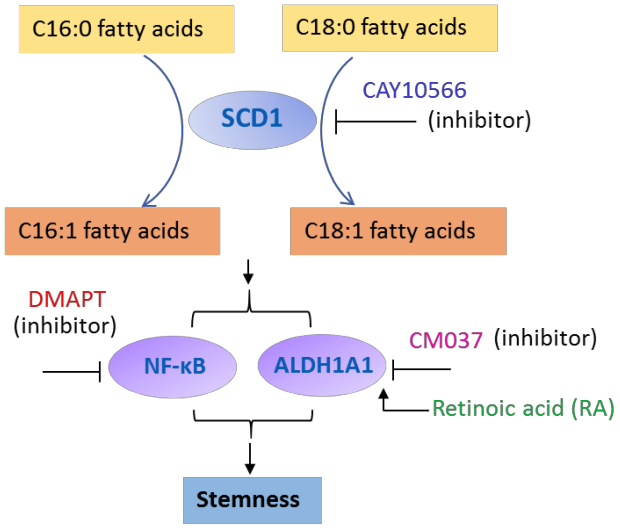

Figure 2.7 Potential mechanisms showing the regulation of unsaturated lipids and fatty acids by SCD1, NF-κB, and ALDH1A1, and their relationship to the stemness of CSCs.

2.4 Conclusions

In this study we successfully applied the SCMS technique to detecting a number of key metabolic features of colon CSCs, including higher levels of metabolites in the TCA cycle and unsaturated fatty acids and lipids. The high abundances of unsaturated lipids and fatty acids are the metabolic features of CSCs. SCD1 is a key factor mediating the expression of unsaturated fatty acids and lipids such as palmitoleic and oleic acid. Inhibiting the activity of SCD1 could significantly suppress the expression of unsaturated fatty acids and lipids. In addition, NF-κB and ALDH1A1 play critical roles in maintaining stemness of CSCs, and also regulate the expression of unsaturated lipids. Together, we demonstrate that SCD1, NF-κB, and ALDH1A1 regulate the metabolism of unsaturated lipids and fatty acids, which are associated with the stemness of CSCs, at single cell level. Our current study indicates that the Single-probe SCMS technique can be applied to analyze live single CSCs, and our findings can promote the understanding

of the biological characters of CSCs. Moreover, because metabolic features and regulatory factors detected here are deeply associated with the stemness and tumorigenicity of colon CSCs, they can be potentially used as the functional biomarkers and new therapeutic targets for colon CSCs.

2.5 References

[1] L.A. Torre, F. Bray, R.L. Siegel, J. Ferlay, J. Lortet-Tieulent, A. Jemal, Global cancer statistics, 2012, CA: Cancer J. Clin, 65 (2015) 87-108.

[2] G. Housman, S. Byler, S. Heerboth, K. Lapinska, M. Longacre, N. Snyder, S. Sarkar, Drug resistance in cancer: an overview, Cancers, 6 (2014) 1769-1792.

[3] T. Reya, S.J. Morrison, M.F. Clarke, I.L. Weissman, Stem cells, cancer, and cancer stem cells, nature, 414 (2001) 105.

[4] D.A. Lawson, N.R. Bhakta, K. Kessenbrock, K.D. Prummel, Y. Yu, K. Takai, A. Zhou, H. Eyob, S. Balakrishnan, C.-Y. Wang, Single-cell analysis reveals a stem-cell program in human metastatic breast cancer cells, Nature, 526 (2015) 131.

[5] D.G. Tang, Understanding cancer stem cell heterogeneity and plasticity, Cell Res., 22 (2012) 457.

[6] B. Bao, A. Ahmad, A.S. Azmi, S. Ali, F.H. Sarkar, Overview of cancer stem cells (CSCs) and mechanisms of their regulation: implications for cancer therapy, Curr Protoc Pharmacol, 61 (2013) 14.25. 11-14.25. 14.

[7] W.B. Dunn, A. Erban, R.J. Weber, D.J. Creek, M. Brown, R. Breitling, T. Hankemeier, R. Goodacre, S. Neumann, J. Kopka, Mass appeal: metabolite identification in mass spectrometry-focused untargeted metabolomics, Metabolomics, 9 (2013) 44-66.

[8] P. Hu, W. Zhang, H. Xin, G. Deng, Single cell isolation and analysis, Front Cell Dev Biol, 4 (2016) 116.

[9] W. Gruber, T. Scheidt, F. Aberger, C.G. Huber, Understanding cell signaling in cancer stem cells for targeted therapy–can phosphoproteomics help to reveal the secrets?, Cell Commun. Signal, 15 (2017) 12.

[10] H.M. Davey, D.B. Kell, Flow cytometry and cell sorting of heterogeneous microbial populations: the importance of single-cell analyses, Microbiol Rev, 60 (1996) 641-696.

[11] K.A. Vermeersch, M.P. Styczynski, Applications of metabolomics in cancer research, J. Carcinog., 12 (2013).

[12] T.M. O'Connell, Recent advances in metabolomics in oncology, Bioanalysis, 4 (2012) 431-451.

[13] M. Waki, Y. Ide, I. Ishizaki, Y. Nagata, N. Masaki, E. Sugiyama, N. Kurabe, D. Nicolaescu, F. Yamazaki, T. Hayasaka, Single-cell time-of-flight secondary ion mass spectrometry reveals that human breast cancer stem cells have significantly lower content of palmitoleic acid compared to their counterpart non-stem cancer cells, Biochimie, 107 (2014) 73-77.

[14] B.M. Turner, Epigenetic responses to environmental change and their evolutionary implications, Philos. Trans. Royal Soc. B, 364 (2009) 3403-3418.

[15] S.G. Villas-Bôas, J. Højer-Pedersen, M. Åkesson, J. Smedsgaard, J. Nielsen, Global metabolite analysis of yeast: evaluation of sample preparation methods, Yeast, 22 (2005) 1155-1169.

[16] M. Peiris-Pagès, U.E. Martinez-Outschoorn, R.G. Pestell, F. Sotgia, M.P. Lisanti, Cancer stem cell metabolism, Breast Cancer Res., 18 (2016) 55.

[17] Y. Zhou, Y. Wang, X. Ju, J. Lan, H. Zou, S. Li, Y. Qi, W. Jia, J. Hu, W. Liang, Clinicopathological significance of ALDH1A1 in lung, colorectal, and breast cancers: a meta-analysis, Biomark. Med, 9 (2015) 777-790.

[18] R.C. Langan, J.E. Mullinax, M.T. Raiji, T. Upham, T. Summers, A. Stojadinovic, I. Avital, Colorectal cancer biomarkers and the potential role of cancer stem cells, J. Cancer, 4 (2013) 241.

[19] J.E. Visvader, G.J. Lindeman, Cancer stem cells in solid tumours: accumulating evidence and unresolved questions, Nat. Rev. Cancer, 8 (2008) 755.

[20] A. Mitra, L. Mishra, S. Li, EMT, CTCs and CSCs in tumor relapse and drug-resistance, Oncotarget, 6 (2015) 10697.

[21] N. Pan, W. Rao, N.R. Kothapalli, R. Liu, A.W. Burgett, Z. Yang, The single-probe: a miniaturized multifunctional device for single cell mass spectrometry analysis, Anal. Chem., 86 (2014) 9376-9380.

[22] N. Pan, W. Rao, R. Liu, N. Kothapalli, A. Burgett, Z. Yang, The single-probe mass spectrometry for single cell analysis and biological tissue imaging, Planta Medica, 81 (2015) IL55.

[23] N. Pan, W. Rao, S.J. Standke, Z. Yang, Using Dicationic Ion-Pairing Compounds To Enhance the Single Cell Mass Spectrometry Analysis Using the Single-Probe: A Microscale Sampling and Ionization Device, Anal. Chem., 88 (2016) 6812.

[24] M. Sun, Z. Yang, B. Wawrik, Metabolomic Fingerprints of Individual Algal Cells Using the Single-Probe Mass Spectrometry Technique, Front. Plant Sci., 9 (2018).

[25] W. Rao, N. Pan, X. Tian, Z. Yang, High-resolution ambient MS imaging of negative ions in positive ion mode: using dicationic reagents with the single-probe, J. Am. Soc. Mass Spectrom., 27 (2016) 124-134.

[26] M. Sun, X. Tian, Z. Yang, Microscale Mass Spectrometry Analysis of Extracellular Metabolites in Live Multicellular Tumor Spheroids, Anal. Chem., (2017).

[27] Z.F. Bielecka, K. Maliszewska-Olejniczak, I.J. Safir, C. Szczylik, A.M. Czarnecka, Three-dimensional cell culture model utilization in cancer stem cell research, Biological Reviews, 92 (2017) 1505-1520.

[28] J. Li, S. Condello, J. Thomes-Pepin, X. Ma, Y. Xia, T.D. Hurley, D. Matei, J.-X. Cheng, Lipid desaturation is a metabolic marker and therapeutic target of ovarian cancer stem cells, Cell stem cell, 20 (2017) 303-314. e305.

[29] S. Condello, C.A. Morgan, S. Nagdas, L. Cao, J. Turek, T.D. Hurley, D. Matei, β-Catenin-regulated ALDH1A1 is a target in ovarian cancer spheroids, Oncogene, 34 (2015) 2297.

[30] I. Lanekoff, B.S. Heath, A. Liyu, M. Thomas, J.P. Carson, J. Laskin, Automated platform for high-resolution tissue imaging using nanospray desorption electrospray ionization mass spectrometry, Anal. Chem., 84 (2012) 8351-8356.

[31] R. Liu, N. Pan, Y. Zhu, Z. Yang, T-Probe: An Integrated Microscale Device for Online In Situ Single Cell Analysis and Metabolic Profiling Using Mass Spectrometry, Anal. Chem., 90 (2018) 11078-11085.

[32] C.V. Dang, Rethinking the Warburg effect with Myc micromanaging glutamine metabolism, Cancer Res., 70 (2010) 859-862.

[33] P.P. Hsu, D.M. Sabatini, Cancer cell metabolism: Warburg and beyond, Cell, 134 (2008) 703-707.

[34] M. Saraste, Oxidative phosphorylation at the fin de siecle, Science, 283 (1999) 1488-1493.

[35] M. Sato, K. Kawana, K. Adachi, A. Fujimoto, M. Yoshida, H. Nakamura, H. Nishida, T. Inoue, A. Taguchi, J. Takahashi, Spheroid cancer stem cells display

reprogrammed metabolism and obtain energy by actively running the tricarboxylic acid (TCA) cycle, Oncotarget, 7 (2016) 33297.

[36] P. Sancho, D. Barneda, C. Heeschen, Hallmarks of cancer stem cell metabolism, Br. J. Cancer, 114 (2016) 1305.

[37] X.Q. Ye, Q. Li, G.H. Wang, F.F. Sun, G.J. Huang, X.W. Bian, S.C. Yu, G.S. Qian, Mitochondrial and energy metabolism-related properties as novel indicators of lung cancer stem cells, Int. J. Cancer, 129 (2011) 820-831.

[38] V. Snyder, T.C. Reed-Newman, L. Arnold, S.M. Thomas, S. Anant, Cancer stem cell metabolism and potential therapeutic targets, Front Oncol., 8 (2018) 203.

[39] A. Mukherjee, H.A. Kenny, E. Lengyel, Unsaturated fatty acids maintain cancer cell stemness, Cell stem cell, 20 (2017) 291-292.

[40] L. Tirinato, F. Pagliari, T. Limongi, M. Marini, A. Falqui, J. Seco, P. Candeloro, C. Liberale, E. Di Fabrizio, An overview of lipid droplets in cancer and cancer stem cells, Stem Cells Int, 2017 (2017).

[41] Y. Gökmen-Polar, H. Nakshatri, S. Badve, Biomarkers for breast cancer stem cells: the challenges ahead, Biomark. Med, 5 (2011) 661-671.

[42] F. Pietrocola, L. Galluzzi, J.M. Bravo-San Pedro, F. Madeo, G. Kroemer, Acetyl coenzyme A: a central metabolite and second messenger, Cell Metab., 21 (2015) 805-821.

[43] L. Chen, J. Ren, L. Yang, Y. Li, J. Fu, Y. Li, Y. Tian, F. Qiu, Z. Liu, Y. Qiu, Stearoyl-CoA desaturase-1 mediated cell apoptosis in colorectal cancer by promoting ceramide synthesis, Sci. Rep., 6 (2016) 19665.

[44] P.V. Deraska, C. O'Leary, H.D. Reavis, S. Labe, T.-K. Dinh, J.-B. Lazaro, C. Sweeney, A.D. D'Andrea, D. Kozono, NF-κB inhibition by dimethylaminoparthenolide

radiosensitizes non-small-cell lung carcinoma by blocking DNA double-strand break repair, Cell Death Discov. , 4 (2018) 10.

[45] H. Nakshatri, H. Appaiah, M. Anjanappa, D. Gilley, H. Tanaka, S. Badve, P. Crooks, W. Mathews, C. Sweeney, P. Bhat-Nakshatri, NF-κB-dependent and-independent epigenetic modulation using the novel anti-cancer agent DMAPT, Cell Death Dis., 6 (2015) e1608.

[46] H. Matsui, T. Yokoyama, K. Sekiguchi, D. Iijima, H. Sunaga, M. Maniwa, M. Ueno, T. Iso, M. Arai, M. Kurabayashi, Stearoyl-CoA desaturase-1 (SCD1) augments saturated fatty acid-induced lipid accumulation and inhibits apoptosis in cardiac myocytes, PLoS One, 7 (2012) e33283.

[47] F. Mohammadzadeh, G. Mosayebi, V. Montazeri, M. Darabi, S. Fayezi, M. Shaaker, M. Rahmati, B. Baradaran, A. Mehdizadeh, M. Darabi, Fatty acid composition of tissue cultured breast carcinoma and the effect of stearoyl-CoA desaturase 1 inhibition, Breast Cancer Res., 17 (2014) 136-142.

[48] Z.F. Bielecka, K. Maliszewska-Olejniczak, I.J. Safir, C. Szczylik, A.M. Czarnecka, Three-dimensional cell culture model utilization in cancer stem cell research, BIOL REV, 92 (2017) 1505-1520.

[49] A.A. Beg, D. Baltimore, An essential role for NF-κB in preventing TNF-α-induced cell death, Science, 274 (1996) 782-784.

[50] D. Jia, W. Yang, L. Li, H. Liu, Y. Tan, S. Ooi, L. Chi, L.G. Filion, D. Figeys, L. Wang, β-Catenin and NF-κB co-activation triggered by TLR3 stimulation facilitates stem cell-like phenotypes in breast cancer, Cell Death Differ, 22 (2015) 298.

[51] C. Gonzalez-Torres, J. Gaytan-Cervantes, K. Vazquez-Santillan, E.A. Mandujano-Tinoco, G. Ceballos-Cancino, A. Garcia-Venzor, C. Zampedri, P. Sanchez-Maldonado, R. Mojica-Espinosa, L.E. Jimenez-Hernandez, NF-κB Participates in the Stem Cell Phenotype of Ovarian Cancer Cells, Arch Med Res., 48 (2017) 343-351.

[52] N. Zakaria, N.M. Yusoff, Z. Zakaria, D. Widera, B.H. Yahaya, Inhibition of NF-κB Signaling Reduces the Stemness Characteristics of Lung Cancer Stem Cells, Front Oncol., 8 (2018).

[53] R.C. Langan, J.E. Mullinax, M.T. Raiji, T. Upham, T. Summers, A. Stojadinovic, I. Avital, Colorectal cancer biomarkers and the potential role of cancer stem cells, Cancer, 4 (2013) 241.

[54] R. Shanmugam, P. Kusumanchi, H. Appaiah, L. Cheng, P. Crooks, S. Neelakantan, T. Peat, J. Klaunig, W. Matthews, H. Nakshatri, A water soluble parthenolide analog suppresses in vivo tumor growth of two tobacco-associated cancers, lung and bladder cancer, by targeting NF-κB and generating reactive oxygen species, Int. J. Cancer, 128 (2011) 2481-2494.

[55] K. Phoenix, X. Hong, S. Tannenbaum, K. Claffey, Expression of the Cancer Stem Cell Marker ALDH1A1 in Primary Breast Cancer: A Mechanism for Chemotherapy Resistance, AACR, 2009.

[56] H. Tomita, K. Tanaka, T. Tanaka, A. Hara, Aldehyde dehydrogenase 1A1 in stem cells and cancer, Oncotarget, 7 (2016) 11018.

[57] R. Zhang, Y. Wang, R. Li, G. Chen, Transcriptional factors mediating retinoic acid signals in the control of energy metabolism, Int J Mol Sci, 16 (2015) 14210-14244.

[58] A.L. Rinkenbaugh, A.S. Baldwin, The NF-κB pathway and cancer stem cells, Cells, 5 (2016) 16.

[59] Y. Xia, S. Shen, I.M. Verma, NF-κB, an active player in human cancers, Cancer Immunol Res., 2 (2014) 823-830.

[60] J. Zhou, H. Zhang, P. Gu, J. Bai, J.B. Margolick, Y. Zhang, NF-κB pathway inhibitors preferentially inhibit breast cancer stem-like cells, Breast Cancer Res. Treat., 111 (2008) 419-427.

[61] C. Gonzalez-Torres, J. Gaytan-Cervantes, K. Vazquez-Santillan, E.A. Mandujano-Tinoco, G. Ceballos-Cancino, A. Garcia-Venzor, C. Zampedri, P. Sanchez-Maldonado, R. Mojica-Espinosa, L.E. Jimenez-Hernandez, NF-κB Participates in the Stem Cell Phenotype of Ovarian Cancer Cells, Arch Med Res, 48 (2017) 343-351.

Chapter 3. Metabolomic Fingerprints of Individual Algae Cells using the Single-Probe Mass Spectrometry Technique

3.1 Introduction

Globally, marine phytoplankton contribute ca. 45 petagrams carbon per annum to net primary production (NPP) [1]. Phytoplankton are thus important drivers of several global biogeochemical cycles, notably of elements that are components of cellular biomass, including carbon (C), nitrogen (N), phosphorus (P), silicate (Si), and others. The abundance of phytoplankton in marine systems is shaped by the availability of nutrients as well as physical oceanic processes. Typically, phytoplankton biomass can be broadly approximated from environmental variables, such as nutrient concentrations, sea surface temperature, and solar irradiance [1, 2]. However, at a more granular level, such as the cellular response of individual phytoplankton to dynamic oceanographic conditions, requisite adaptations are often not well understood. In particular, whether phytoplankton are nutrient limited in the environment has long attracted the attention of oceanographers who are trying to understand the controls on NPP, given the large impact that limitation may have on the structure of marine ecosystems.

Historically, both N and P have been understood to, at times, limit productivity in marine systems [3], but other nutrient, such as iron [4, 5], also appear to play an important role. Additionally, phytoplankton can be co-limited by more than one nutrient due to their limited absolute abundance (i.e., kinetic limitations), or the acquisition of one nutrient may be dependent on the concentration of another [6]. Understanding requisite limitations in natural systems is unfortunately not a straightforward matter, given the

restricted methodological options available to researchers. For example, nutrient limitation is frequently invoked via nutrient ratios (Liebig's law of the minimum), yet this ignores that turnover rates can be high in the face of low, but non-limiting ambient concentrations [7, 8]. Similarly, bottle incubations (spiking nutrients) are used to infer nutrient limitation via measurements of cellular activity (e.g., carbon fixation), biomass (e.g., chl *a*), or photosynthetic capacity (F_v/F_m), but interpretation of requisite data can be challenging, given that measurements are made on bulk communities in which individual phytoplankton species may exhibit differential behavior. Changes in elemental uptake ratios (C: P or C: N) have been used to infer nutrient limitation [7, 9], but such analyses suffer from drawbacks similar to those of bottle incubations, in that measurements are conducted on bulk communities.

An alternate avenue has been the development of specific molecular probes for the expression of marker genes. This approach draws on a long tradition of studies that aim to develop molecular targets for specific microbial nutrient cycling activities in the environment [10-12](and many more). For example, the expression of the global nitrogen regulator NtcA in marine cyanobacteria has been used to assess the nutritional status of natural populations of *Synechococcus* [13]. Similarly, the expression of the *nifH* gene is widely distributed in marine systems [14], indicator of cellular alleviation of N limitation in some microbial populations. However, while this approach is powerful, it typically requires a fairly good understanding of the underlying molecular mechanisms and genetic diversity of related genes to allow for the derivation of probes or primers. Other studies have applied less targeted, transcriptomic approaches to detect nutrient limitation in marine phytoplankton [15-17], but analogous studies are more difficult in

diverse natural assemblages for which genetic information is not necessarily available. Given this, our understanding of the degree and severity of nutrient limitation in the marine environment, especially at the induvial species and cellular level, remains poorly constrained.

Recently, several approaches have been developed to perform the single cell analysis. These include fluorescence, capillary electrophoresis, and mass spectrometry (MS)[18-22]. Here we report the application of a novel technology that allows for the analysis of the metabolome of single phytoplankton cells to assess their physiological status. The approach utilizes the 'Single-probe', a micro-scale sampling and ionization device, that is coupled to an XYZ-stage to directly insert into single phytoplankton cells to extract cellular metabolites for real-time MS analysis [23, 24]. Our aims were threefold. First, we intended to establish a proof of concept, i.e. demonstrate that metabolome data could be generated for single marine phytoplankton cells. Second, we aimed to demonstrate that physiological changes at the cellular level could be detected via analysis cellular metabolites sampled. Lastly, we aimed to demonstrate that single cell metabolomics can be utilized to assess whether cells are experiencing different illumination levels and nutrient limitation.

3.2 Materials and methods

3.2.1 Cultures

Non-axenic *Scrippsiella trochoidea* CCMP 3099 was originally obtained from the National Center for Marine Algae and Microbiota (Provasoil-Guillard NCMA, Boothbay Harbor, ME). For maintenance, cultures were grown in L1 seawater media [25-27].

Media was prepared from natural seawater collected near Key West (salinity of 33), which was aged for at least six month in the dark and autoclaved. Maintenance and experimental cultures were grown in a light/dark incubator at 23-24 °C and 30-40 μmol quanta·$m^{-2}s^{-1}$ light under a 12-h light:12-h dark cycle.

3.2.2 Experimental Culture Setup. For the light/dark comparisons, cultures were grown under replete conditions in full L1 media containing 880 μM $NaNO_3$ and 36 μM NaH_2PO_4 (N/P ratio 24:1). Experimental cultures were started as a 1:10 inoculum from exponentially growing cultures into 1L of media in 2.5 L Pyrex Fernbach flasks without shaking and monitored daily via cell counts and chlorophyll measurements. Cell counts were conducted by addition of 1% Lugol's iodine and direct counting of cells in 96-well microtiter plates using a dissection microscope. Dilutions were made as necessary and at least 10 wells containing 100 μL diluted culture were counted to average cell counts. Chlorophyll *a* was measured via fluorometry [28] by filtering 5 mL of culture in triplicate onto GF/F filters, over-night extraction with methanol, and quantification using a Turner Trilogy Laboratory Fluorometer. Cultures were grown into late-log phase (data not shown) and then sampled three hours before and three hours after the light was turned on. Cultures were sub-sampled for MS analysis, making sure to keep 'dark' sample exposure to light to a minimum by wrapping sampling tubes in aluminum foil.

N-deplete cultures were generated by first growing cells on L1 media with an N:P ratio of 2.4:1 (88 mM nitrate: 36mM phosphate) analogous what has been previously described [15]. This lower ratio stoichiometrically limited cultures in nitrogen and at least three transfers were performed to ensure no carryover from higher nutrient full L1 medium. Cultures were monitored daily via cell counts (see above), chlorophyll *a*

quantification (see above), and quantification of nitrate/nitrite via a Vanadium reduction method [29]. Parallel cultures were set up in which one culture was allowed to run out of nitrogenous nutrients (N-deplete), while the culture (control) was fed additional nitrate every second day to bring total nitrate/nitrite concentrations back to starting levels. Once nitrate/nitrite levels dropped below the limit of detection (~1-2 μM) in the N-deplete culture, cultures were grown for an additional 24 hours before sampling to ensure that N-depletion was complete. Both the N-deplete and replete cultures were then sampled for MS analysis of single cells.

3.2.3 MS

Individual cells of *S. trochoidea* were analyzed via the 'Single-probe' MS techniques. Detailed fabrication protocols of the Single-probe have been previously described [23, 30, 31]. Briefly, a Single-probe (Figure 3.1A) has three components: a dual-bore quartz tubing (outer diameter (OD) 500 μm; inner diameter (ID) 127 μm, Friedrich & Dimmock, Inc., Millville, NJ, USA) pulled using a laser pipette puller (P-2000 micropipette puller, Sutter Instrument, Novato, CA, USA), a fused silica capillary (OD 105 μm; ID 40 μm, Polymicro Technologies, Phoenix, AZ, USA), and a nano-ESI emitter made from the same type of fused silica capillary. A Single-probe is fabricated by embedding a fused silica capillary and a nano-ESI emitter into both of the channels of the laser-pulled dual-bore quartz needle.

For the analysis, cells were deposited onto 0.2 μm polycarbonate membranes by gentle filtration, and the cells were rinsed with phosphate buffered saline (PBS; 137 mM NaCl, 2.7 mM KCl, 4.3 mM Na_2HPO_4, 1.47 mM KH_2PO_4; pH of 7.4) to remove culture medium. Filters were then placed on a home-built XYZ−translation stage system and

spatial motion was controlled by a custom designed LabView software package [32]. The Single-probe tip (<10 μm) was then precisely insert into single *S. trochoidea* cells (typically ~20-30 μm cellular diameter) using a microscope as a guide (Figure 3.1B). During the experiment, a syringe (250 μl; Hamilton Co., Reno, NV, USA) was used to continuously provide the sampling solvent (acetonitrile; Sigma-Aldrich St. Louis, MO, USA), and a liquid junction formed at the Single-probe tip to perform highly efficient extraction of cellular contents. The analytes were withdrawn by capillary action towards the nano-ESI emitter, and ionized for analysis using a Thermo LTQ Orbitrap XL mass spectrometer (Thermo Scientific, Waltham, MA, USA)(Figure 3.1C). Mass analyze parameters were as follows: mass resolution 60,000, +4 kV ionization voltage at positive ion mode (0.05-0.07 μA of ion current), 1 microscan, 100 ms max injection time, and automatic gain control on.

3.2.4 Data Analysis

The Thermo Xcalibur Qual Browser (Thermo Scientific, Waltham, MA, USA) was used to export MS data (m/z values with relative intensities) as tab-delimited data files. As a conservative approach, only relatively abundant peaks with ion intensities > 10^3 were exported. This approach excluded 6% of low signal peaks as background while retaining 94 % of total signal intensity. The relative ion intensities were normalized to the total ion current to minimize the influence induced by fluctuations of ion signals during experiments. The Geena 2 online software tool (http://bioinformatics.hsanmartino.it/geena2/) was then used for peak alignment [33], and the aligned m/z values were then used for comparisons. Parameters used in Geena 2 include analysis range (from 100m/z to 1500 m/z), maximum number of isotopic replicas

(5), maximum delta between isotopic peaks (0.05 Da), and maximum delta for aligning replicates (0.01 Da). Metaboanalyst 3.0 (http://www.metaboanalyst.ca/) was used to

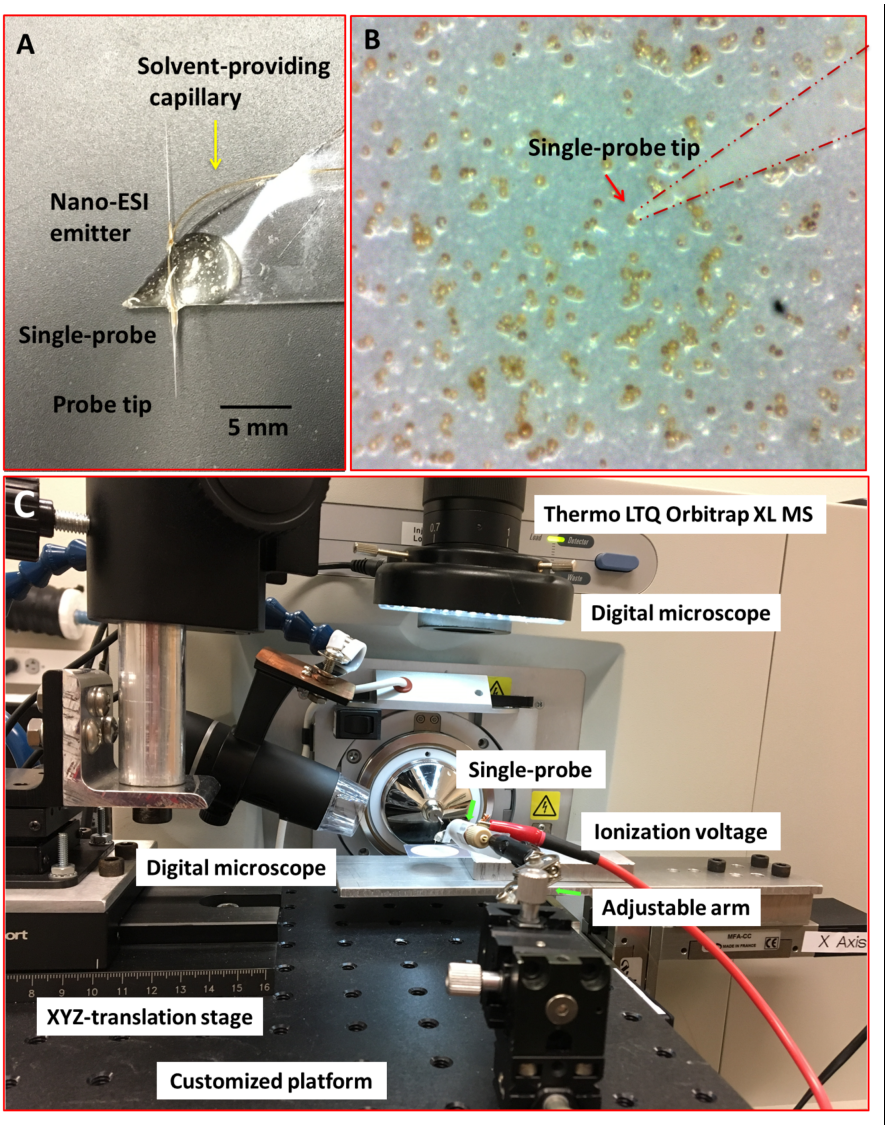

Figure 3.1 Experimental setup to measure single *S. trochoidea* cells using the "Single-probe" MS techniques. (A) Photograph of the Single-probe device with its different components labeled (B) Image from microscope-linked camera used to target single *S. trochoidea* cell with the Single-probe; (C) Setup used to manipulate the Single-probe MS device with components labeled.

tentatively label all ions of interest [36, 37], to perform hierarchical clustering, and to generate heat maps. Lastly, Pathos (http://motif.gla.ac.uk/Pathos/) was used to attempt identification of significantly regulated metabolic pathways by considering all KEGG maps in all organisms [38].

3.3 Result

The main aims of this study were to develop a single-cell-based metabolomic methodology that could be applied to individual algal cells and to demonstrate that this technology can detect physiological responses to environmental stimuli. The described setup allowed us to sample individual cells by targeting them with the tip of the Single-probe (Figure 3.1B). Our 'proof of concept' experiment involved a comparison of cells in the context of diurnal illumination changes, which are known to induce significant changes in algal cellular metabolomes [39].

Using the Single-probe MS technique, distinct and clear differences were observed in the *S. trochoidea* metabolome under different light levels. A total of 1,085 and 1,103 metabolites were detected under light and dark conditions respectively. Of these, 306 and 321 were differentially abundant among treatments (*t*-test; $p < 0.05$). Partial Least Squares Discriminant Analysis of all detected metabolites (PLS-DA) (Figure 3.2A and Table 3.2) revealed that metabolic features formed distinct clusters (15 cells in each group), and this difference was highly significant ($p = 5*10^{-4}$; permutation test in Metaboanalyst 3.0). To investigate which metabolic pathways may have been significantly impacted by the difference in illumination levels, all ions with significant differences ($p<0.05$) were selected and tentatively labeled by searching their m/z values

in Pathos, considering all KEGG metabolites, and retaining pathways for which at least 2 hits were observed (Table 3.1). A criterion of two hits to an individual pathway was used, because the reliability of assignments for metabolites based on m/z values alone is limited. Most strikingly, only 12 (5%) and 16 (19%) of differentially abundant metabolites could be assigned to KEGG pathways for light and dark conditions respectively, indicating that the majority of the metabolic response to light changes in *S. trochoidea* is not captured in KEGG metabolic maps. With respect to pathways with at least two hits (Table 3.1), light favors biosynthesis of molecules potentially linked to the production of 12-, 14- and 16-membered macrolides. In particular, several hits in the pathway for Avermectin were observed (Table 3.1A). Under dark conditions, identified pathways included those for polyketides, porphyrin, chlorophylls, terpenoids, and limonene (Table 3.1B). With respect to the four hits in porphyrin and chlorophyll metabolism, all were linked to the production of phycobillins.

Pathway	# of Metabolites	Metabolite	Counter-ion
(A)			
Biosynthesis of 12−, 14−, and 16-membered macrolides	7	6-Deoxyerythronolide B ($C_{21}H_{38}O_6$)*	($+Na^+$)
		Avermectin A2a ($C_{49}H_{76}O_{15}$)*	($+H^+$)
		Avermectin A2a aglycone ($C_{35}H_{52}O_9$) *	($+Na^+$)
		Avermectin B2b ($C_{47}H_{72}O_{15}$) *	($+Na^+$)
		Demethyllactenocin ($C_{37}H_{61}NO_{14}$) *	($+NH_4^+$)
		Erythronolide B ($C_{21}H_{38}O_7$) *	($+K^+$)
		L-Oleandrosyl-oleandolide ($C_{27}H_{46}O_{10}$) *	($+Na^+$)
(B)			
Porphyrin and chlorophyll metabolism	4	(3Z)-Phytochromobilin ($C_{33}H_{36}N_4O_6$)	($+Na^+$)
		15,16-Dihydrobiliverdin ($C_{33}H_{36}N_4O_6$)	($+Na^+$)
		Bilirubin ($C_{33}H_{36}N_4O_6$)	($+Na^+$)
		I-Urobilinogen ($C_{33}H_{44}N_4O_6$) *	($+K^+$)
Biosynthesis of type II polyketide products	2	19-Hydroxytetrangulol ($C_{19}H_{12}O_5$)	($+K^+$)
		Dehydrorabelomycin ($C_{19}H_{12}O_5$)	($+K^+$)
Limonene and pinene degradation	2	(3R)-3-Isopropenyl-6-oxoheptanoate ($C_{10}H_{16}O_3$)	($+NH_4^+$)
		(3S)-3-Isopropenyl-6-oxoheptanoate ($C_{10}H_{16}O_3$)	($+NH_4^+$)
Monoterpenoid biosynthesis	2	1,6,6-Trimethyl-2,7-dioxabicyclo[3.2.2]nonan-3-one ($C_{10}H_{16}O_3$)	($+NH_4^+$)
		4,5-Dihydro-5,5-dimethyl-4-(3-oxobutyl)furan-2(3H)-one ($C_{10}H_{16}O_3$)	($+NH_4^+$)

Metabolites were analyzed using Pathos (http://motif.gla.ac.uk/Pathos/pathos.html) by considering all KEGG maps in all organisms under positive ion mode.
**Denotes that the formula is unique among all metabolites in KEGG maps.*

Table 3.1 Pathways containing more than one metabolite with significantly different abundance under (Table 3.1A) illuminated conditions compared to cultures during (Table 3.1B) dark condition. Metabolites were analyzed using Pathos (http://motif.gla.ac.uk/Pathos/pathos.html) by considering all KEGG maps in all organisms under positive ion mode.

Given the successful proof of concept for light/dark conditions, we aimed to investigate whether single cell metabolomic analysis might be utilized to investigate the nutritional status of individual phytoplankton cells. As shown in Figure 3.2B and Table 3.2, PLS-DA results indicated that single cellular metabolomes of *S. trochoidea* under N-limited condition were clearly different from those in nitrogen replete cells (n = 10). As with the light-dark treatments, N limitation induced a highly significant response ($p= 1*10^{-3}$; permutation test in Metaboanalyst 3.0). KEGG pathway analysis was attempted, but yielded no metabolites in the significantly upregulated pool that could be matched to KEGG. Similarly, only 8 (<4.5%) metabolites from the down-regulated pool could be mapped with KEGG and no pathways contained more than a single hit. Little information could therefore be gleaned about requisite physiological responses via KEGG analysis, and an alternative approach to analysis was therefore taken. First, we hypothesized that N-limitation should be reflected in the C/N and N/P rations of the cellular metabolome, as cells might physiologically adjust to environmental conductions by choosing cellular metabolites with lower N content [7, 40]. Second, metabolites were analyzed for the putatively detected N-containing lipids (e.g. phosphoethanolamine), given that physiological responses are often manifest in the lipid pool.

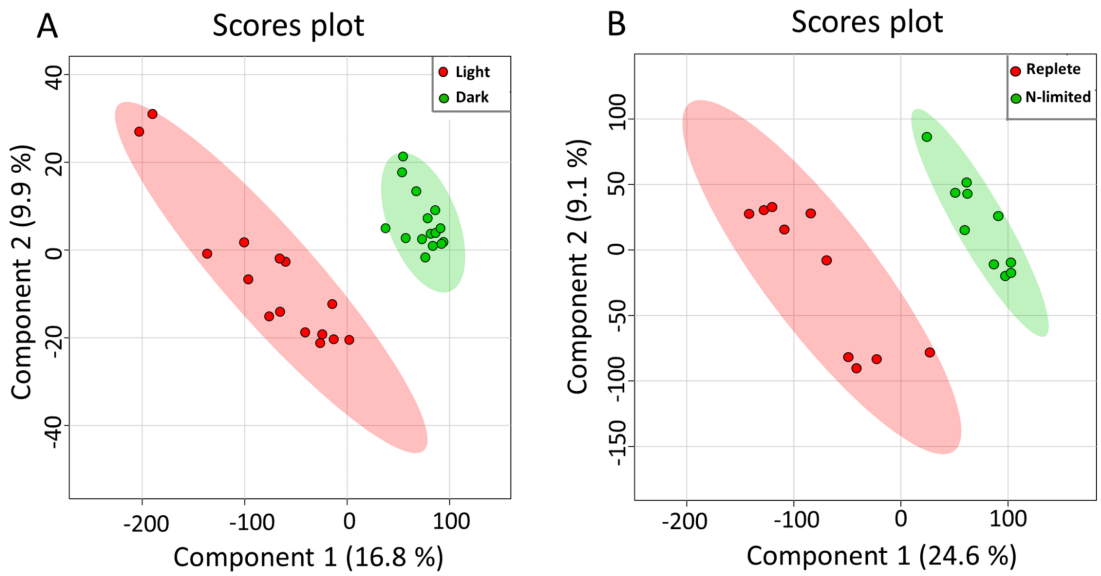

Figure 3.2 Partial Least Squares Discriminant Analysis (PLS-DA) of MS data. All detected metabolites were analyzed, visualizing the overall effect on the metabolome of single *S. trochoidea* cells by (A) light vs dark conditions (results are reported from 15 replicates (n=15) in each group), and (B) N-limited vs. replete conditions (n=10 for each group).

(A) R^2 and Q^2 values for light vs dark model

Measure	1 comps	2 comps	3 comps	4 comps	5 comps
Accuracy	0.97619	0.97619	0.97619	0.97619	0.97619
R2	0.86165	0.97386	0.99618	0.99883	0.99974
Q2	0.72835	0.8285	0.84477	0.84725	0.84978

(B) R^2 and Q^2 values for N-limited vs replete model

Measure	1 comps	2 comps	3 comps	4 comps	5 comps
Accuracy	0.9	0.95	0.9	0.9	0.9
R2	0.79324	0.96464	0.89568	0.89955	0.89994
Q2	0.59696	0.64163	0.63966	0.64254	0.64297

Table 3.2 PLS-DA cross-validation results. Presented are the performance measures (R^2 and Q^2) for different number of components.

C: N and C: P ratios were calculated by summing the product of the number of C, N, P atoms in each metabolite with its relative abundance across all metabolites. This analysis reveals that N-limited *S. trochoidea* has significantly higher C:N ratios in regulated metabolites as compared to replete conditions ($p=4*10^{-6}$). Similarly, C:P ratios were affected and were significantly higher under N-limitation ($p< 0.044$). Concurrently, the abundances of at least some cellular lipids were significantly affected. When all significantly regulated metabolites putatively identified as lipids are considered (Figure 3.4), it appears that the availability of light correlates with both up- and down-regulation of specific lipid complements (Figure 3.4A). Under N-limitation, however, a significant decrease lipid abundances is observed ($p<0.05$) (Figure 3.4B).

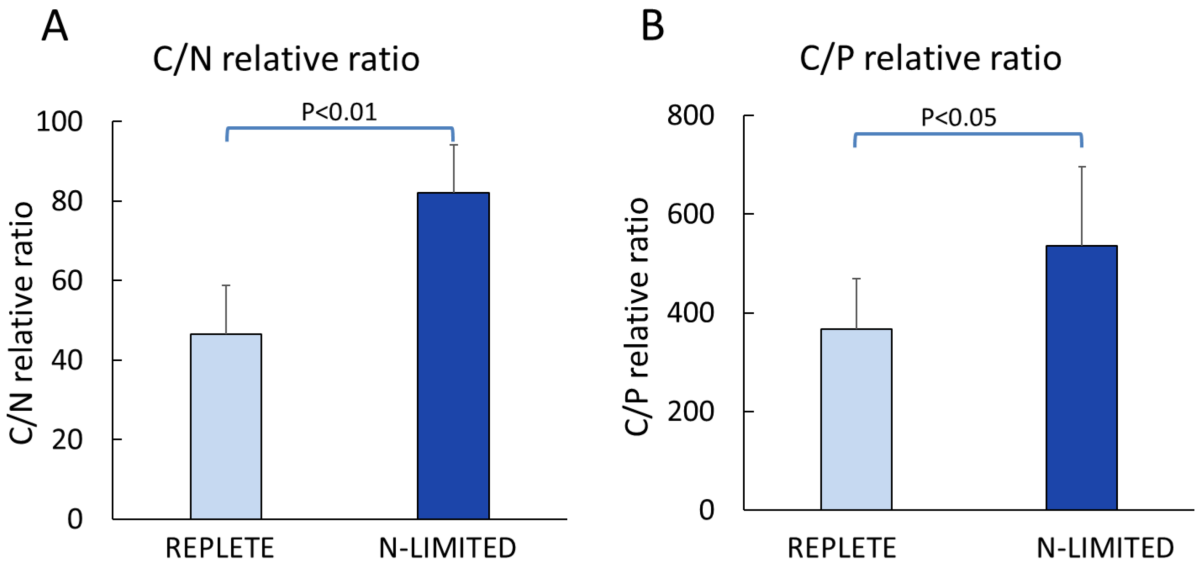

Figure 3.3 Elemental ratios of significantly regulated metabolites. (A) Carbon to Nitrogen ratio; (B) Carbon to Phosphorus ratio.

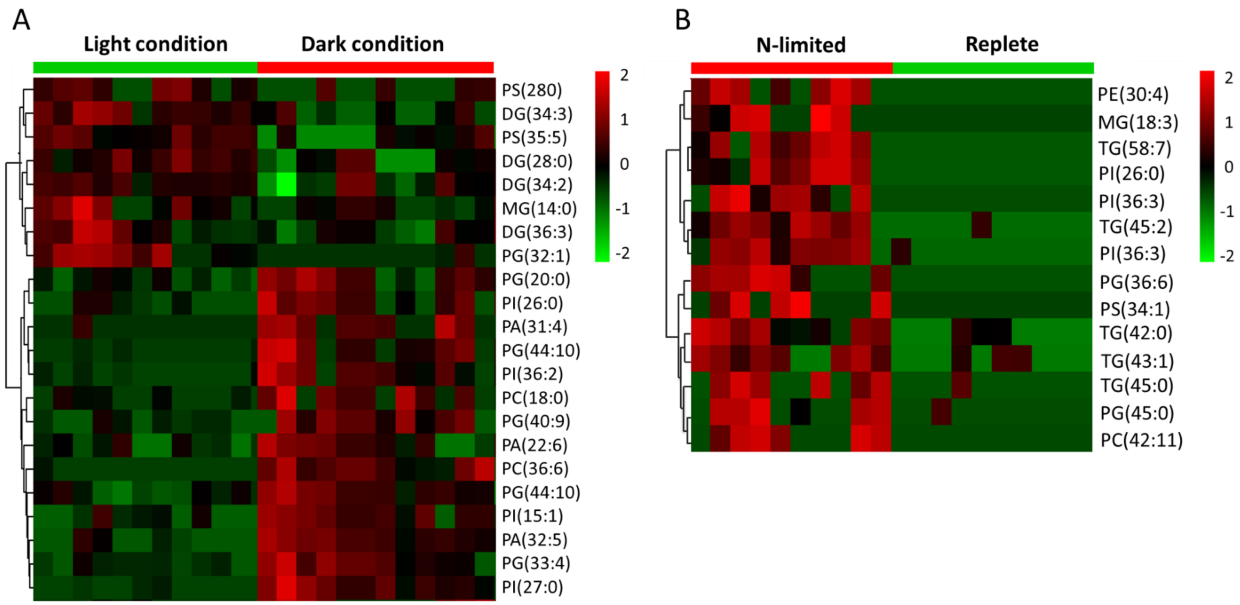

Figure 3.4 Heat maps generated from hierarchically clustering summarizing the cellular lipids measured from single *S. trochoidea* cell under different light and nutrient conditions. Only lipids for which abundances were significantly different among treatment pairs are shown. Shown are differences for (A) light vs. dark conditions and (B) replete vs nitrogen (N) limiting conditions. Red indicates elevated and green indicates decreased signal with respect to the mean signal observed for all tested cells. PA (phosphatic acid), PE (phosphoethanolamine), PG (phosphatidylglycerol), PS (phosphatidylserine), PI (phosphatidylinositol), PC (phosphatidylcholine), MG (monoglycerides), DG (diglycerides), TG (triglyceride)

3.4 Discussion

Historically, the majority of oceanographic research has targeted natural populations of phytoplankton via bulk filtration techniques (e.g. filtration onto GF/F filters) to assess physiological responses to environmental factors such as light or nutrient limitation. While much has been learned using bulk filtration, requisite approaches suffer from important limitations. Most notably, individual populations or different species are not adequately resolved in this manner. It is also now well appreciated that cellular functions, such as gene expression, proliferation, or programmed cell death, are subject to significant stochasticity, leading to high cellular chemical and phenotypic diversity at the single cell level, potentially obscuring some important patterns [41-43]. Single-cell analysis is therefore an attractive methodological choice when studying rare types of cells (cells available are inadequate for bulk analysis) or cells in heterogenous populations, where cell separation or sorting are impractical. Here we present the first report of a single cell-based metabolomic technology that allows for the analysis of intracellular intermediates of individual phytoplankton cells. The Single-probe directly collects cellular contents of living cells, and it does this without significant sample preparation steps (e.g. filtration or solvent extraction), thereby allowing for real-time and targeted analysis that minimizes sampling artifacts.

We note that bulk analyses (e.g., liquid chromatography (LC)/MS, gas chromatography (GC)/MS), or direct-injection MS without separation) were not conducted in this study. It is likely that the number and the types of metabolites detected here differs from those that might have been observed in bulk measurements. Traditional LC/MS and GC/MS techniques have certainly been used in the analysis of marine algae

[44, 45], and their value is clear in requisite studies. However, a direct comparison was not conducted, because we do not view the use of the Single-probe as a replacement for more traditional bulk biomass approaches. Rather, single-cell analysis can serve as a complementary methods that allows exploration of inherent cell-to-cell variability in complex and heterogeneous systems that may not be resolved using more traditional approaches.

Given the tip size of the Single-probe, which is ca. 10 μm in diameter, analysis is currently limited to larger phytoplankton and protists. However, the currently applicable size range includes many important bloom forming algae, including toxin producing genera such as *Karenia* (20-40 μm) or *Pseudonitschia* (40-175 μm). The Single-probe might therefore offer unique opportunities to help understand the biological forces that shape the success of these organisms in an ecosystem by revealing their metabolomic responses to changing environmental conditions or experimental treatments at the cellular level. We note that the expensive and bulky configuration of equipment described here still precludes easy field deployment, making the Single-probe MS technique most useful under conditions where direct access to the lab is available, or when experimental cultures are assayed. Further development in the miniaturization of high-resolution mass spectrometer or sample preservation maybe be helpful in this regard. In addition, due to the limited amount of cytoplasm found in an individual cell and limitation on the achievable sensitivity of mass spectrometers, most single cell MS studies to date are primarily focused on the analysis of relatively small molecules such as metabolites and peptides [46]. The detection of larger molecules, such as proteins presenting as relatively lower abundances, at single cell level remains very challenging.

Despite these limitations, single-cell MS technique holds great promise for environmental research. The Single-probe MS technique has been successfully used to study live single cancer cells [23, 47], to map biomolecules on animal tissues with high spatial resolutions [24, 30, 48], and to analyze the extracellular metabolites inside spheroids [31]. With respect to the ability to detect a large range of cellular metabolites from single cells (i.e. from only a few pico-litters of cytoplasm sampled from a cell with a diameter of approximately10 μm), the Single-probe MS setup provides excellent detection sensitivity. We note, however, that single cell MS measurements are not strictly repeatable (cellular contents are consumed in each measurement), and that it is impractical to evaluate reproducibility in this regard. Multiple cells must therefore be measured (e.g., n = 10-15 in each group in the current study) to normalized intensities for statistical data analysis and to minimize the influence of uncertainties such as fluctuation of ion signals, minor changes of experimental tuning conditions, instrument noise, and variances associated with the matrix effect.

Here, were extend these advances by demonstrating that the physiological status of phytoplankton with respect to light and nutrients can be assessed. The availability of light was correlated with a highly significant response in the metabolite profile of *S. trochoidea* cells (Figure 3.2). As might be expected, metabolites related to porphyrin and chlorophyll pathways stood out. In particular, the detected metabolites are related to phytochrome metabolism, which is consistent with the notion that phytochromes are signal-transducing photoreceptors [49]. Beyond phototaxis and a handful of secondary metabolite intermediates, however, few metabolites could be assigned to KEGG pathways. This, perhaps, speaks to our limited understanding of metabolism in

Dinoflagellate algae. Transcriptomic analysis of *S. trochoidea* (same strain used here) indicated that this species makes perhaps in excess of 10^5 transcripts, the majority of which could not be annotated [16].

Cellular lipids have been used to parse physiological responses of living cells under different illumination conditions [50, 51]. For example, under dark conditions, mRNA for some genes involved in lipid biosynthesis have been observed to be elevated in *Chlorella* [51]. Differential responses of lipid abundance have also been observed in the marine dinoflagellate *Prorocentrum minium* under dark vs. light conditions [52], and light-induced significant changes in the fatty acid profiles have been reported for freshwater diatom, chrysophyte, cryptophyte, and zygnematophyte algae [50]. Differences in requisite light-dependent cellular lipid profiles are thought to be related to alterations of energy storage and the compositions of chloroplast membranes [53-55]. Consistently, our experiments indicated both up- and down-regulation of lipids in response to light in *S. trochoidea*. The pattern of changes in lipid composition in response to N-limitation was, however, quite different from that observed under light limitation. Most notably, all differentially regulated lipids were more abundant under the nutrient limiting conditions. This is potentially the result of limitation induced imbalances in cellular elemental composition. Under N-limitation almost all parts of central metabolism are impacted (and potentially slowed due to limiting resources), yet lipids, for the most part, do not contain N atoms and their biosynthesis might thereby proceed so long photosynthesis can proceed. Whether lipid accumulation in *Scrippsiella* is adaptive, however, by possibly allowing energy storage to gain advatages when nutrients are more readily available, or is simply a consequence of the onset of

senescence remains to be investigated. Changes in the C:N and C:P ratios do appear to be reflected in the metabolome overall (Figure 3.3). This observation is consistent with the notion that elemental ratios have considerable plasticity based on nutrient availability [40]. Previous studies have suggested that nutrient deficiency can cause the accumulation of lipids, such as triglyceride [56-58], and that phytoplankton funnel excess NADPH to the biosynthesis of triglyceride and fatty acids to regenerate $NADP^+$ [56, 59, 60]. Correspondingly, we observed that a number of triglycerides significantly increased in the N-limited group (Figure 3B). We also note that C:N and C:P ratios reported here deviate from Redfield's expectations (C:N:P ~ 106:16:9) (Figure 3.3A). However, these observations are consistent with our approach. The elemental Redfield ratios are based on all cellular components, yet data analyzed here only covers a subset of all cellular constituents. For example, the Single-probe MS techniques cannot currently measure large biomolecules such as proteins and nucleic acids which are N-rich. The absence of nucleic acids in calculations likely leads to high C:P ratio estimates [40, 61, 62]. Values reported here are therefore not inconsistent with generally expected elemental ratios for phytoplankton biomass.

In summary, we report the development of a methodology for single-cell metabolomics of small protists such as marine dinoflagellate algae. Using the Single-probe MS technology we can efficiently monitor the cellular physiological responses of phytoplankton under different illumination and nutrient conditions. This offers the opportunity for real-time analysis of natural populations and has the potential ability to provide information about the dynamic metabolic response of individual cells to environment stimulation.

3.5 References

[1] P.G. Falkowski, R.T. Barber, V.V. Smetacek, Biogeochemical Controls and Feedbacks on Ocean Primary Production, Science, 281 (1998) 200-207.

[2] D. Antoine, J.M. Andre, A. Morel, Oceanic primary production .2. Estimation at global scale from satellite (coastal zone color scanner) chlorophyll, Global Biogeochem Cy, 10 (1996) 57-69.

[3] R.W. Howarth, Nutrient Limitation of Net Primary Production in Marine Ecosystems, Annual Review of Ecology and Systematics, 19 (1988) 89-110.

[4] K.H. Coale, K.S. Johnson, S.E. Fitzwater, S.P.G. Blain, T.P. Stanton, T.L. Coley, IronEx-I, an in situ iron-enrichment experiment: Experimental design, implementation and results, Deep-Sea Res Pt Ii, 45 (1998) 919-945.

[5] M.R. Landry, J. Constantinou, M. Latasa, S.L. Brown, R.R. Bidigare, M.E. Ondrusek, Biological response to iron fertilization in the eastern equatorial Pacific (IronEx II). III. Dynamics of phytoplankton growth and microzooplankton grazing, Marine Ecology Progress Series, 201 (2000) 57-72.

[6] M.A. Saito, T.J. Goepfert, J.T. Ritt, Some thoughts on the concept of colimitation: Three definitions and the importance of bioavailability, Limnology and Oceanography, 53 (2008) 276-290.

[7] J. Beardall, E. Young, S. Roberts, Approaches for determining phytoplankton nutrient limitation, Aquatic Sciences, 63 (2001) 44-69.

[8] B. Wawrik, J.H. Paul, D.A. Bronk, D. John, M. Gray, High Rates of Ammonium Recycling Drive Phytoplankton Productivity in the Offshore Mississippi River Plume, Aquat Microbiol Ecol, 35 (2004) 175-184.

[9] A.P. Rees, N.J.P. Owens, M.R. Heath, D.H. Plummer, R.S. Bellerby, Seasonal Nitrogen Assimilation and Carbon Fixation in a Fjordic Sea Loch, J Plankton Res, 17 (1995) 1307-1324.

[10] A.E. Allen, M.G. Booth, M.E. Frischer, P.G. Verity, J.P. Zehr, S. Zani, Diversity and detection of nitrate assimilation genes in marine bacteria, Applied and Environmental Microbiology, 67 (2001) 5343-5348.

[11] D.J. Scala, L.J. Kerkhof, Nitrous oxide reductase (nosZ) gene-specific PCR primers for detection of denitrifiers and three nosZ genes from marine sediments, FEMS Microbiology Letters, 162 (1998) 61-68.

[12] B. Wawrik, J.H. Paul, F.R. Tabita, Real-time PCR quantification of rbcL (ribulose-1,5-bisphosphate carboxylase/oxygenase) mRNA in diatoms and pelagophytes, Applied and Environmental Microbiology, 68 (2002) 3771-3779.

[13] D. Lindell, A.F. Post, Ecological aspects of ntcA gene expression and its use as an indicator of the nitrogen status of marine Synechococcus spp, Applied and Environmental Microbiology, 67 (2001) 3340-3349.

[14] K.A. Turk, A.P. Rees, J.P. Zehr, N. Pereira, P. Swift, R. Shelley, M. Lohan, E.M. Woodward, J. Gilbert, Nitrogen fixation and nitrogenase (nifH) expression in tropical waters of the eastern North Atlantic, ISME Journal, 5 (2011) 1201-1212.

[15] M.J. Harke, A.R. Juhl, S.T. Haley, H. Alexander, S.T. Dyhrman, Conserved Transcriptional Responses to Nutrient Stress in Bloom-Forming Algae, Frontiers in Microbiology, 8 (2017) 1279.

[16] J.T. Cooper, G.A. Sinclair, B. Wawrik, Transcriptome Analysis of Scrippsiella trochoidea CCMP 3099 Reveals Physiological Changes Related to Nitrate Depletion, Frontiers in Microbiology, 7 (2016).

[17] Y.S. Hwang, G. Jung, E. Jin, Transcriptome analysis of acclimatory responses to thermal stress in Antarctic algae, Biochemical and Biophysical Research Communications, 367 (2008) 635-641.

[18] D. Cohen, J.A. Dickerson, C.D. Whitmore, E.H. Turner, M.M. Palcic, O. Hindsgaul, N.J. Dovichi, Chemical Cytometry: Fluorescence-Based Single-Cell Analysis, Annu Rev Analyt Chem, 1 (2008) 165-190.

[19] L.A. Woods, T.P. Roddy, A.G. Ewing, Capillary electrophoresis of single mammalian cells, Electrophoresis, 25 (2004) 1181-1187.

[20] L.A. Woods, A.G. Ewing, Analysis of single mammalian cells with capillary electrophoresis, Analyt. Bioanalyt. Chem., 376 (2003) 281-283.

[21] J.F. Cahill, T.K. Darlington, C. Fitzgerald, N.G. Schoepp, J. Beld, M.D. Burkart, K.A. Prather, Online analysis of single cyanobacteria and algae cells under nitrogen-limited conditions using aerosol time-of-flight mass spectrometry, Anal. Chem., 87 (2015) 8039-8046.

[22] P.L. Urban, T. Schmid, A. Amantonico, R. Zenobi, Multidimensional analysis of single algal cells by integrating microspectroscopy with mass spectrometry, Anal. Chem., 83 (2011) 1843-1849.

[23] N. Pan, W. Rao, N.R. Kothapalli, R. Liu, A.W. Burgett, Z. Yang, The single-probe: a miniaturized multifunctional device for single cell mass spectrometry analysis, Analytical Chemistry, 86 (2014) 9376-9380.

[24] W. Rao, N. Pan, Z. Yang, Applications of the Single-probe: Mass Spectrometry Imaging and Single Cell Analysis under Ambient Conditions, JoVE, (2016) e53911-e53911.

[25] R.R.L. Guillard, P.E. Hargraves, Stichochrysis immobilis is a diatom, not a chrysophyte, Phycologia, 32 (1993) 234-236.

[26] R.R.L. Guillard, P. Kilham, T.A. Jackson, Kinetics of silicon-limited growth in the marine diatom Thalassiosira pseudonana Hasle And Heimdal (=Cyclotella nana Hustedt), Journal of Phycology, 9 (1973) 233-237.

[27] R.R.L. Guillard, J.H. Ryther, Studies of marine planktonic diatoms: I. Cyclotella nana Hustedt, and Detonula confervacea (Cleve) Gran, Canadian Journal of Microbiology, 8 (1962) 229-239.

[28] N.A. Welschmeyer, Fluorometric Analysis of Chlorophyll-a in the Presence of Chlorophyll-b and Pheopigments, Limnology and Oceanography, 39 (1994) 1985-1992.

[29] K.M. Miranda, M.G. Espey, D.A. Wink, A Rapid, Simple Spectrophotometric Method for Simultaneous Detection of Nitrate and Nitrite, Nitric Oxide, 5 (2001) 62-71.

[30] W. Rao, N. Pan, Z. Yang, High resolution tissue imaging using the single-probe mass spectrometry under ambient conditions, Journal of the American Society for Mass Spectrometry, 26 (2015) 986-993.

[31] M. Sun, X. Tian, Z. Yang, Microscale Mass Spectrometry Analysis of Extracellular Metabolites in Live Multicellular Tumor Spheroids, Analytical Chemistry, (2017).

[32] I. Lanekoff, B.S. Heath, A. Liyu, M. Thomas, J.P. Carson, J. Laskin, Automated platform for high-resolution tissue imaging using nanospray desorption electrospray ionization mass spectrometry, Anal. Chem., 84 (2012) 8351-8356.

[33] P. Romano, A. Profumo, M. Rocco, R. Mangerini, F. Ferri, A. Facchiano, Geena 2, improved automated analysis of MALDI/TOF mass spectra, BMC Bioinformat, 17 (2016) 61.

[34] J. Xia, I.V. Sinelnikov, B. Han, D.S. Wishart, MetaboAnalyst 3.0—making metabolomics more meaningful, Nucleic Acids Res., 43 (2015) W251-W257.

[35] J. Xia, D.S. Wishart, Using MetaboAnalyst 3.0 for comprehensive metabolomics data analysis, Curr Protoc Bioinformatics, (2016) 14.10. 11-14.10. 91.

[36] C. Guijas, J.R. Montenegro-Burke, X. Domingo-Almenara, A. Palermo, B. Warth, G. Hermann, G. Koellensperger, T. Huan, W. Uritboonthai, A.E. Aisporna, METLIN: A Technology Platform for Identifying Knowns and Unknowns, Anal. Chem., (2018).

[37] C.A. Smith, G. O'Maille, E.J. Want, C. Qin, S.A. Trauger, T.R. Brandon, D.E. Custodio, R. Abagyan, G. Siuzdak, METLIN: a metabolite mass spectral database, Drug Monit, 27 (2005) 747-751.

[38] D.P. Leader, K. Burgess, D. Creek, M.P. Barrett, Pathos: a web facility that uses metabolic maps to display experimental changes in metabolites identified by mass spectrometry, Rapid Commun. Mass Spectrom., 25 (2011) 3422-3426.

[39] C. Vidoudez, G. Pohnert, Comparative metabolomics of the diatom Skeletonema marinoi in different growth phases, Metabolomics, 8 (2012) 654-669.

[40] R.J. Geider, J. La Roche, Redfield revisited: variability of C [ratio] N [ratio] P in marine microalgae and its biochemical basis, Europ J Phycol, 37 (2002) 1-17.

[41] O. Guillaume-Gentil, T. Rey, P. Kiefer, A.J. Ibáñez, R. Steinhoff, R. Brönnimann, L. Dorwling-Carter, T. Zambelli, R. Zenobi, J.A. Vorholt, Single-cell mass spectrometry of metabolites extracted from live cells by fluidic force microscopy, Anal. Chem., 89 (2017) 5017-5023.

[42] T.J. Comi, T.D. Do, S.S. Rubakhin, J.V. Sweedler, Categorizing cells on the basis of their chemical profiles: progress in single-cell mass spectrometry, J Amer Chem Soc, 139 (2017) 3920-3929.

[43] S.R. Fagerer, T. Schmid, A.J. Ibáñez, M. Pabst, R. Steinhoff, K. Jefimovs, P.L. Urban, R. Zenobi, Analysis of single algal cells by combining mass spectrometry with Raman and fluorescence mapping, Analyst, 138 (2013) 6732-6736.

[44] A. Barofsky, P. Simonelli, C. Vidoudez, C. Troedsson, J.C. Nejstgaard, H.H. Jakobsen, G. Pohnert, Growth phase of the diatom Skeletonema marinoi influences the metabolic profile of the cells and the selective feeding of the copepod Calanus spp, J Plankton Res, 32 (2009) 263-272.

[45] M.S. Burriesci, T.K. Raab, J.R. Pringle, Evidence that glucose is the major transferred metabolite in dinoflagellate–cnidarian symbiosis, J Exp Biol, 215 (2012) 3467-3477.

[46] S.S. Rubakhin, E.V. Romanova, P. Nemes, J.V. Sweedler, Profiling metabolites and peptides in single cells, Nat. Methods, 8 (2011) S20.

[47] N. Pan, W. Rao, S.J. Standke, Z. Yang, Using Dicationic Ion-Pairing Compounds To Enhance the Single Cell Mass Spectrometry Analysis Using the Single-Probe: A Microscale Sampling and Ionization Device, Analytical Chemistry, 88 (2016) 6812.

[48] W. Rao, N. Pan, X. Tian, Z. Yang, High-resolution ambient MS imaging of negative ions in positive ion mode: using dicationic reagents with the single-probe, Journal of the American Society for Mass Spectrometry, 27 (2016) 124-134.

[49] H. Smith, Phytochromes and light signal perception by plants--an emerging synthesis, Nature, 407 (2000) 585-591.

[50] A. Wacker, M. Piepho, J.L. Harwood, I.A. Guschina, M.T. Arts, Light-Induced Changes in Fatty Acid Profiles of Specific Lipid Classes in Several Freshwater Phytoplankton Species, Frontiers Plant Sci, 7 (2016).

[51] T. Chen, J. Liu, B. Guo, X. Ma, P. Sun, B. Liu, F. Chen, Light attenuates lipid accumulation while enhancing cell proliferation and starch synthesis in the glucose-fed oleaginous microalga Chlorella zofingiensis, Scientific reports, 5 (2015) 14936.

[52] K. Manoharan, T.K. Lee, J.M. Cha, J.H. Kim, W.S. Lee, M. Chang, C.W. Park, J.H. Cho, Acclimation of Prorocentrum minimum (Dinophyceae) to prolonged darkness by use of an alternative carbon source from triacylglycerides and galactolipids, J Phycol, 35 (1999) 287-292.

[53] E.M. Trentacoste, R.P. Shrestha, S.R. Smith, C. Glé, A.C. Hartmann, M. Hildebrand, W.H. Gerwick, Metabolic engineering of lipid catabolism increases microalgal lipid accumulation without compromising growth, Proc Nat Acad Sci USA, 110 (2013) 19748-19753.

[54] G. d'Ippolito, A. Sardo, D. Paris, F.M. Vella, M.G. Adelfi, P. Botte, C. Gallo, A. Fontana, Potential of lipid metabolism in marine diatoms for biofuel production, Biotechnol Biofuels, 8 (2015) 28.

[55] F. Guihéneuf, V. Mimouni, L. Ulmann, G. Tremblin, Combined effects of irradiance level and carbon source on fatty acid and lipid class composition in the microalga Pavlova lutheri commonly used in mariculture, J Exp Mar Biol Ecol, 369 (2009) 136-143.
[56] H.Y. El-Kassas, Growth and fatty acid profile of the marine microalga Picochlorum sp. grown under nutrient stress conditions, Egypt J Aquat Res, 39 (2013) 233-239.
[57] L. Xin, H. Hong-ying, G. Ke, S. Ying-xue, Effects of different nitrogen and phosphorus concentrations on the growth, nutrient uptake, and lipid accumulation of a freshwater microalga Scenedesmus sp, Biores Technol, 101 (2010) 5494-5500.
[58] M. Takagi, K. Watanabe, K. Yamaberi, T. Yoshida, Limited feeding of potassium nitrate for intracellular lipid and triglyceride accumulation of Nannochloris sp. UTEX LB1999, Appl Microbiol Biotechnol, 54 (2000) 112-117.
[59] G.A. Thompson, Lipids and membrane function in green algae, Biochimica et Biophysica Acta (BBA)-Lipids and Lipid Metabolism, 1302 (1996) 17-45.
[60] Q. Hu, M. Sommerfeld, E. Jarvis, M. Ghirardi, M. Posewitz, M. Seibert, A. Darzins, Microalgal triacylglycerols as feedstocks for biofuel production: perspectives and advances, Plant J, 54 (2008) 621-639.
[61] H. Maske, Ammonium-Limited Continuous Culures of Skeletonema costatum in Steady and Transitional State: Experimental Results and Model Simulations, J Mar Biol Assoc UK, 62 (1982) 919-943.
[62] E.A. Laws, D.G. Redalje, D.M. Karl, M.S. Chalup, A theoretical and experimental examination of the predictions of two recent models of phytoplankton growth, J Theoret Biol, 105 (1983) 469-491.

Chapter 4. Cancer Cells Escape Irinotecan Chemotherapy by Entering Stemness Associated with the SCD1

4.1 Introduction

Cancer is the one of the devastating disease in the world[1], and chemotherapy is one of the major treatment options for cancer [2], which can be used to treat cancers with different stages and also be used as an adjuvant therapy for advanced after surgery.[3] Drug resistance can largely reduce the therapeutic efficiency and finally cause the chemotherapy failure.[4] Therefore, it is important to understand the drug resistant mechanisms to promote the development of more efficient therapy for cancer.

Previous studies have revealed a number of general drug resistant mechanisms, including enhanced drug efflux, increased drug inactivation, promoted DNA damage repair, and suppressed apoptosis pathway.[4, 5] Accumulating evidence indicates that the development of drug resistance is associated with alteration of metabolic profiles. For example, previous studies indicated that amino acids and nucleobases (i.e., pyrimidines and purines) are enriched by irinotecan treatment.[6-8] However, the specific metabolic different have not been fully understood, and the role of metabolic changes in the development of drug resistance in cancer cells is largely unknown. Additionally, studies of cells with the acquired resistance in clinic were generally based on long-term chemotherapy [9]. For example, in many studies cancer cells were treated with anticancer drug for more than a year to develop the drug-resistant cell models, which possess over 100-time higher drug resistance than their parental cells. However, a very few studies have been focused on the metabolic features and biological changes of cancer cells at the

early stage of drug resistance development. Understanding the metabolic changes and gene regulation involved in the beginning of drug resistance development can reveal the relevant mechanisms and eventually benefit the disease management.

In addition to the metabolic changes, recent studies reported that chemotherapy treatment leads to the induced cancer stem cells (iCSCs), which are stem-like cells with self-renew and spheroid formation characteristics [10]. The iCSCs can be isolated from various types of tumors, and they possess high levels of resistant to many anticancer drugs such as oxaliplatin and 5-fluorouracil.[11, 12] Importantly, iCSCs also promote tumor recurrence and metastasis.[13, 14] However, the specific mechanism of drug induced stemness still remains unclear, limiting the efficacy of clinical thermotherapy. Due to the limited quantity of iCSCs, particularly from patients in clinical treatment, it is impractical to perform molecular analysis using traditional analytical methods (e.g. LC-MS). Therefore, techniques allowing for analysis at the single-cell level would provide a great advantage to study CSCs. Single-cell mass spectrometry (SCMS) analysis is a promising technique which can effectively utilize the limited resources of CSCs due to its high detection sensitivity and broad range of molecular analysis.

In this study, we applied the Single-probe SCMS technique [15-18] to explore the metabolic differences between drug-resistant cells and their parental cells at the single-cell level, and to investigate the molecular mechanism at the emergence of drug resistance. Irinotecan, a widely used antitumor drug, was employed in this study to develop the early-stage drug resistant cell line, which were further used to measure their metabolomic features at the single-cell level. We discovered a new drug resistant mechanism, in which drug-resistant cells upregulate the expression of stearoyl-CoA

desaturase-1 (SCD1), resulting in the promoted cancer stemness and reactive oxygen species (ROS) level. This study can promote our understanding of how cancer cells develop resistance to anticancer drugs such as irinotecan, and potentially benefit early diagnosis of patients with drug-resistance and the development of novel therapeutic strategies.

4.2 Methods

4.2.1 Materials and Chemicals

Irinotecan was purchased from Life Technologies (Grand Island, NY, USA). The stock solution of irinotecan was prepared in dimethyl sulfoxide (DMSO; Sigma-Aldrich, St. Louis, MO, USA) and further diluted into McCoy's 5A cell culture medium (Life Technologies, Grand Island, NY, USA). The MTT ((3-(4,5-Dimethylthiazol-2-yl)-2,5-Diphenyltetrazolium Bromide) was purchased from Biotium(Hayward, CA, USA).

4.2.2 Cell lines and Cell culture

HCT-116 cells were originally obtained from American Type Culture Collection (ATCC) (Rockville, MD). The cells were cultured in McCoy's 5A cell culture medium containing 10% FBS (fetal bovine serum; Life Technologies, Grand Island, NY, USA) and 1% Pen Strep (Life Technologies, Grand Island, NY, USA) at 37°C in an incubator with 5% CO_2 supply (HeraCell, Heraeus, Germany). In order to obtain irinotecan-resistant cells, we exposed the cells to a relatively high dose of irinotecan (1 μM) for different treatment time (i.e.,). Survived cells were then passaged at 80% confluence, and incubated at the same concentration of irinotecan. These processes were repeated until the resistant cell populations (i.e., 10- and 20-day resistant cells) were obtained.

4.2.3 Cytotoxicity assay

The MTT ((3-(4,5-Dimethylthiazol-2-yl)-2,5-Diphenyltetrazolium Bromide) was used to determine the growth inhibitory effect of irinotecan on HCT-116 cell viability after 72 hr drug exposure. IC_{50} values were calculated by using Grahpad Prism software.

4.2.4 Fabrication of the Single-probe

The fabrication process of the Single-probe has been described in previous studies.[17, 19] Briefly, there are three components in a Single-probe: a needle pulled from dual-bore quartz tubing (outer diameter (OD): 500 μm; inner diameter (ID): 127 μm, Friedrich & Dimmock, Inc., Millville, NJ, USA) using a laser pipet puller (P-2000 micropipette puller, Sutter Instrument, Novato, CA, USA), a fused silica capillary (OD: 105 μm; ID: 40 μm, Polymicro Technologies, Phoenix, AZ, USA), and a nano-ESI emitter produced using the same type of fused silica capillary. A Single-probe is fabricated by embedding a laser-pulled dual-bore quartz needle with a fused silica capillary and a nano-ESI emitter.

4.2.5 The Single-probe SCMS Set-up

Irinotecan-resistant cells and parental cells were attached on the glass sides through over-night culture, and slides containing cells were placed onto a motorized XYZ−translation stage system. The stage system was controlled using a LabView software package. A syringe (250 μl; Hamilton Co., Reno, NV, USA) was used to continuously provide the sampling solvent (acetonitrile; Sigma-Aldrich St. Louis, MO, USA), and a stable liquid junction was formed at the Single-probe tip to extract cellular contents during the experiment. Using the microscope as a visual guide, the tip of the

Single-probe (OD ~10 μm) was precisely inserted into a targeted cell. Cellular contents were withdrawn towards the nano-ESI emitter through the capillary action and immediately ionized by a voltage applied on the conductive union followed by MS analysis using a Thermo LTQ Orbitrap XL mass spectrometer (Thermo Scientific, Waltham, MA, USA). Mass analysis parameters are listed as follows: mass range (m/z), 200–1500; mass resolution, 60 000; ionization voltage at positive ion mode, +4.5 kV; microscan, 1; max injection time, 100 ms; AGC (automatic gain control) on.

4.2.6 Data analysis

The pretreatment of SCMS data was performed prior to statistical analysis. SCMS data (m/z values with their relative intensities) were exported as tab-delimited data files using Thermo Xcalibur Qual Browser (Thermo Scientific, Waltham, MA, USA). Only relatively abundant peaks (intensity > 10^3) were exported, whereas background signals, such as peaks from solvent and cell culture medium, were subtracted from MS data. To minimize the influence induced by fluctuations of ion signals during experiments, ion intensities were normalized to the total ion current (TIC). We used Geena 2 online software to preform peak alignment. Student's t-test (for data with equal variance) was then applied to obtain ions with significantly different abundance between two groups ($p < 0.05$).

4.2.7 Western blot analysis

Cell lysates were prepared using radioimmunoprecipitation assay (RIPA) buffer containing protease inhibitor (Thermo Scientific). Equal amount of proteins was separated by 12% sodium dodecyl sulfate-polyacrylamide gel electrophoresis (SDS-PAGE) and transferred to nitrocellulose membrane (GH, Healthcare Life Science).

Membrane was blocked by 10% non-fat milk (Bio-Rad) incubate overnight with primary antibody at 4°C. The following primary antibodies were used for Western blot: anti-SCD1 antibody (Thermo Fisher Scientific) and anti-tubulin antibody (Abcam, UK). The corresponding secondary antibody (Thermo Fisher Scientific) was added during the incubation (1hr, at room temperature), and then membranes were washed using PBS buffer for three times. Finally, protein bands were vitalized using the Opti-4CN western blot detection kit (Bio-Rad).

4.2.8 Flow cytometry analysis

The Stratedigm S1400Exi flow cytometer platform was used to determine the expression of cancer stem cell biomarker CD133 and CD24 in drug-resistant cells and parental cells. Briefly, cells were suspended in the solution containing 0.5% bovine serum albumin (BSA, Sigma-Aldrich, St. Louis) and antibodies (human anti-CD24-FITC and human anti-CD133-PE, Miltenyi Biotec) on ice. CD133 and CD24 double-positive cells (CD133+/CD24+) were gated using control cells that incubated with IgG1 isotype control FITC-conjugated antibody and PE-conjugated antibody (Biolegend, San Diego, CA).

For reactive oxygen species (ROS) detection, cells were incubated in McCoy's 5A cell culture medium containing 1μM CM-H2DCFDA (Thermo Fisher Scientific) for 30 min at 37 °C, and then washed with PBS buffer based on previous studies. Cells were analyzed using the Stratedigm S1400Exi flow cytometer platform.

4.2.9 RNA extraction and Quantitative real-time polymerase chain reaction (qPCR)

The RNeasy Mini Kit (Qiagen, Valencia, CA) was used to isolate RNA from cells according to the manufacturer's instructions. The potential genomic DNA contaminants

were removed using a DNA-free™ DNA Removal Kit (Thermo Fisher Scientific). iScript™ Reverse Transcription Supermix (Bio-Rad Laboratories, CA) was used to synthesize the cDNA, and then qPCR experiments were performed using a Bio-Rad CFX96 Touch™ Real-Time PCR Detection System using SsoAdvanced™ Universal SYBR® Green Supermix (Bio-Rad).

The sequences of the primers and annealing temperatures were as follows:

Scd1: (5'- TTCAGAAACACATGCTGATCCTCATAATTCCC-3' and 5'-ATTAAGCACCACAGCATATCGCAAGAAAGTGG-3'), CD133: (5'-CTGGGGCTGCTGTTTATTATTCTG-3' and 5'-ACGCCTTGTCCTTGGTAGTGTTG-3'),

CD24: (5'- TCCAAGGCACCCAGCATCCTGCTAGA-3' and 5'-TAGAAGACGTTTCTTGGCCTGAGTCT-3'), ALDH1A1: (5'-CGGGAAAAGCAATCTGAAGAGGG-3' and 5'-GATGCGGCTATACAACACTGGC-3')

Actin: (5'- CGTCACCAACTGGGACGACA-3' and 5'-CTTCTCGCGGTTGGCCTTGG-3')

The relative expression of each gene was calculated using the ΔΔCT method with CFX manager software (Bio-Rad), and the target gene expression was normalized by the endogenous housekeeping gene β-actin. In addition, No-RT controls and No-template controls were used to avoid potential genomic DNA/RNA contaminants or other technical contaminants.

4.3 Results

4.3.1 Irinotecan-resistant cells have higher abundance of unsaturated lipids and fatty acids than parental cells

Irinotecan resistant cells were established by exposure to irinotecan in cell culture medium for 3, 10 and 20 days. The drug resistance of each group of cells was determined by MTT viability assay for 72hr. As shown in Figure 4.1A, the MTT results indicated that parental cells were more sensitive to irinotecan compared to drug-treated cells with IC_{50} values of 3.0 μM, 5.3 μM, 7.8 μM and 11.0 μM. Previous studies demonstrated that the cell lines displaying two to eight folds resistance compared to parental cell lines could be considered as clinically relevant drug-resistant cells.[24] Therefore, based on the MTT test results, the cells treated with irinotecan for 10 days and 20 days are considered as drug-resistant cells.

In this study, our aim is to investigate the specific mechanism of cancer cells at the initial stage of irinotecan resistance, so cancer cells treated with irinotecan for 10days is our target. We compared the metabolic difference between irinotecan-resistant cells and parental cells based on the results obtained from single-probe mass spectrometry[20, 23, 25, 26], and single-probe based metabolomics studies provided metabolic clues to study the mechanism of irinotecan resistance. We found that irinotecan-resistant cells have significant higher levels of multiple unsaturated lipids, including PC(33:4), PC(34:4), PC(38:5), PC(34:3), PC(35:1), PC(36:3), PC(34:2), PC(34:1) and PC(36:6)) (Figure 4.1B). Moreover, four major fatty acids (C18:0 (stearic acid), C18:1 (oleic acid), C16:0 (palmitic acid) and C16:1 (palmitoleic acid)) were also enriched in irinotecan-resistant cells compared to control cells (Figure 4.1C). In addition, the ratios of monounsaturated

fatty acids (MUFAs) to saturated fatty acids (SFAs), such as palmitic acid/palmitoleic acid (C16:0/C16:1) and stearic acid/oleic acid (C18:0/C18:1), were dramatically increased in irinotecan-resistant cells, as shown in Figure 4.1D. Taken together, the single-cell metabolomics suggests that irinotecan-resistant cells have a much higher level of unsaturated lipids and fatty acids than control cells.

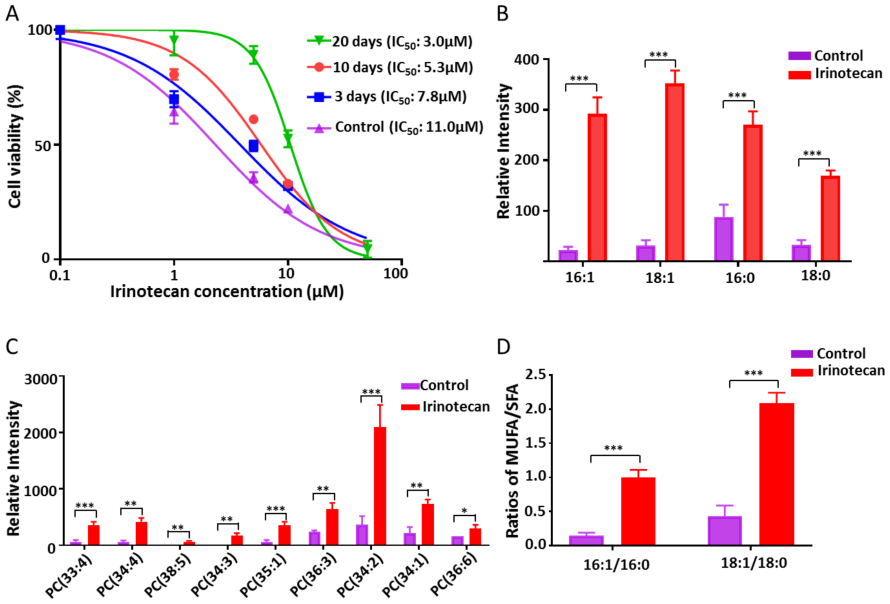

Figure 4.1 Irinotecan-resistant cells have high abundance of unsaturated lipids/fatty acids. (A) The IC_{50} of irinotecan against control, 3days, 10days and 20days treatment cells. (B) Relative abundances of fatty acids (C16:0, C16:1, C18:0, and C18:1) detected in drug-resistant cells and control cells. (C) Unsaturated lipids accumulated in irinotecan-resistant cells. (D) Ratios of unsaturated fatty acid (UFA) to saturated fatty acid (SFA) in drug-resistant cells and control cells. (From t-test: *, $p < 0.05$; **, $p < 0.01$; ***, $p < 0.001$.)

4.3.2 The high level of fatty acids/ lipids is mediated by SCD1

SCD1 is one of the most important desaturases that catalyzing SFAs to MUFAs, and the major products of SCD1 are oleic acid and palmitoleic acid.[27] Previous studies indicate that higher levels of unsaturated lipids and fatty acids are mainly produced by lipids desaturase SCD1 enzyme.[28] Therefore, we hypothesized that SCD1 induced the enrichment of unsaturated lipids and fatty acids in irinotecan-resistant cells. To investigate this hypothesis, we measured the SCD1 level through RT-PCR and western blotting, and SCD1 mRNA and protein levels were higher in irinotecan-resistant cells than in control cells (Figure 4.2A and 4.2B). Then we treated irinotecan-resistant cells with CAY10566, a specific inhibitor of SCD1[29], to further the study of functions of SCD1. CAY10566 significantly reduced the levels of multiple unsaturated lipids and dramatically suppressed the metabolic flux from SFAs to MUFAs (the ratios of C16:1/C16:0 and C18:1/C18:0) in irinotecan-resistant cells (Figure 4.2C-E). According to the result, SCD1 inhibitor altered the level of unsaturated lipids/ fatty acids in irinotecan-resistant cells, which is similar to the level in control cells. In conclusion, these results indicated that the high level of unsaturated lipids and fatty acids in irinotecan-resistant cells were induced by SCD1.

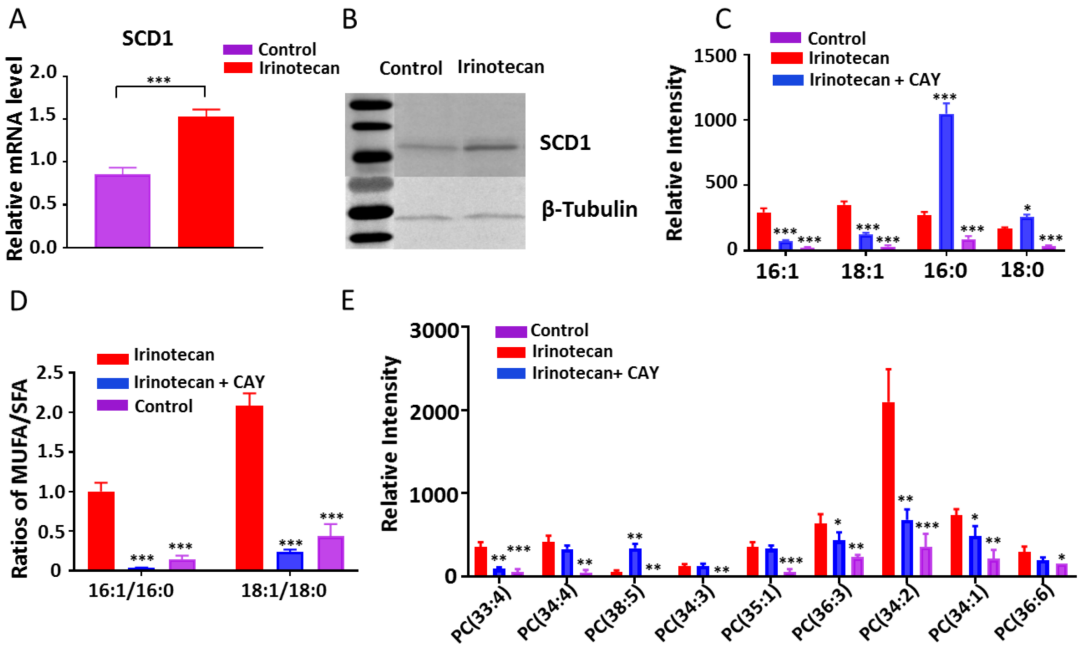

Figure 4.2 SCD1 upregulated in drug-resistant cells and mediated the high level of unsaturated lipids. (A) RT-PCR measurement of SCD1 mRNA level in drug-resistant cells and control cells. (B) Western blot for SCD1 protein expression in drug-resistant cells and control cells. SCD1 inhibitor has significantly decreased expression of (C) unsaturated fatty acids, (D) ratio of MUFA/SFA and (E) unsaturated lipids.

4.3.3 SCD1 modulates drug resistance in irinotecan-resistant cells

In order to investigate whether high SCD1 level played a role in the development of irinotecan resistance of colon cancer cells. We inhibited SCD1 activity by treating irinotecan-resistant cells with CAY10566 and the inhibition of SCD1 significantly reduced the resistance to irinotecan in drug-resistant cells, causing an around two-fold decrease of IC_{50} (Figure 4.3A). On the other hand, oleic acid is the major product of SCD1, and inhibiting the activity of SCD1 will apparently lead to a reduced production of oleic acid successfully rescued the cell viability under the treatment of CAY10566

(Figure 4.3B). Because oleic acid is an important product of ALDH1A1 inhibiting the activity of ALDH1A1 will apparently lead to a reduced production of RA. This consequence is likely related to the altered properties of CSCs such as the reduced stemness. It is reasonable to hypothesize that increasing RA supply during the cell culture will likely alleviate the inhibition by CM037. Taken together, SCD1 activity modulates the irinotecan resistance.

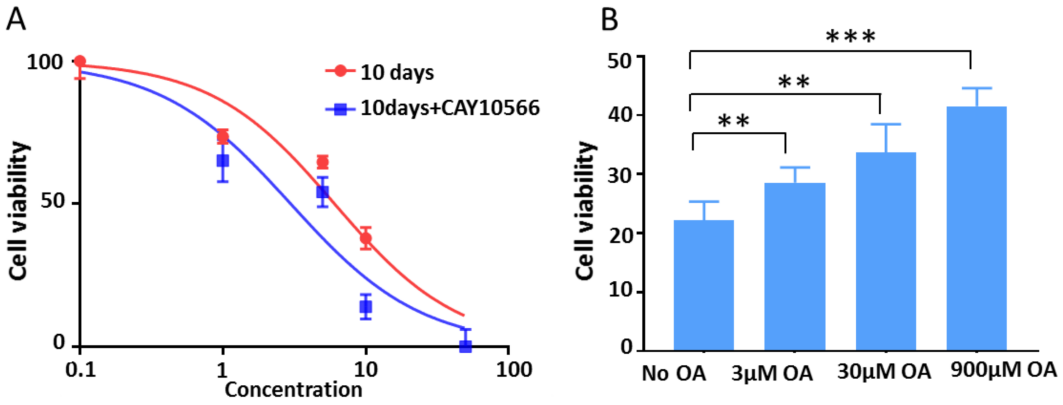

Figure 4.3 SCD1 affected the drug resistance in irinotecan-resistant cells. (A) The IC_{50} of control, irinotecan and irinotecan inhibitor treated groups against irinotecan. (B) Cell proliferation of HCT116 cells were measured under treatment of irinotecan, irinotecan inhibitor and oleic acid separately.

4.3.4 Irinotecan treatment induced cancer stemness in irinotecan-resistant cells

Previous studies found that cancer therapy (e.g., radiochemotherapy and chemotherapy) could directly transform the non-stem cancer cells (NSCCs) into induced cancer stem cells (iCSCs), which contain relatively higher levels of SCD1 and unsaturated lipids. Moreover, iCSCs generally have high drug resistance compared to non-stem cancer cells. Therefore, we investigate whether SCD1 could induce the

stemness in irinotecan-resistant cells. We compared the lipid pattern among the control cells, irinotecan-resistant cells and CSCs. As shown in Figure 4A, the overall unsaturated lipids level in 10-day irinotecan-resistant cells and CSCs are higher than the levels in control cells. Likewise, major fatty acid levels, as well as the ratio of MUFAs/SFAs, in irinotecan-resistant cells were close to CSCs (Figure 4B and 4C). To further investigate the stemness of irinotecan-resistant cells, we measured the levels of three colon CSCs biomarkers (CD133, CD24, and ALDH1A1). The mRNA levels of ALDH1A1, CD133 and CD24 were significantly increased in irinotecan-resistant cells compared to control cells (Figure 4D), and the enrichment of CD133 and CD24 in irinotecan-resistant cells also were also been confirmed by flow cytometry assay (Figure 4E and 4F). Therefore, these results indicate that irinotecan-resistant cells acquired stemness.

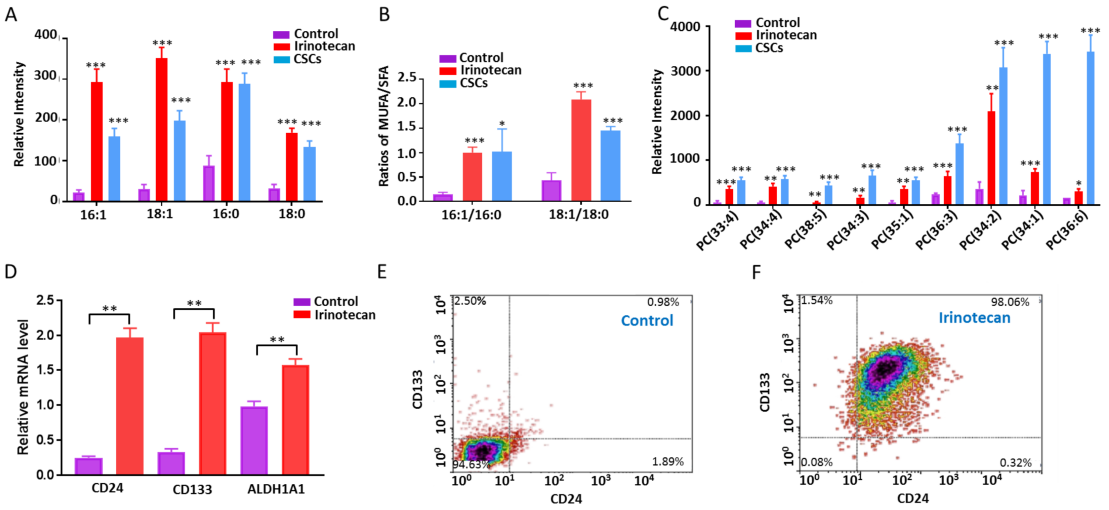

Figure 4.4 Influence of irinotecan treatment on cancer stemness. 10-day irinotecan-resistant cells possess similar metabolic features as the CSCs, including (A) levels of unsaturated fatty acids, (B) ratios of MUFA/SFA, and (C) levels of unsaturated lipids.

(D) RT-PCR measurements of mRNA levels of CD24, CD 133, CD ALDH1A1 in 10-day drug-resistant and control cells. Flow cytometry measurement of CD24 and CD133 CSC surface biomarkers in (E) control and (F) 10-day drug-resistant cells.

4.3.5 SCD1 regulates the expression of cancer stem cell biomarker ALDH1A1

Given that SCD1 are essential for the maintenance of stemness in CSCs[22], we investigated whether a high level of SCD1 could promote the development of stemness in irinotecan-resistant cells. We treated 10-day irinotecan-resistant cells with SCD1 inhibitor (CAY10566), and results indicated that inhibiting SCD1 has no significant influence on the expression level of CD24 and CD133 in drug-resistant cells. However, interestingly, CAY10566 significantly reduced the mRNA level ALDH1A1. Moreover, oleic acid, the major product of SCD1, could successfully rescue the mRNA level of ALDH1A1 in 10-day irinotecan-resistant cells under CAY10566 treatment (Figure 4.5A). These results suggest that SCD1 specifically upregulates the expression of ALDH1A1, which potentially promotes the stemness development of IR cells.

4.3.6 ALDH1A1 were associated to the reactive oxygen species (ROS) level in drug-resistant cells

The function of ALDH1A1 is to catalyze oxidation of aldehydes, which contributes to the cellular detoxification, retinoic acid metabolism, and protection from reactive oxygen species (ROS)[24, 25]. Moreover, high level of ROS can induce oxidative stress and promote cell death in cancer cells. For example, multiple anticancer drugs can result in the enrichment of ROS to induce cell apoptosis[26, 27]. To further understand the role of ALDH1A1 in the irinotecan-resistant cells, we suppressed ALDH1A1 activity using its inhibitor (N, N-diethylaminobenzaldehyde, DEAB). As

shown in Figure 4.5B, the ROS level was significantly increased by DEAB in 10-day IR cells. In contrast, adding retinoic acid, which is a major product of ALDHIA1, drastically decreased the ROS level. Likewise, SCD1 inhibitor (CAY10566) also increased the ROS level in IR cells, whereas oleic acid (a major product of SCD1) rescued the inhibition (Figure 4.5B). Our results indicate that in irinotecan-resistant cells contain overexpressed SCD1, which further results in upregulated ALDH1A1, promoted stemness, and decreased ROS level. All above factors contribute to increased drug resistance.

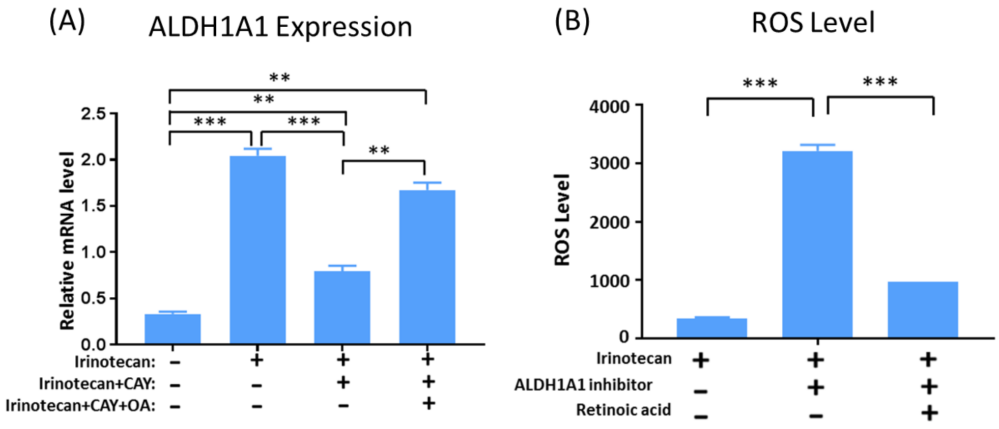

Figure 4.5 Influence of SCD1 on the expression of ALDH1A1 and the level of ROS. Measurements of (A) ALDH1A1 mRNA and (B) ROS of 10-day IR cells under different treatment conditions.

4.4 Discussion

Irinotecan is a widely used antitumor drug to against multiple cancers, including brain cancer, breast cancer, lung cancer, and especially metastatic colon caner. Specifically, irinotecan is the first- or second-line treatment for metastatic colon cancer.[28-30] Irinotecan targets DNA topoisomerase I, and results in double–stand DNA breakage and finally causes cell death.[31-33] However, the clinical activity of irinotecan

is frequently limited by de novo or acquired clinical resistance.[34, 35] Previous studies found the chemoresistance of cancer cells is generally associated with metabolic reprogramming.[36-39]. For example, to escape from the irinotecan chemotoxity, cancer cells may require a large supply of metabolic substrates to access a series of defense activities through enhancing glycolysis and lipogenesis.[36, 40] For example, it has been reported lipid accumulation occurs in cancer cells with irinotecan treatment,[41] and de novo lipids synthesis enzymes were enriched in the irinotecan resistance cells. [42] However, it is still unknown how lipogenesis contributes to irinotecan resistance.

The current study revealed a novel mechanism that irinotecan induces the activation of lipid desaturase SCD1, resulting in accumulations of unsaturated lipids/fatty acids. SCD1 is one of the major lipid desaturases catalyzing the conversion of SFAs (e.g., stearic (C18:0) and palmitic acid (C16:0)) to MUFAs (e.g., oleic acid (C18: 1) and palmitoleic acid (C16: 1)) in mammalian cells. In addition, SCD1 stimulates the conversion of FAs into triglycerides, phospholipids, and cholesterol ester, which contribute to cell membrane synthesis during cell mitosis. However, little is known about the role of SCD1 in irinotecan-resistant cells. Previous studies indicated that the inhibition of SCD1 impacted cell growth and proliferation process, and overexpressed SCD1 facilitated tumor survival in liver, lung, and pancreatic cancers. Moreover, inhibiting SCD1 reverted the resistance to cisplatin and sorafenib in different types of CSCs such as lung, hepatocellular carcinomas, and ovarian CSCs. These studies implied the importance of SCD1 in chemoresistance. For the first time, we demonstrated the SCD1 could enhance the resistance to irinotecan in HCT-116 colon cancer cell line.

Interestingly, we found irinotecan treatment produced drug-resistance cells possessing features of CSCs, i.e., overexpressed CSC biomarkers CD133, CD24, and ALDH1A1[43], compared with their parental cells. CSCs are a rare subset of cancer cells with the ability to self-renew, initiate tumors, and resistant chemotherapy.[44] In general, CSCs confers the resistance to traditional therapeutic methods through multiple ways, including entering a protective quiescent state, up-regulating the expression of ABC transporters, and decreasing ROS level.[45] Recent studies indicated that the ionizing radiotherapy could generate CSCs by dedifferentiation of NSCCs through up-regulated signaling pathways (e.g., Notch, Wnt, ect.).[13] Because SCD1 is an important intermediate in Wnt protein biogenesis[46], it is suggested as a key factor affecting cancer stemness and tumor initiation capacity in ovarian and colon CSCs.[18, 22] Our current study indicate that the levels of unsaturated lipids/fatty acids and the ratios of MUFA/SFA in irinotecan-resistant cells are comparable to those CSCs compared to parental cells. According to previous studies, the ratio of palmitic acid/palmitoleic acid (C16:0/C16:1) and stearic acid/oleic acid (C18:0/C18:1) reflect the expression and activity of SCD1 enzyme[47]. These results may suggest that SCD1 contributes to the development of cancer stemness in irinotecan-resistant cells. Thus, a better understanding of the potential role of SCD1 in the characteristics of irinotecan resistance cells, especially the development of cancer stemness, is of great significance for study the mechanism of irinotecan resistance. However, inhibiting the activity of SCD1 had no significant influence on the expression of CD133 and CD24, whereas the level of ALDH1A1 mRNA drastically decreased after treatment with CAY10566. In general, SCD1 specifically regulate the expression of ALDH1A1 rather than other CSCs

biomarkers. ALDH1A1 is a well-known CSCs biomarker[48, 49], and its major function is to oxidize retinal to retinoic acid (RA), which contributes to the cellular detoxification, retinoic acid metabolism, and protection from oxygen species (ROS) in CSCs[50]. Previous studies indicate that ROS belong to metabolomic byproducts of aerobic respiration, and they play essential roles to maintain redox homeostasis. Increased levels of ROS induce oxidative stress and DNA damage, and eventually lead cell death.[51] Our experimental results indicate that inhibiting the activity of ALDH1A1 and SCD1 can significantly increase the ROS level, suggesting SCD1 and ALDH1A1 can likely protect cancer cells from apoptosis by maintaining the level of ROS.

Our finding demonstrates that the irinotecan-resistant cells upregulate the expression of SCD1, and result in higher levels of unsaturated lipids/fatty acids, which can be potential biomarkers of drug resistance. In addition, SCD1 directly regulates the expression of ALDH1A1, a stem cell biomarker of colon cancer, and contributes to the generation of the CSCs. Moreover, ALDH1A1 protects cancer cells from irinotecan chemotherapy by decrease the level of ROS to avoid apoptosis. Given the important role of SCD1 in irinotecan-resistant cells, combining SCD1 inhibitors and irinotecan can be potentially effective for colon cancer treatment.

4.5 Reference

[1] R. Siegel, K. Miller, A. Jemal, Cancer statistics, 2018, CA: Cancer J. Clin., 68 (2018) 7-30.

[2] J. Mishra, J. Drummond, S.H. Quazi, S.S. Karanki, J. Shaw, B. Chen, N. Kumar, Prospective of colon cancer treatments and scope for combinatorial approach to enhanced cancer cell apoptosis, Crit. Rev. Oncol. Hematol. , 86 (2013) 232-250.

[3] K. Van der Jeught, H.-C. Xu, Y.-J. Li, X.-B. Lu, G. Ji, Drug resistance and new therapies in colorectal cancer, World J. Gastroenterol., 24 (2018) 3834.

[4] G. Housman, S. Byler, S. Heerboth, K. Lapinska, M. Longacre, N. Snyder, S. Sarkar, Drug resistance in cancer: an overview, Cancers, 6 (2014) 1769-1792.

[5] M.M. Gottesman, Mechanisms of cancer drug resistance, Annu. Rev. Med. , 53 (2002) 615-627.

[6] X. Chen, R. Liao, D. Li, J. Sun, Induced cancer stem cells generated by radiochemotherapy and their therapeutic implications, Oncotarget, 8 (2017) 17301.

[7] M. Nishi, H. Akutsu, A. Kudoh, H. Kimura, N. Yamamoto, A. Umezawa, S.W. Lee, A. Ryo, Induced cancer stem-like cells as a model for biological screening and discovery of agents targeting phenotypic traits of cancer stem cell, Oncotarget, 5 (2014) 8665.

[8] L.B. Saltz, J.V. Cox, C. Blanke, L.S. Rosen, L. Fehrenbacher, M.J. Moore, J.A. Maroun, S.P. Ackland, P.K. Locker, N. Pirotta, Irinotecan plus fluorouracil and leucovorin for metastatic colorectal cancer, N. Engl. J. Med., 343 (2000) 905-914.

[9] J.A. Conti, N.E. Kemeny, L.B. Saltz, Y. Huang, W.P. Tong, T.-C. Chou, M. Sun, S. Pulliam, C. Gonzalez, Irinotecan is an active agent in untreated patients with metastatic colorectal cancer, J. Clin. Oncol., 14 (1996) 709-715.

[10] J. Douillard, D. Cunningham, A. Roth, M. Navarro, R. James, P. Karasek, P. Jandik, T. Iveson, J. Carmichael, M. Alakl, Irinotecan combined with fluorouracil compared with fluorouracil alone as first-line treatment for metastatic colorectal cancer: a multicentre randomised trial, Lancet, 355 (2000) 1041-1047.

[11] Y. Kawato, M. Aonuma, Y. Hirota, H. Kuga, K. Sato, Intracellular roles of SN-38, a metabolite of the camptothecin derivative CPT-11, in the antitumor effect of CPT-11, Cancer Res., 51 (1991) 4187-4191.

[12] R.H. Mathijssen, R.J. Van Alphen, J. Verweij, W.J. Loos, K. Nooter, G. Stoter, A. Sparreboom, Clinical pharmacokinetics and metabolism of irinotecan (CPT-11), Clin. Cancer Res., 7 (2001) 2182-2194.

[13] Y.-H. Hsiang, R. Hertzberg, S. Hecht, L. Liu, Camptothecin induces protein-linked DNA breaks via mammalian DNA topoisomerase I, J. Biol. Chem., 260 (1985) 14873-14878.

[14] Y. Xu, M. Villalona-Calero, Irinotecan: mechanisms of tumor resistance and novel strategies for modulating its activity, Ann. Oncol., 13 (2002) 1841-1851.

[15] A. Petitprez, A. K Larsen, Irinotecan resistance is accompanied by upregulation of EGFR and Src signaling in human cancer models, Curr. Pharm. Des., 19 (2013) 958-964.

[16] M.L.V. Costa, R.C.P. Lima-Júnior, K.S. Aragão, R.P. Medeiros, R.D. Marques-Neto, L. de Sá Grassi, L.L. Leite, L.G. Nunes, J.W.B. de Mesquita Neto, G.A. de Castro Brito,

Chemotherapy-associated steatohepatitis induced by irinotecan: a novel animal model, Cancer Chemother. Pharmacol., 74 (2014) 711-720.

[17] Y. Zhou, L.R. Bollu, F. Tozzi, X. Ye, R. Bhattacharya, G. Gao, E. Dupre, L. Xia, J. Lu, F. Fan, ATP citrate lyase mediates resistance of colorectal cancer cells to SN38, Mol. Cancer Ther., (2013) molcanther. 0098.2013.

[18] X. Bao, J. Wu, S. Kim, P. LoRusso, J. Li, Pharmacometabolomics Reveals Irinotecan Mechanism of Action in Cancer Patients, J. Clin. Pharmacol., (2019).

[19] M. McDermott, A. Eustace, S. Busschots, L. Breen, M. Clynes, N. O'Donovan, B. Stordal, In vitro development of chemotherapy and targeted therapy drug-resistant cancer cell lines: a practical guide with case studies, Front Oncol., 4 (2014) 40.

[20] N. Pan, W. Rao, N.R. Kothapalli, R. Liu, A.W. Burgett, Z. Yang, The single-probe: a miniaturized multifunctional device for single cell mass spectrometry analysis, Anal. Chem., 86 (2014) 9376-9380.

[21] M. Sun, Z. Yang, Metabolomic Studies of Live Single Cancer Stem Cells Using Mass Spectrometry, Anal. Chem., 91 (2018) 2384-2391.

[22] W. Rao, N. Pan, Z. Yang, Applications of the Single-probe: Mass Spectrometry Imaging and Single Cell Analysis under Ambient Conditions, J. Vis. Exp., (2016) e53911-e53911.

[23] M. Sun, X. Tian, Z. Yang, Microscale Mass Spectrometry Analysis of Extracellular Metabolites in Live Multicellular Tumor Spheroids, Anal. Chem., (2017).

[24] M. McDermott, A. Eustace, S. Busschots, L. Breen, M. Clynes, N. O'Donovan, B. Stordal, In vitro development of chemotherapy and targeted therapy drug-resistant cancer cell lines: a practical guide with case studies, Front. Oncol. , 4 (2014) 40.

[25] N. Pan, W. Rao, S.J. Standke, Z. Yang, Using Dicationic Ion-Pairing Compounds To Enhance the Single Cell Mass Spectrometry Analysis Using the Single-Probe: A Microscale Sampling and Ionization Device, Anal. Chem., 88 (2016) 6812.

[26] M. Sun, Z. Yang, Metabolomic Studies of Live Single Cancer Stem Cells Using Mass Spectrometry, Anal. Chem., (2018).

[27] A.D. Southam, F.L. Khanim, R.E. Hayden, J.K. Constantinou, K.M. Koczula, R.H. Michell, M.R. Viant, M.T. Drayson, C.M. Bunce, Drug redeployment to kill leukemia and lymphoma cells by disrupting SCD1-mediated synthesis of monounsaturated fatty acids, Cancer Res., 75 (2015) 2530-2540.

[28] J. Li, S. Condello, J. Thomes-Pepin, X. Ma, Y. Xia, T.D. Hurley, D. Matei, J.-X. Cheng, Lipid desaturation is a metabolic marker and therapeutic target of ovarian cancer stem cells, Cell stem cell, 20 (2017) 303-314. e305.

[29] G. Liu, J.K. Lynch, J. Freeman, B. Liu, Z. Xin, H. Zhao, M.D. Serby, P.R. Kym, T.S. Suhar, H.T. Smith, Discovery of potent, selective, orally bioavailable stearoyl-CoA desaturase 1 inhibitors, J. Med. Chem., 50 (2007) 3086-3100.

[30] S. Singh, C. Brocker, V. Koppaka, Y. Chen, B.C. Jackson, A. Matsumoto, D.C. Thompson, V. Vasiliou, Aldehyde dehydrogenases in cellular responses to oxidative/electrophilicstress, Free Radic Biol Med, 56 (2013) 89-101.

[31] D.W. Clark, K. Palle, Aldehyde dehydrogenases in cancer stem cells: potential as therapeutic targets, Ann Transl Med., 4 (2016).

[32] I.S. Okon, M.-H. Zou, Mitochondrial ROS and cancer drug resistance: Implications for therapy, Pharmacol. Res, 100 (2015) 170-174.

[33] A.T. Dharmaraja, Role of reactive oxygen species (ROS) in therapeutics and drug resistance in cancer and bacteria, J. Med. Chem., 60 (2017) 3221-3240.

[34] S. Dai, Y. Yan, Z. Xu, S. Zeng, L. Qian, L. Huo, X. Li, L. Sun, Z. Gong, SCD1 Confers Temozolomide resistance to human glioma cells via the Akt/GSK3β/β-Catenin signaling axis, Front Pharmacol., 8 (2018) 960.

[35] F. Guerra, A.A. Arbini, L. Moro, Mitochondria and cancer chemoresistance, Biochim Biophys Acta Mol Basis Dis., 1858 (2017) 686-699.

[36] F. Guerra, A.A. Arbini, L. Moro, Mitochondria and cancer chemoresistance, Biochim. Biophys. Acta, 1858 (2017) 686-699.

[37] X. Qian, W. Xu, J. Xu, Q. Shi, J. Li, Y. Weng, Z. Jiang, L. Feng, X. Wang, J. Zhou, Enolase 1 stimulates glycolysis to promote chemoresistance in gastric cancer, Oncotarget, 8 (2017) 47691.

[38] Y. Zhao, E.B. Butler, M. Tan, Targeting cellular metabolism to improve cancer therapeutics, Cell Death Dis., 4 (2013) e532.

[39] M. Lindskog, C. Spenger, J.r. Jarvet, A. Gräslund, P. Kogner, Predicting resistance or response to chemotherapy by proton magnetic resonance spectroscopy in neuroblastoma, J. Natl. Cancer Inst., 96 (2004) 1457-1466.

[40] Y. Zhou, L.R. Bollu, F. Tozzi, X. Ye, R. Bhattacharya, G. Gao, E. Dupre, L. Xia, J. Lu, F. Fan, ATP citrate lyase mediates resistance of colorectal cancer cells to SN38, Mol Cancer Ther. , (2013) molcanther. 0098.2013.

[41] R.C. Langan, J.E. Mullinax, M.T. Raiji, T. Upham, T. Summers, A. Stojadinovic, I. Avital, Colorectal cancer biomarkers and the potential role of cancer stem cells, J. Cancer, 4 (2013) 241.

[42] B. Bao, A. Ahmad, A.S. Azmi, S. Ali, F.H. Sarkar, Overview of cancer stem cells (CSCs) and mechanisms of their regulation: implications for cancer therapy, Curr Protoc Pharmacol. , 61 (2013) 14.25. 11-14.25. 14.

[43] M. Prieto-Vila, R.-u. Takahashi, W. Usuba, I. Kohama, T. Ochiya, Drug resistance driven by cancer stem cells and their niche, Int. J. Mol. Sci., 18 (2017) 2574.

[44] J. Rios-Esteves, M.D. Resh, Stearoyl CoA desaturase is required to produce active, lipid-modified Wnt proteins, Cell Rep., 4 (2013) 1072-1081.

[45] N. Rodriguez‐Perez, E. Schiavi, R. Frei, R. Ferstl, P. Wawrzyniak, S. Smolinska, M. Sokolowska, N. Sievi, M. Kohler, P. Schmid‐Grendelmeier, Altered fatty acid metabolism and reduced stearoyl‐coenzyme a desaturase activity in asthma, Allergy, 72 (2017) 1744-1752.

[46] K. Phoenix, X. Hong, S. Tannenbaum, K. Claffey, Expression of the Cancer Stem Cell Marker ALDH1A1 in Primary Breast Cancer: A Mechanism for Chemotherapy Resistance, AACR, 2009.

[47] C. Kahlert, E. Gaitzsch, G. Steinert, C. Mogler, E. Herpel, M. Hoffmeister, L. Jansen, A. Benner, H. Brenner, J. Chang-Claude, Expression analysis of aldehyde dehydrogenase 1A1 (ALDH1A1) in colon and rectal cancer in association with prognosis and response to chemotherapy, Ann. Surg. Oncol, 19 (2012) 4193-4201.

[48] S. Singh, C. Brocker, V. Koppaka, Y. Chen, B.C. Jackson, A. Matsumoto, D.C. Thompson, V. Vasiliou, Aldehyde dehydrogenases in cellular responses to oxidative/electrophilicstress, Free Radic Biol Med., 56 (2013) 89-101.

[49] C. Yokoyama, Y. Sueyoshi, M. Ema, Y. Mori, K. Takaishi, H. Hisatomi, Induction of oxidative stress by anticancer drugs in the presence and absence of cells, Oncol. Lett., 14 (2017) 6066-6070.

Chapter 5 Microscale Mass Spectrometry Analysis of Extracellular Metabolites in Live Multicellular Tumor Spheroids

5.1 Introduction

Cancer recurrence is one of the major threats for the health of patients receiving chemotherapy.[1, 2] For example, around 40% patients with breast cancers can develop recurrent metastatic diseases after chemotherapy.[3, 4] Recent studies indicate that central tumor cells play crucial roles in cancer recurrence.[5, 6] Due to the distribution gradients of oxygen, nutrients, and energy, tumors possess gradients of proliferation cells and metabolites abundances from outer to inner regions.[7-9] Generally, central tumor cells stop cell cycle progression and become dormant due to their microenvironment, while cells in outer regions of tumors have high proliferative activities.[5] Because cytostatic drugs mainly target proliferating cells, central cancer cells with low proliferating rate could survive from drug treatment and potentially cause the disease relapse after the therapy.[5, 6, 10] Previous studies found that extracellular compounds are critical in multiple biological behaviors of tumors,[11, 12] including tumor growth and progression, cell-cell communication, and cancer cell migration and metastasis.[13, 14] Studying extracellular compounds produced by central tumor cells can potentially identify more specific cancer biomarkers, reveal the characteristic responses of cancer cell under drug treatment, and provide guidelines for the amelioration of current cancer therapies.

Conventionally, two-dimensional (2D) cell monolayers are widely used for drug discovery studies.[15] However, results obtained from 2D cultured cells cannot be directly translated into *in vivo* settings because of their totally different microenvironment compared with cells in actual tissues. For example, the 2D cell monolayers are exposed to

sufficient oxygen and nutrients, whereas the microenvironment of cells in solid tumors contains gradients of oxygen, energy, and some critical chemicals.[16] Previous studies indicate that the extracellular compounds secreted by 2D-cultured cells are much less abundant than those in a three-dimensional (3D) environment, suggesting that interactions among cells in 2D models are different from those in 3D environment.[17] It is evident that, compared with 2D culture, 3D cell cultures can better mimic the microenvironment and cell-cell interactions of *in vivo* tumors.[18] The multicellular tumor spheroids (hereinafter referred to as spheroids) are widely used 3D tumor models.[19, 20] Spheroids have been proven to possess numerous characteristics similar to *in vivo* tumors, such as extracellular compounds and protein production patterns,[20, 21] making them more accurate ideal models for the research of extracellular molecules.

However, studies of broad ranges of molecules inside live tumors have not been widely carried out due to the lack of appropriate analytical techniques. In a long time, the detection of extracellular biomolecules is limited by their low concentrations, especially once they diffuse into the cell culture medium or dilute in body fluid. Microdialysis devices, which use a semipermeable membrane to enrich molecules, have been utilized to study the extracellular compounds of tumors or tissues.[22-24] However, the general sizes of microdialysis probes range between 200 and 500 μm, with the smallest one around 200 μm,[25-27] resulting in limited spatial resolution. Therefore, it is very challenging to use these techniques to study relatively small targets such as spheroids (sizes are generally less than 1 mm),[19-21] tumors at early stages, or small regions inside large tissues. In addition, lipophilic compounds may be retained by the tubing or other

probe components, resulting in a discrepancy of components sampling and low or no analyte recovery the amount of sample solution needed.[28, 29]

In this study, we developed a microscale device, the micro-funnel, to collect the extracellular molecules produced from cells in the central region of spheroids. The micro-funnel has a small tip size (~25 μm), which allows it to be implanted into a live spheroid for direct collection of extracellular compounds without being diluted and selected. A Single-probe device is inserted into the orifice of the micro-funnel to extract the collected extracellular molecules for direct MS analysis. The Single-probe is a miniaturized multifunctional sampling and ionization device that can be coupled with MS for the real-time microscale bioanalysis. The Single-probe MS techniques have been successfully used to study live single cells (single cell MS), and to map biomolecules on animal tissues (MS imaging) with high spatial resolutions.[30-34] Due to its extremely small sampling probe size (<10 μm) and high efficiency of extraction and ionization, the Single-probe is an ideal device to analyze small amounts of biomolecules collected in the micro-funnel device. By combining the micro-funnel with the Single-probe, we measured anticancer drug irinotecan and its major metabolites in the central region of spheroids, and determined their abundance changes under different treatment concentrations and time lengths. In addition, we investigated the influence of irinotecan treatment on the compositions of extracellular metabolites. Our study provides a new tool for the research of extracellular drug metabolites and cell metabolites in live spheroids.

5.2 Experimental section

5.2.1 Fabricate the Single-probe and the micro-funnel

The detailed fabrication protocols of the Single-probe were provided in our previous work.[30, 34] Briefly, a Single-probe (Figure 5.1(a)) consists of three components: a dual-bore quartz tubing (outer diameter (OD) 500 μm; inner diameter (ID) 127 μm, Friedrich & Dimmock, Inc., Millville, NJ, USA) pulled using a laser pipette puller (P-2000 micropipette puller, Sutter Instrument, Novato, CA, USA), a fused silica capillary (OD 105 μm; ID 40 μm, Polymicro Technologies, Phoenix, AZ, USA), and a nano-ESI emitter produced using the same type of fused silica capillary. A Single-probe is fabricated by embedding a laser-pulled dual-bore quartz needle with a fused silica capillary and a nano-ESI emitter.[30, 34] The micro-funnel (Figure 5.1(b)) is produced using a fused silica capillary (OD 360 μm; ID 70 μm, Polymicro Technologies, Phoenix, AZ, USA). Upon removing the coating material, the fused silica capillary is pulled using the laser pipette puller (tip size ~25 um), and cut into a micro-funnel with a desired length (~5 mm).

5.2.2 Implant micro-funnels in spheroids

The colon carcinoma cell line HCT-116 was used as the model to culture spheroids. First, we cultured cells following the standard protocols. Cells were cultured in McCoy's 5A cell culture medium (Life Technologies, Grand Island, NY, USA) containing 10% FBS (fetal bovine serum; Life Technologies, Grand Island, NY, USA) and 1% Pen Strep (Life Technologies, Grand Island, NY, USA). A CO_2 incubator (HeraCell, Heraeus, Germany) was used to culture cells under well-controlled conditions (5% CO_2, 37 °C), and cell passage was performed every two days. Second, we cultured spheroids using

HCT-116 cells. The culture protocol of spheroids was generally adopted from previous studies with some modifications.[35-37] To foster the accumulation of cells and promote the success rate of culturing spheroids, agarose-coated 96-well plates (with U-bottom wells) were utilized in our modified protocols. Briefly, 60 µL of agarose gel (1.8 %; Sigma-Aldrich, St. Louis, MO, USA) was added into individual wells in a 96-well plate (U-bottom; VWR, Radnor, PA, USA). 200 µl of cell solution (containing ~12,000 cells) was added into the agarose-coated wells, and the micro-funnel was horizontally placed on the top of agarose coating with its tip positioned in the well center. Because the fused silica is a biocompatible material,[38] cells incubated under normal conditions (5% CO_2, 37 °C) can attach to and grow around the micro-funnel tip. Culture medium was changed every 48 hours, and spheroids with implanted micro-funnels were collected after 14 days of culture. Using an inverted microscope, we selected the similar size (diameters ~1 mm) of spheroids, in which the micro-funnels tips were implanted in the center regions. Eight (n = 8) samples were used in each group for drug treatment and control experiments. The screening process and replicated measurements allow us to minimize the influence of sample variation on experimental results.

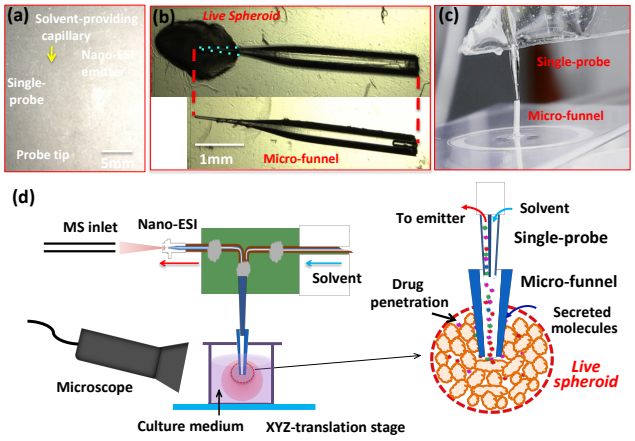

Figure 5.1 The combined micro-funnel and Single-probe technique for MS analysis of extracellular compounds in live spheroids. (a) A photo of a Single-probe device. (b) A photo of a micro-funnel before and after implanted into a spheroid. (c) Coupled micro-funnel and Single-probe device. (d) Real-time MS analysis of extracellular compounds in a live spheroid using the coupled micro-funnel and Single-probe device.

5.2.3 Drug treatment of spheroids

Irinotecan was purchased from Life Technologies (Grand Island, NY, USA). The stock solution of irinotecan was prepared in dimethyl sulfoxide (DMSO; Sigma-Aldrich, St. Louis, MO, USA), and further diluted into McCoy's 5A cell culture medium to prepare drug solutions with a series of concentrations. To perform drug treatment, a plastic microscope slide (VWR, Radnor, PA, USA) with a pinhole (diameter: ~360 um) was prepared and placed on the top a well in the 96-well plate (Figure 5.1(c)). The pinhole on the plastic slide was used to vertically hold the micro-funnel implanted into a spheroid. Irinotecan solutions were added into wells to submerge spheroid, whereas the orifice of the micro-funnel was retained above the treatment solution, eliminating any infusion of treatment solution into micro-funnels. We have conduced both concentration- and time-dependent studies. In the concentration-dependent experiments, spheroids were treated for 5 hrs using a series of concentrations (5, 20.6, 50, 100, 200, 300, 400, and 500 μM). In time-dependent studies, we used the IC_{50} of irinotecan (20.6 uM)[39] and treated them for various lengths of time (5, 12, 24, and 48 hrs). Untreated spheroids were used as the control group in experiments.

5.2.4 Couple the Micro-funnel with the Single-probe MS setup

The extracellular contents collected in the micro-funnel present in a very small volume (~1.2 nL) that is challenging for conventional MS analysis. The Single-probe device, which is designed for microscale MS analysis, is appropriate for analysis of molecules collected in the micro-funnel. To conduct an experiment, the 96-well plates containing spheroids were placed on a home-built XYZ−translation stage system (Figure 5.1(d)),[30, 34] and the spatial motion of the stage was controlled with the LabView software package.[40] Using the microscope as a visual guide, the tip of the Single-probe (OD ~10 μm) was precisely placed on the orifice of a micro-funnel (ID ~70 μm); a small gap between the Single-probe tip and micro-funnel orifice is present due to the size difference. The sampling solvent (acetonitrile; Sigma-Aldrich St. Louis, MO, USA) was continuously provided (~0.1μL/min) by a syringe (250 μl; Hamilton Co., Reno, NV, USA), and a liquid junction formed at the Single-probe tip performs a highly efficient extraction of extracellular contents collected inside the micro-funnel. The extracted molecular species were withdrawn by the nano-ESI emitter through the capillary action, and immediately ionized by a voltage applied on the conductive union followed by MS analysis using a Thermo LTQ Orbitrap XL mass spectrometer (Thermo Scientific, Waltham, MA, USA). Mass analyze parameters are listed as follows: mass range (m/z = 200−1,500), mass resolution 60,000, +4 kV ionization voltage at positive ion mode, 1 microscan, 100 ms max injection time, and AGC (automatic gain control) on.

Under the optimized conditions, stable ion signals can be obtained without having bubbles inside the emitter (i.e., solvent flow rate is too low) or solvent dripping on the Single-probe tip (i.e., solvent flow rate is too high). Due the gap between the Single-

probe tip and micro-funnel orifice as well as the optimized flow rate, the sampling solvent is unlikely to be delivered into spheroids through the micro-funnel affecting cell growth environment. The solvent transport through diffusion is also negligible. A MS measurement of a spheroid is usually accomplished within 5 minutes, which is marginal compared with the time needed for acetonitrile molecules to diffuse through the micro-funnel to reach cells (~1.2 hrs). The diffusion time can be estimated using $t = x^2/2D$, in which x (5 mm) is the diffusion distance and D (1.445×10^{-5} cm^2/s) is the diffusion coefficient of acetonitrile in water.

5.2.5 Data processing

The molecular identification of irinotecan and its metabolites was performed by comparing their accurate *m/z* values with theoretical results. More confident analyses were carried by conducting tandem MS analysis (MS/MS or MS^2, i.e. fragments analysis of selected ions) and comparing with results from the standard irinotecan sample and published work.[39, 41] However, a real biological tissue consists of complex histological structures and chemical components, and a large amount of information is present within each mass spectrum. Manual analysis of MS data can only provide the limited and selected information of species among numerous amounts of data. In contrast, statistical analysis methods, including Principle Component Analysis (PCA), t-test, and Analysis of Variance (ANOVA), are powerful tools to extract features from a complex MS data.[42-45] We utilized statistical data analysis methods to analyze MS results obtained from spheroids experiments. First, we export peaks (with *m/z* values and relative intensities) into Excel data format using Thermo Xcalibur Qual Browser (Thermo Scientific, Waltham, MA, USA). Due to the extremely complexed MS data, we only

export relatively abundant peaks (i.e., ion intensities higher than 10^4) for analysis; the background noise level is $<10^3$. To minimize the influence induced by fluctuations of ion signals during experiments, we used the relative ion intensities normalized to the total ion current (TIC). Second, we upload the Excel data onto online software *Geena2* (http://bioinformatics.hsanmartino.it/geena2/)[46] for peak alignment. Third, we import treated data into *Metaboanalyst 3.0* (http://www.metaboanalyst.ca/faces/ModuleView.xhtml)[47-55] to conduct statistical data analysis, including PCA and the *t*-test. PCA was utilized to detect the difference of chemical compositions between drug treated and control groups, whereas the t-test was applied to extract characteristic molecular peaks with significant abundance changes ($P < 0.05$) upon drug treatment. Finally, we use online database METLIN (https://metlin.scripps.edu/metabo_batch.php)[56] and human metabolome database (HMDB; http://www.hmdb.ca)[57-59] to tentatively label all ions of interest, which can be grouped them into a few different major categories using the heat maps.

5.3 Results and Discussions

5.3.1 Detection of irinotecan and its metabolites

Although the distribution of irinotecan and its metabolites in spheroids has recently been reported,[39, 60] the drug abundance change and the metabolites composition in the microenvironment inside a living tumor are still unclear. The combined micro-funnel and Single-probe design aims to collect and detect anticancer drugs, drug metabolites, and cell metabolites inside live spheroids. As shown in Figure 5.2, using our techniques we have successfully detected the drug compound and multiple drug metabolites, including

SN-38 (*m/z* 393.1437), hydroxyl-irinotecan (*m/z* 603.2802), decarboxyl-irinotecan (*m/z* 543.2956), and dehydro-irinotecan (*m/z* 585.2697). MS/MS analysis has been performed to further confirm the structures of irinotecan and its metabolites accumulated by micro-funnel. Irinotecan and its metabolites were not detected in tumors in the control group.

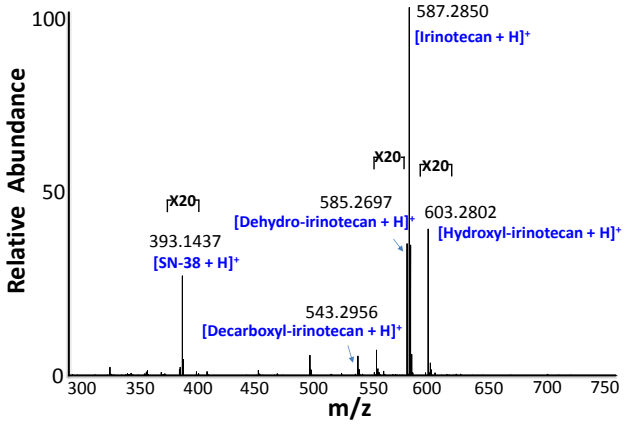

Figure 5.2 Detection of irinotecan and its metabolites from extracellular compounds accumulated by the micro-funnel.

Irinotecan (7-ethyl-10-[4-(1-piperidino)-1-piperidino]-carbonyloxy camptothecin) has been widely used in clinical treatment of colon cancer and lung cancer.[61] The metabolic pathways of irinotecan have already been reported,[39, 62] as partially summarized in Figure 5.3. Irinotecan is a pro-drug that can be metabolized by carboxylesterases into the active compound SN-38, a cytotoxic metabolite that is 300 to 1000-fold more active than irinotecan.[41, 63-65] SN-38 can irreversible induced DNA damage by targeting *Topoisomerase I* and stabilizing the DNA cleavable complex, and result in cancer cell death.[66, 67] The detection of irinotecan from extracellular contents inside tumors is expected since the drug molecules can be delivered into inner regions through molecular diffusion.[8] The drug metabolite SN-38 detected in extracellular

environment is likely from the secretion of cancer cells.[68] Previous studies demonstrated that SN-38 can be expelled by colon cancer cells through efflux mechanism, which is directly related to their drug resistance capabilities.[69, 70] For example, P-glycoprotein (P-gp), an ATP-binding cassette transporter, has been considered as the major transporter of irinotecan and SN-38.[7, 69] Similarly, the multidrug resistance-associated protein was also identified as a transporter of irinotecan and its metabolites.[71]

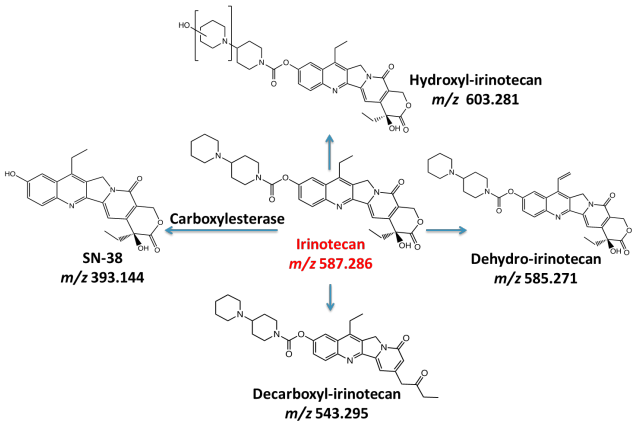

Figure 5.3 Scheme of irinotecan metabolism in tumor cells. All metabolites were detected as the singly protonated species in our experiments.

Another interesting observation is that, for spheroids treated with irinotecan, the abundances of decarboxyl-irinotecan (*m/z* 543.2956) has a similar trend to that of irinotecan (Figure 5.4). Although decarboxylated species was regarded as one of irinotecan metabolites[39] (Figure 5.3), we have detected this compound (with ~1% relative ion intensities compared with irinotecan) in irinotecan water solutions (i.e., 5, 20, 100, and 500 μM). It is plausible that decarboxyl-irinotecan is produced through the in-source fragmentation of irinotecan parent ion. We further performed two types of

experiments to better represent the influence of matrix effect on the detection irinotecan and its metabolites. (a) We used spheroids (control group) to prepared cell lysate solutions containing irinotecan with the above concentrations. (b) We added irinotecan solutions (with the above concentrations) in the syringe, and inserted the Single-probe tip into the micro-funnel implanted in spheroids (control group) to conduct MS measurements. The relative ion intensities of decarboxyl-irinotecan are ~1 % compared with irinotecan in both types of experiments. However, this ratio ranges between 3% and 20% in the spheroid experiments depending on the treatment conditions: higher concentration and longer treatment time lead to more abundant SN-38 (Figure 5.4). Therefore, it is very likely that the extracellular decarboxyl-irinotecan detected from spheroids is primarily from irinotecan metabolism.

5.3.2 Abundance Change of extracellular irinotecan and its metabolites in concentration- and time-dependent experiments

In addition to the detection of molecules of interest inside live spheroids, we have investigated the abundance change of irinotecan and its metabolites under different treatment conditions. We have conducted comprehensive studies of spheroids treated using a series of concentrations and different lengths of time. In concertation-dependent experiments, we treated spheroids (n = 8 for each treatment concentration and control groups) with irinotecan using a series of concentrations (5, 20.6, 50, 100, 200, 300, 400, and 500 μM) for 5 hrs. We measured the relative abundances, which were normalized to the TIC, of extracellular irinotecan and its metabolites. As shown in Figure 5.4(a), the ion intensities of irinotecan increase with higher drug concentrations for treatment. Hydroxyl-irinotecan and SN-38 started to appear inside tumors at relatively higher

treatment concentrations (i.e., 100 and 300 μM for hydroxyl-irinotecan and SN-38, respectively). All four major metabolites were detected from tumors treated with 500 μM irinotecan.

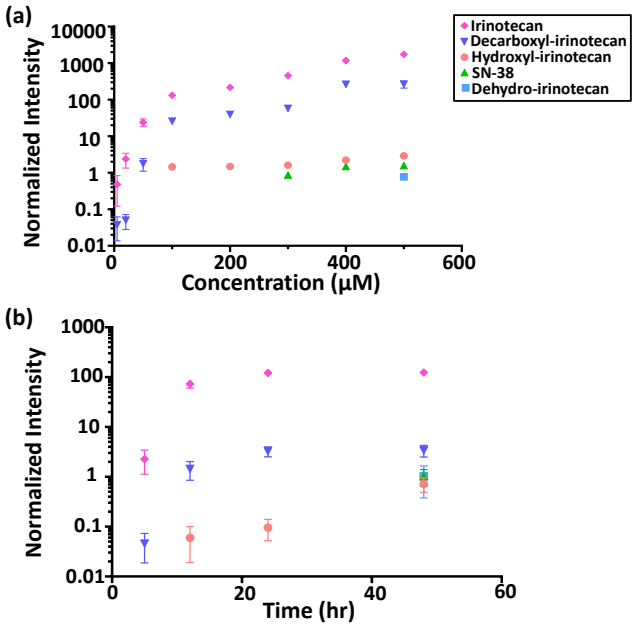

Figure 5.4 Concentration- and time-dependent measurements of extracellular irinotecan and its metabolites in live spheroids. (a) The normalized ion intensities of irinotecan and its metabolites measured from spheroids treated using 5, 20.6, 50, 100, 200, 300, 400, and 500 μM irinotecan for 5 hrs. (b) The normalized intensities of irinotecan and its metabolites measured from spheroids treated for 5, 12, 24, and 48 hrs using the IC_{50} of irinotecan (20.6 μM). Results are the averaged values (with standard deviations) from eight replicates (n = 8) for each concentration and time length.

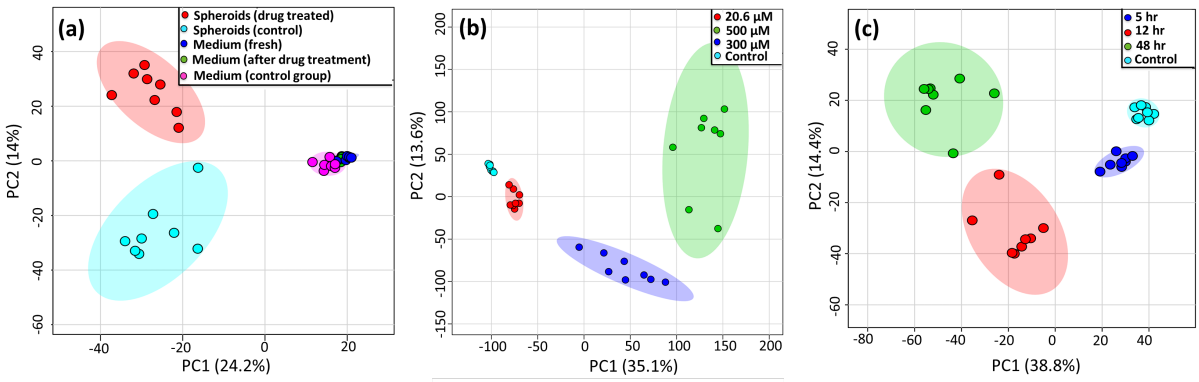

Figure 5.5 Principle component analysis (PCA) of mass spectra. (a) PCA results of culture medium (fresh medium, medium after spheroids culture (control), and medium after drug treatment (50 µM irinotecan)) and extracellular compounds in micro-funnels (spheroids from control and drug treated (50 µM irinotecan) groups). (b) PCA results of extracellular compounds in spheroids in concentrations-dependent experiments (20.6, 300, and 500 µM). (c) PCA results of extracellular compounds in spheroids in time-dependent experiments (5, 12, and 48 hrs). Results are reported from eight replicates (n = 8) in each group, and each symbol represents an independent experiment.

For time-dependent measurements, the adopted drug concentration was 20.6 μM, which is the IC_{50} of irinotecan for HCT-116 spheroids reported from previously studies.[39, 72] We treated spheroids (n = 8 for each treatment time) with 20.6 μM irinotecan for various lengths of time (5, 12, 24, 48, and 72 hrs). However, the treatment of 72 hrs resulted in a complete detachment of spheroids from micro-funnels, the corresponding MS measurements were not conducted. In general, abundances of irinotecan and its metabolites as well as the number of drug metabolites increase along with longer treatment time (Figure 5.4(b)). For example, the hydroxyl-irinotecan and SN-38 were detected after 12 and 48 hrs, respectively; however, they were not observed from samples with shorter time drug treatments.

The combined micro-funnel and Single-probe device has been proven to successfully detect the extracellular drug and its metabolites in the central regions of spheroids treated under a variety of different conditions. Our techniques can be used to study the pharmacokinetics of drugs (such as the drug absorption and excretion) and the rate of drug metabolism inside live tumors. These techniques can potentially provide an effective approach to investigate the fundamentals of anti-drug ability of tumor cells, and facilitate the determination of appropriate drug concentration needed in drug screening studies.

5.3.3 Influence of drug treatment on the extracellular metabolites inside spheroids

The molecular compositions of cell metabolites (including both intracellular and extracellular species) can rapidly response to the changes of cell status and the living environment. Previous analyses of cell metabolites from tissues are

primarily conducted using cell lysate prepared from tissues. The corresponding experimental results cannot discriminate between intracellular and extracellular

metabolites of living tissues. This previously intractable task can be accomplished using the combined micro-funnel and Single-probe device. Due to the critical roles of extracellular compounds on cell-cell communication and cancer cell migration and metastasis, we applied our techniques to investigate whether drug treatment can modulate the composition of extracellular compounds inside spheroids.

First, we demonstrated that compounds in culture medium have no interference with the analysis of molecules collected in the micro-funnels, although our experiments were designed to prohibit the infusion of culture medium into the micro-funnel during the drug treatment (Figure 5.1(d)). We conducted PCA of mass spectra obtained from three medium groups (i.e., the fresh medium, medium collected after spheroids culture, and the medium collected after 50 μM irinotecan treatment) as well as samples collected in micro-funnels from irinotecan-treated spheroids and the control group (Figure 5.5(a)). PCA results indicate that the molecular compositions in culture media are significantly different from those extracellular compounds inside spheroids. In fact, culture medium is composed of inorganic salts, amino acids, vitamins, and glucose. In contrast, the major metabolites detected in tumor environments include phospholipids, glycerides, fatty acids, and glycoside deviates (please refer to Figure 5.6 for details). These results demonstrate that the micro-funnel device can effectively accumulate extracellular compounds in center regions of spheroids without having the leakage of culture medium.

Second, we investigated the general trends of composition change of extracellular compounds induced by drug treatment under different conditions. PCA results show that samples from different treatment concentrations (Figures 5.5(b)) and time lengths (Figures 5.5(c)) exhibit different metabolic signatures. Moreover, the data points are generally located farther away from the control groups, and their

distributions are broader for samples with higher concentrations (Figure 5.5(b)) or longer time (Figure 5.5(c)) for drug treatment. It is very likely that these trends are attributed to the metabolites change as cellular drug uptake increases, which are induced by higher drug concentration or longer time for treatment. Farther distance (i.e., higher scores on PCA plots) is due to the increased abundance of extracellular metabolites; broader distribution is likely associated with sample diversity (e.g. such as minor differences in size of spheroids and location of micro-funnel implant), and the caused variations in cell metabolite become more significant as the drug uptake increases.

Third, for a better understanding of cell metabolic regulation and the response of tumor cells to drug treatment, we classified the extracellular metabolites that are significantly altered by anticancer drug treatment based on t-test results. We tentatively assigned the extracellular compounds collected in micro-funnels by searching the measured accurate *m/z* values in METLIN and HMDB database (mass accuracy < 5 ppm). Because previous studies found that drug treatment affects the metabolism of the extracellular lipids,[73] we focused our current study on analyzing the irinotecan-induced extracellular lipid change. As summarized in the heat maps (Figures 5.6(a) and 5.6(b)), the patterns of extracellular lipids are different between control and irinotecan-treated tumors, and their compositions also change with the increase of drug concentration and treating time length. Specifically, lipids significantly changed by irinotecan treatment include phospholipids (phosphatidic acids (PAs), phosphoethanolamines (PEs), phosphatidylglycerols (PGs), phosphatidylserines (PSs), and phosphatidylinositols (PIs)), and glycerolipids (diglycerides (DGs) and triglycerides (TGs)). Although it is impractical to obtain the exact structure information of all tentatively assigned peaks, we can confidently

classify these species into different groups such as PA, PE, PG, PS, PI, DG, TG. In addition, our technology allows us to conduct MS^2 analysis of ions of interest for more confident structure identification. For example, four compounds (i.e., DG (38:5), PC (34:5), PC (40:7), TG (50:3)) have been confirmed by performing MS^2 analysis and comparing our mass spectra with the METLIN database. MS^3 and above analyses were not carried out due to inadequate ion intensities.

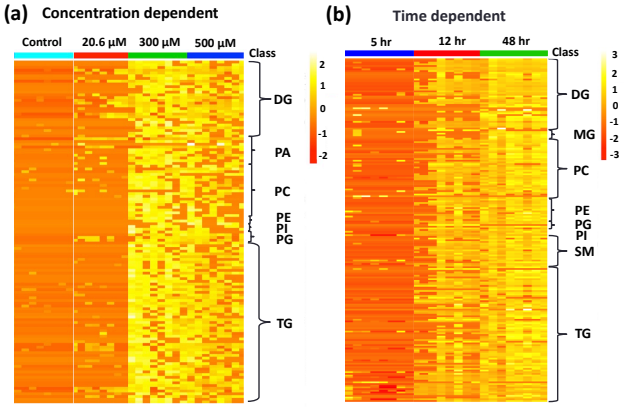

Figure 5.6 Heat maps summarizing the categorized extracellular lipids measured from spheroids under different treatment conditions. The compositions of extracellular lipids were significant changed by anticancer drug treatment under (a) different concentrations (20.6, 300, and 500 μM) and (b) different treatment times (5, 12, and 48 hrs). Results are reported from eight replicates (n = 8) in each group. PA (phosphatic acid), PE (phosphoethanolamine), PG (phosphatidylglycerol), PS (phosphatidylserine), PI (phosphatidylinositol), PC (phosphatidylcholine), MG (monoglycerides), DG (diglycerides), TG (triglyceride), SM (sphingomyelin).

Previously studies found that some colorectal cancer cells can develop resistance to the SN-38 through regulating their cellular metabolism.[74, 75] For example, under irinotecan treatment, colon cancer cells can enhance *de novo* lipogenesis to accumulate cellular TGs and phospholipids, which can promote cell survival[76, 77] and develop the resistance to chemotherapy.[78, 79] TGs are used by

cells for energy storage; phospholipids are essential components for biological membrane, and they are also found as second messengers for transduction of intercellular signals.[80-82] Both TGs and phospholipids are critical for cell proliferation and apoptosis.[83-85] The enhanced lipogenesis in drug-treated cells can increase lipids secretion and result in increased concentrations of extracellular lipids.[79] Correspondingly, in our live spheroids studies, we did observe the increase of extracellular lipids (e.g., phospholipids, TGs, and DGs) under irinotecan treatment (Figures 5.6(a) and 5.6(b)), which was likely attributed to the trigged drug resistance of cancer cells inside central regions of tumors. Detailed interpretation of more MS data is needed to better understand other significant implications, which potentially present in our experimental results, of cancer biology and anticancer drug mechanisms; however, this goal is beyond the scope of current study.

5.4 Conclusion

We reported a study of using combined microscale devices, the micro-funnel and the Single-probe, to collect extracellular contents inside live spheroids for real-time MS analysis. The micro-funnel is produced from laser-pulled fused silica capillary, a biocompatible material, with small tip size (~25 μm). This type of microscale device can be implanted into live spheroids cultured from cancer cells to collect the extracellular compounds in inner region of spheroids. The spheroids were treated using anticancer drug irinotecan under a series of conditions. The collected extracellular contents in the micro-funnel were then efficiently extracted by the Single-probe, a microscale sampling and ionization device, for real-time MS analysis. We successfully detected irinotecan, drug metabolites, and cellular metabolites using our technologies. Statistical data analyses, including PCA and t-test, have been carried

out to obtain the overall feathers of cell metabolomic changes induced by anticancer drug treatment. Our results indicate that extracellular compounds in inner tumor regions are significantly altered by irinotecan treatment, and different treatment conditions result in significant differences in metabolic signatures. In particular, the increased abundances of phospholipids and glycerolipids reflect cellular responses to drug treatment, and may indicate the drug resistance of central tumor cells. Our current study demonstrates that the combined micro-funnel and Single-probe MS technique can be used to monitor extracellular metabolites in the microenvironment inside spheroids. However, we may not be able to completely eliminate the possibility of sampling intracellular molecules in experiments. Dead cells (e.g., due to the lack of oxygen and nutrients as well as the present of drug molecules) may be present inside spheroids. Cellular contents released by dead cells can be mixed with extracellular metabolites and collected by the micro-funnel in MS measurements. Future studies are necessary to test this possibility. This novel technique can be potentially applied to studies of live tissues in different areas, including fundamental research of the regulation of extracellular compounds in tumor development, drug penetration and metabolism in tumor treatment, and biomarker discovery in cancer diagnosis.

5.5 References

[1] R. Demicheli, A. Abbattista, R. Miceli, P. Valagussa, G. Bonadonna, Time distribution of the recurrence risk for breast cancer patients undergoing mastectomy: further support about the concept of tumor dormancy, Breast Cancer Res. Treat., 41 (1996) 177-185.

[2] T.G. Karrison, D.J. Ferguson, P. Meier, Dormancy of mammary carcinoma after mastectomy, J. Natl. Cancer Inst., 91 (1999) 80-85.

[3] J. Pfitzenmaier, W.J. Ellis, E.W. Arfman, S. Hawley, P.O. McLaughlin, P.H. Lange, R.L. Vessella, Telomerase activity in disseminated prostate cancer cells, BJU Int., 97 (2006) 1309-1313.

[4] D. Weckermann, P. MÜller, F. Wawroschek, R. Harzmann, G. RiethmÜller, G. Schlimok, Disseminated cytokeratin positive tumor cells in the bone marrow of patients with prostate cancer: detection and prognostic value, J. Urol., 166 (2001) 699-704.

[5] J.A. Aguirre-Ghiso, Models, mechanisms and clinical evidence for cancer dormancy, Nat. Rev. Cancer., 7 (2007) 834-846.

[6] A.H. Kyle, J.H. Baker, A.I. Minchinton, Targeting quiescent tumor cells via oxygen and IGF-I supplementation, Cancer Res., 72 (2012) 801-809.

[7] T. Bansal, A. Awasthi, M. Jaggi, R.K. Khar, S. Talegaonkar, Pre-clinical evidence for altered absorption and biliary excretion of irinotecan (CPT-11) in combination with quercetin: possible contribution of P-glycoprotein, Life Sci., 83 (2008) 250-259.

[8] A.I. Minchinton, I.F. Tannock, Drug penetration in solid tumours, Nat. Rev. Cancer, 6 (2006) 583-592.

[9] I. Tannock, The relation between cell proliferation and the vascular system in a transplanted mouse mammary tumour, Br. J. Cancer, 22 (1968) 258.

[10] O. Trédan, C.M. Galmarini, K. Patel, I.F. Tannock, Drug resistance and the solid tumor microenvironment, J. Natl. Cancer Inst., 99 (2007) 1441-1454.

[11] M.Y. Ali, C.-Y. Chuang, M.T.A. Saif, Reprogramming cellular phenotype by soft collagen gels, Soft Matter, 10 (2014) 8829-8837.

[12] R. Harisi, J. Dudás, F. Timár, G. Pogány, J. Timár, I. Kovalszky, M. Szendrői, A. Jeney, Invasive growth and topoisomerase-switch induced by tumorous extracellular matrix in osteosarcoma cell culture, Cell Biol. Int, 29 (2005) 959-967.

[13] T. Triulzi, P. Casalini, M. Sandri, M. Ratti, M.L. Carcangiu, M.P. Colombo, A. Balsari, S. Ménard, R. Orlandi, E. Tagliabue, Neoplastic and stromal cells contribute to an extracellular matrix gene expression profile defining a breast cancer subtype likely to progress, PLOS One, 8 (2013) e56761.

[14] R. Harisi, A. Jeney, Extracellular matrix as target for antitumor therapy, Onco Targets Ther., 8 (2015) 1387.

[15] D.W. Hutmacher, D. Loessner, S. Rizzi, D.L. Kaplan, D.J. Mooney, J.A. Clements, Can tissue engineering concepts advance tumor biology research?, Trends Biotechnol., 28 (2010) 125-133.

[16] G. Mehta, A.Y. Hsiao, M. Ingram, G.D. Luker, S. Takayama, Opportunities and challenges for use of tumor spheroids as models to test drug delivery and efficacy, J. Control. Release, 164 (2012) 192-204.

[17] E. Fennema, N. Rivron, J. Rouwkema, C. van Blitterswijk, J. de Boer, Spheroid culture as a tool for creating 3D complex tissues, Trends Biotechnol., 31 (2013) 108-115.

[18] D. Antoni, H. Burckel, E. Josset, G. Noel, Three-dimensional cell culture: a breakthrough in vivo, Int. J. Mol. Sci., 16 (2015) 5517-5527.

[19] T. Nederman, B. Norling, B. Glimelius, J. Carlsson, U. Brunk, Demonstration of an extracellular matrix in multicellular tumor spheroids, Cancer Res., 44 (1984) 3090-3097.

[20] T.T. Goodman, C.P. Ng, S.H. Pun, 3-D tissue culture systems for the evaluation and optimization of nanoparticle-based drug carriers, Bioconjugate Chem., 19 (2008) 1951-1959.

[21] N.S. Waleh, J. Gallo, T.D. Grant, B.J. Murphy, R.H. Kramer, R.M. Sutherland, Selective down-regulation of integrin receptors in spheroids of squamous cell carcinoma, Cancer Res., 54 (1994) 838-843.

[22] C. Liu, Q. Wu, A.C. Harms, R.D. Smith, On-line microdialysis sample cleanup for electrospray ionization mass spectrometry of nucleic acid samples, Anal. Chem., 68 (1996) 3295-3299.

[23] R.W. Kondrat, K. Kanamori, B.D. Ross, In vivo microdialysis and gas-chromatography/mass-spectrometry for 13 C-enrichment measurement of extracellular glutamate in rat brain, J. Neurosci. Methods, 120 (2002) 179-192.

[24] L. Wu, Q.-L. Zhang, X.-Y. Zhang, C. Lv, J. Li, Y. Yuan, F.-X. Yin, Pharmacokinetics and blood–brain barrier penetration of (+)-catechin and (−)-epicatechin in rats by microdialysis sampling coupled to high-performance liquid chromatography with chemiluminescence detection, J. Agric. Food Chem., 60 (2012) 9377-9383.

[25] Z. Li, Z. Cui, Application of microdialysis in tissue engineering monitoring, Prog. Nat. Sci., 18 (2008) 503-511.

[26] P. Nandi, S.M. Lunte, Recent trends in microdialysis sampling integrated with conventional and microanalytical systems for monitoring biological events: a review, Anal. Chim. Acta, 651 (2009) 1-14.

[27] M.I. Davies, A review of microdialysis sampling for pharmacokinetic applications, Anal. Chim. Acta, 379 (1999) 227-249.

[28] N. Plock, C. Kloft, Microdialysis—theoretical background and recent implementation in applied life-sciences, Eur. J. Pharm. Sci., 25 (2005) 1-24.

[29] F. Erdő, Microdialysis Techniques In Pharmacokinetic and Biomarker Studies, Clin. Exp. Pharmacol. Physiol., 5 (2015) 2161-1459.1000180.

[30] N. Pan, W. Rao, N.R. Kothapalli, R. Liu, A.W. Burgett, Z. Yang, The single-probe: a miniaturized multifunctional device for single cell mass spectrometry analysis, Anal. Chem., 86 (2014) 9376-9380.

[31] N. Pan, W. Rao, S.J. Standke, Z. Yang, Using Dicationic Ion-Pairing Compounds To Enhance the Single Cell Mass Spectrometry Analysis Using the Single-Probe: A Microscale Sampling and Ionization Device, Anal. Chem., 88 (2016) 6812.

[32] W. Rao, N. Pan, Z. Yang, High resolution tissue imaging using the single-probe mass spectrometry under ambient conditions, J. Am. Soc. Mass Spectrom., 26 (2015) 986-993.

[33] W. Rao, N. Pan, X. Tian, Z. Yang, High-resolution ambient MS imaging of negative ions in positive ion mode: using dicationic reagents with the single-probe, J. Am. Soc. Mass Spectrom., 27 (2016) 124-134.

[34] W. Rao, N. Pan, Z. Yang, Applications of the Single-probe: Mass Spectrometry Imaging and Single Cell Analysis under Ambient Conditions, J. Vis. Exp., (2016) e53911-e53911.

[35] H. Li, A.B. Hummon, Imaging mass spectrometry of three-dimensional cell culture systems, Anal. Chem., 83 (2011) 8794-8801.

[36] D.R.A. Wheatcraft, X. Liu, A.B. Hummon, Sample preparation strategies for mass spectrometry imaging of 3D cell culture models, J. Vis. Exp., (2014) e52313-e52313.

[37] O. Sirenko, T. Mitlo, J. Hesley, S. Luke, W. Owens, E.F. Cromwell, High-content assays for characterizing the viability and morphology of 3D cancer spheroid cultures, Assay Drug Dev Technol, 13 (2015) 402-414.

[38] Y.-H. Joung, Development of implantable medical devices: from an engineering perspective, Int Neurourol J, 17 (2013) 98-106.

[39] X. Liu, E.M. Weaver, A.B. Hummon, Evaluation of therapeutics in three-dimensional cell culture systems by MALDI imaging mass spectrometry, Anal. Chem., 85 (2013) 6295-6302.

[40] I. Lanekoff, B.S. Heath, A. Liyu, M. Thomas, J.P. Carson, J. Laskin, Automated platform for high-resolution tissue imaging using nanospray desorption electrospray ionization mass spectrometry, Anal. Chem., 84 (2012) 8351-8356.

[41] Y. Kawato, M. Aonuma, Y. Hirota, H. Kuga, K. Sato, Intracellular roles of SN-38, a metabolite of the camptothecin derivative CPT-11, in the antitumor effect of CPT-11, Cancer Res., 51 (1991) 4187-4191.

[42] E.A. Jones, S.O. Deininger, P.C.W. Hogendoorn, A.M. Deelder, L.A. McDonnell, Imaging mass spectrometry statistical analysis, J. Proteomics, 75 (2012) 4962-4989.

[43] J. Jaumot, R. Tauler, Potential use of multivariate curve resolution for the analysis of mass spectrometry images, Analyst, 140 (2015) 837-846.

[44] B. Vaezian, C.R. Anderton, M.L. Kraft, Discriminating and Imaging Different Phosphatidylcholine Species within Phase-Separated Model Membranes by Principal

Component Analysis of TOF-Secondary Ion Mass Spectrometry Images, Anal. Chem., 82 (2010) 10006-10014.

[45] I. Yao, Y. Sugiura, M. Matsumoto, M. Setou, In situ proteomics with imaging mass spectrometry and principal component analysis in the Scrapper-knockout mouse brain, Proteomics, 8 (2008) 3692-3701.

[46] P. Romano, A. Profumo, M. Rocco, R. Mangerini, F. Ferri, A. Facchiano, Geena 2, improved automated analysis of MALDI/TOF mass spectra, BMC Bioinform., 17 (2016) 61.

[47] J. Xia, D.S. Wishart, MetPA: a web-based metabolomics tool for pathway analysis and visualization, Bioinformatics, 26 (2010) 2342-2344.

[48] J. Xia, I.V. Sinelnikov, D.S. Wishart, MetATT: a web-based metabolomics tool for analyzing time-series and two-factor datasets, Bioinformatics, 27 (2011) 2455-2456.

[49] J. Xia, D.S. Wishart, Metabolomic Data Processing, Analysis, and Interpretation Using MetaboAnalyst, Curr Protoc Bioinformatics, John Wiley & Sons, Inc.2002.

[50] J. Xia, D.I. Broadhurst, M. Wilson, D.S. Wishart, Translational biomarker discovery in clinical metabolomics: an introductory tutorial, Metabolomics, 9 (2013) 280-299.

[51] J. Xia, D.S. Wishart, Web-based inference of biological patterns, functions and pathways from metabolomic data using MetaboAnalyst, Nat. Protocols, 6 (2011) 743-760.

[52] J. Xia, R. Mandal, I.V. Sinelnikov, D. Broadhurst, D.S. Wishart, MetaboAnalyst 2.0—a comprehensive server for metabolomic data analysis, Nucleic Acids Res., 40 (2012) W127-W133.

[53] J. Xia, N. Psychogios, N. Young, D.S. Wishart, MetaboAnalyst: a web server for metabolomic data analysis and interpretation, Nucleic Acids Res., 37 (2009) W652-W660.

[54] J. Xia, I.V. Sinelnikov, B. Han, D.S. Wishart, MetaboAnalyst 3.0—making metabolomics more meaningful, Nucleic Acids Res., 43 (2015) W251-W257.

[55] J. Xia, D.S. Wishart, MSEA: a web-based tool to identify biologically meaningful patterns in quantitative metabolomic data, Nucleic Acids Res., 38 (2010) W71-W77.

[56] C.A. Smith, G. O'Maille, E.J. Want, C. Qin, S.A. Trauger, T.R. Brandon, D.E. Custodio, R. Abagyan, G. Siuzdak, METLIN: a metabolite mass spectral database, Ther Drug Monit, 27 (2005) 747-751.

[57] D.S. Wishart, T. Jewison, A.C. Guo, M. Wilson, C. Knox, Y. Liu, Y. Djoumbou, R. Mandal, F. Aziat, E. Dong, S. Bouatra, I. Sinelnikov, D. Arndt, J. Xia, P. Liu, F. Yallou, T. Bjorndahl, R. Perez-Pineiro, R. Eisner, F. Allen, V. Neveu, R. Greiner, A. Scalbert, HMDB 3.0—The Human Metabolome Database in 2013, Nucleic Acids Res., 41 (2013) D801-D807.

[58] D.S. Wishart, C. Knox, A.C. Guo, R. Eisner, N. Young, B. Gautam, D.D. Hau, N. Psychogios, E. Dong, S. Bouatra, R. Mandal, I. Sinelnikov, J. Xia, L. Jia, J.A. Cruz, E. Lim, C.A. Sobsey, S. Shrivastava, P. Huang, P. Liu, L. Fang, J. Peng, R. Fradette, D. Cheng, D. Tzur, M. Clements, A. Lewis, A. De Souza, A. Zuniga, M. Dawe, Y. Xiong, D. Clive, R. Greiner, A. Nazyrova, R. Shaykhutdinov, L. Li, H.J. Vogel, I. Forsythe, HMDB: a knowledgebase for the human metabolome, Nucleic Acids Res., 37 (2009) D603-D610.

[59] D.S. Wishart, D. Tzur, C. Knox, R. Eisner, A.C. Guo, N. Young, D. Cheng, K. Jewell, D. Arndt, S. Sawhney, C. Fung, L. Nikolai, M. Lewis, M.-A. Coutouly, I.

Forsythe, P. Tang, S. Shrivastava, K. Jeroncic, P. Stothard, G. Amegbey, D. Block, D.D. Hau, J. Wagner, J. Miniaci, M. Clements, M. Gebremedhin, N. Guo, Y. Zhang, G.E. Duggan, G.D. MacInnis, A.M. Weljie, R. Dowlatabadi, F. Bamforth, D. Clive, R. Greiner, L. Li, T. Marrie, B.D. Sykes, H.J. Vogel, L. Querengesser, HMDB: the Human Metabolome Database, Nucleic Acids Res., 35 (2007) D521-D526.

[60] G.J. LaBonia, S.Y. Lockwood, A.A. Heller, D.M. Spence, A.B. Hummon, Drug penetration and metabolism in 3D cell cultures treated in a 3D printed fluidic device: assessment of irinotecan via MALDI imaging mass spectrometry, Proteomics, 16 (2016) 1814-1821.

[61] Y. Xu, M. Villalona-Calero, Irinotecan: mechanisms of tumor resistance and novel strategies for modulating its activity, Ann. Oncol., 13 (2002) 1841-1851.

[62] K. Sai, N. Kaniwa, S. Ozawa, J.-i. Sawada, A new metabolite of irinotecan in which formation is mediated by human hepatic cytochrome P-450 3A4, Drug Metab. Dispos., 29 (2001) 1505-1513.

[63] H. Zhao, B. Rubio, P. Sapra, D. Wu, P. Reddy, P. Sai, A. Martinez, Y. Gao, Y. Lozanguiez, C. Longley, Novel prodrugs of SN38 using multiarm poly (ethylene glycol) linkers, Bioconjugate Chem., 19 (2008) 849-859.

[64] Z. Liu, J.T. Robinson, X. Sun, H. Dai, PEGylated nano-graphene oxide for delivery of water insoluble cancer drugs, J. Am. Chem. Soc., 130 (2008) 10876.

[65] E.-J. Kim, S. Bhuniya, H. Lee, H.M. Kim, C. Cheong, S. Maiti, K.S. Hong, J.S. Kim, An activatable prodrug for the treatment of metastatic tumors, J. Am. Chem. Soc., 136 (2014) 13888-13894.

[66] Y.-H. Hsiang, M.G. Lihou, L.F. Liu, Arrest of replication forks by drug-stabilized topoisomerase I-DNA cleavable complexes as a mechanism of cell killing by camptothecin, Cancer Res., 49 (1989) 5077-5082.

[67] A. Wallin, J. Svanvik, B. Holmlund, L. Ferreud, X.-F. Sun, Anticancer effect of SN-38 on colon cancer cell lines with different metastatic potential, Oncol. Rep., 19 (2008) 1493-1498.

[68] L. Iyer, J. Ramírez, D.R. Shepard, C.M. Bingham, D.-K. Hossfeld, M.J. Ratain, U. Mayer, Biliary transport of irinotecan and metabolites in normal and P-glycoprotein-deficient mice, Cancer Chemother. Pharmacol., 49 (2002) 336-341.

[69] T. Hu, Z. Li, C.-Y. Gao, C.H. Cho, Mechanisms of drug resistance in colon cancer and its therapeutic strategies, World J. Gastroenterol., 22 (2016) 6876.

[70] W.T. Bellamy, P-glycoproteins and multidrug resistance, Annu. Rev. Pharmacool. Toxicol., 36 (1996) 161-183.

[71] F.R. Luo, P.V. Paranjpe, A. Guo, E. Rubin, P. Sinko, Intestinal transport of irinotecan in Caco-2 cells and MDCK II cells overexpressing efflux transporters Pgp, cMOAT, and MRP1, Drug Metab. Dispos., 30 (2002) 763-770.

[72] X. Liu, A.B. Hummon, Quantitative determination of irinotecan and the metabolite SN-38 by nanoflow liquid chromatography-tandem mass spectrometry in different regions of multicellular tumor spheroids, J. Am. Soc. Mass. Spectrom., 26 (2015) 577-586.

[73] H. Järveläinen, A. Sainio, M. Koulu, T.N. Wight, R. Penttinen, Extracellular matrix molecules: potential targets in pharmacotherapy, Pharmacol. Rev., 61 (2009) 198-223.

[74] M. Tamada, O. Nagano, S. Tateyama, M. Ohmura, T. Yae, T. Ishimoto, E. Sugihara, N. Onishi, T. Yamamoto, H. Yanagawa, Modulation of glucose metabolism by CD44 contributes to antioxidant status and drug resistance in cancer cells, Cancer Res., 72 (2012) 1438-1448.

[75] K. Hiller, C.M. Metallo, Profiling metabolic networks to study cancer metabolism, Curr. Opin. Biotechnol., 24 (2013) 60-68.

[76] J.A. Menendez, R. Lupu, Fatty acid synthase and the lipogenic phenotype in cancer pathogenesis, Nat. Rev. Cancer, 7 (2007) 763-777.

[77] Y. Zhou, L.R. Bollu, F. Tozzi, X. Ye, R. Bhattacharya, G. Gao, E. Dupre, L. Xia, J. Lu, F. Fan, ATP citrate lyase mediates resistance of colorectal cancer cells to SN38, Mol. Cancer Ther., 12 (2013) 2782-2791.

[78] B. Qiu, D. Ackerman, D.J. Sanchez, B. Li, J.D. Ochocki, A. Grazioli, E. Bobrovnikova-Marjon, J.A. Diehl, B. Keith, M.C. Simon, HIF2α-dependent lipid storage promotes endoplasmic reticulum homeostasis in clear-cell renal cell carcinoma, Cancer Discov., 5 (2015) 652-667.

[79] S. Beloribi-Djefaflia, S. Vasseur, F. Guillaumond, Lipid metabolic reprogramming in cancer cells, Oncogenesis, 5 (2016) e189.

[80] K. Petzold, A. Olofsson, A. Arnqvist, G. Gröbner, J.r. Schleucher, Semiconstant-time P, H-COSY NMR: analysis of complex mixtures of phospholipids originating from Helicobacter pylori, J. Am. Chem. Soc., 131 (2009) 14150-14151.

[81] M. Ma, A. Paredes, D. Bong, Intra-and intermembrane pairwise molecular recognition between synthetic hydrogen-bonding phospholipids, J. Am. Chem. Soc., 130 (2008) 14456-14458.

[82] Y. Nishizuka, Intracellular signaling by hydrolysis of phospholipids and activation of protein kinase C, Science, 258 (1992) 607-615.

[83] C. Berland, C. Cansell, T.S. Hnasko, C. Magnan, S. Luquet, Dietary triglycerides as signaling molecules that influence reward and motivation, Curr. Opin. Behav. Sci., 9 (2016) 126-135.

[84] N.D. Ridgway, The role of phosphatidylcholine and choline metabolites to cell proliferation and survival, Crit. Rev. Biochem. Mol. Biol., 48 (2013) 20-38.
[85] S.-M. Huang, J.M. Bock, P.M. Harari, Epidermal growth factor receptor blockade with C225 modulates proliferation, apoptosis, and radiosensitivity in squamous cell carcinomas of the head and neck, Cancer Res., 59 (1999) 1935-1940.